TRADE STUDY OF NUCLEAR SPACE POWER AND PROPULSION SYSTEM ARCHITECTURES FOR ADVANCED INTERPLANETARY TRAVEL

By

JACLYN CICHON

A THESIS PRESENTED TO THE GRADUATE SCHOOL
OF THE UNIVERSITY OF FLORIDA IN PARTIAL FULFILLMENT
OF THE REQUIREMENTS FOR THE DEGREE OF
MASTER OF SCIENCE

UNIVERSITY OF FLORIDA

2007

I would like to dedicate this work to my parents.

ACKNOWLEDGMENTS

The material presented in this thesis is the culmination of both hard work and dedicated studies in the fields of aerospace and nuclear engineering. Presenting this thesis in its final form has only been done through the support and assistance of many people.

I would first like to thank my parents for their support throughout my life, and most notably their encouragement of my intellectual pursuits. I would like to thank Dr. John-Paul Clarke, my UROP advisor at MIT who assured me that I would get through college and someday be a successful graduate student. I would like to thank Dr. Samim Anghaie for convincing me to further my studies in graduate school and allowing me the opportunity to pursue a Nuclear Engineering master's degree. I owe much gratitude to my Pratt & Whitney mentor, Russ Joyner, who gave me the time and the tools I needed to begin and complete this thesis. Lastly, I would like to thank all of my friends and peers both at MIT and UF for their constant words of encouragement, especially those who truly believed I could someday become the "President of NASA."

TABLE OF CONTENTS

page

LIST OF TABLES

LIST OF FIGURES

Abstract of Dissertation Presented to the Graduate School
of the University of Florida in Partial Fulfillment of the
Requirements for the Degree of Master of Science

TRADE STUDY OF NUCLEAR SPACE POWER AND PROPULSION SYSTEM ARCHITECTURES FOR ADVANCED INTERPLANETARY TRAVEL

By

Jaclyn Cichon

May 2007

Chair: Samim Anghaie
Major: Nuclear Engineering Sciences

Past mission analysis studies for interplanetary missions have typically focused on assessing one power and propulsion system applied to a singular mission. This has led to a lack of comparable results for different power and propulsion systems, and limited systematic procedures for mission planning. We attempted to address these faults through a comprehensive trade study on NTR, NEP, and Hybrid power and propulsion systems, grouped by NTR fuel type or electric thruster type into eleven configurations. Ephemeris codes were used to investigate mission planning and departure options, and vehicle models were developed and then analyzed through parametric performance plots. Lastly, measures of effectiveness were defined and used to assess a tradespace matrix containing all vehicle configurations applied to twelve optimized reference missions. This assessment provided a simplified ranking of specific vehicle designs for each given interplanetary mission, along with a comparison of vehicle performance based on important figures of merit such as propellant mass and IMLEO.

CHAPTER 1
INTRODUCTION

Motivation

The desire to travel though space and reach distant planets has no doubt existed for ages, yet the actual planning of interplanetary missions truly began in the United States approximately 60 years ago. This is when Werner Von Braun, former aerospace engineer and National Aeronautics and Space Administration (NASA) administrator, conducted the first engineering analysis of a manned mission to Mars. By the late 1960s Von Braun had become a proponent for nuclear thermal rocket-powered spacecraft, while his Soviet contemporary Korolev believed nuclear electric propulsion was the best option to go to Mars. Cancellation of the Apollo program in the 1970s led to a sharp decline in nuclear propulsion and Mars exploration research.[1] In 1988 President George H. Bush appointed NASA to create the Mars Office of Exploration as part of the Space Exploration Initiative, resulting in a resurgency in reports on manned missions to the moon and Mars.[2] It was believed that the moon would be a stepping stone to Mars, as one report states: "the Moon provides a unique database for life science and operational verification in a reduced gravity environment, combined with the psychological realism of operations at a harsh extraterrestrial location."[3]

Although the goals sought by the Space Exploration Initiative never came to fruition, a renewed interest in moon and Mars exploration was expressed by George W. Bush under the 'Moon Mars and Beyond' initiative in 2002. NASA has indeed answered this call for a return to the moon and then to Mars, doing so at a pace commensurate with its appropriated funding and resources. The government agency, with the help of its industry partners, is currently in the initial phases of its Constellation project, which hopes to return man to the moon by 2014 and eventually replace the outdated and complex Space Shuttle with the Orion Crew Exploration

Vehicle. Despite all the preparation a return to the moon would provide for a future Mars mission, one of the main differences would be that a vastly different propulsion system would be needed to make the much longer journey to Mars. In fact it has been noted by mission planners that "the choice of a transportation system is the key trade in performance for Mars exploration."[3] This is why it is paramount to invest now in Mars mission planning studies that assess the various power and propulsion architectures that have the capabilities that will be required to carry man to the surface of Mars and back.

Project Statement

Our study aimed to provide this necessary mission analysis and to do so from as broad a scope as possible. Past studies have provided results for specific missions using only one propulsion system, making it difficult to try and compare all possible propulsion systems for the same mission. Our study attempted to provide a comparison of the major power and propulsion system architectures considered for future manned interplanetary missions and to compare them on an "even playing field." This involved elements of mission analysis, system modeling and optimization, and parametric analysis that culminated in a large trade study. Although the end-goal was to provide an answer to which power and propulsion system model best completes the attempted interplanetary missions using the aide of a tradespace matrix, analysis of non-mission-specific vehicle performance and interplanetary trajectories was also assessed. It was the hope of this author that the approach taken was broad enough in context to allow application to a myriad of future space mission profiles, yet specific enough to provide valid and useful results of vehicle performance. This mission analysis study promises a unique perspective on the subject matter given the combined systems engineering perspective and fundamentals of nuclear reactor design, astrodynamics, and rocket propulsion.

Through investigation of previously completed Mars mission studies, a commonality found was that the primary objective of each study was to safely send and return humans to Mars.[2] Although this objective was inherent as well to this study, a very important secondary objective was to provide a comparison of different vehicle architectures on an 'apples-to-apples' level, such that bias towards or against a particular system was completely withheld. Each of the architecture models was pieced together following the same methodology, with the same design constraints and without regard to particular mission profiles. Thus, the optimization of vehicle performance for each mission profile produced results that could provide an honest comparison of the different propulsion systems currently under consideration by both NASA and other members of the aerospace community for future manned interplanetary missions. An extra feature of this study was that even more challenging missions to Saturn and Jupiter were attempted so that a more in-depth understanding of the capabilities of the technologies being assessed could be gleaned.

Previous Work and Contributions

Many of the first formal studies comparing advanced propulsion methods for interplanetary missions came about during the Space Exploration Initiative period, which focused on missions to the moon and then to Mars. At that point in time, it was desired to compare the conventional chemical propulsion system with that of a nuclear thermal or electric propulsion system. One report that was done by Boeing for presentation to NASA was the "Space Transfer Concepts and Analysis for Exploration Missions" report. This comprehensive report attempted to compare the possible propulsion methods through various analyses, diagrams, and charts. Initial Mass in Low Earth Orbit (IMLEO) charts were presented in many different fashions, but one of the most useful was a chart showing the optimal IMLEO versus trip time for all the opposition opportunities in the Earth-Mars synodical cycle.

This chart showed these opportunity bands, with the lower boundary of each propulsion system option formed by the best year (2018), and the upper boundary by the most difficult year (2025), given all opportunities between the years 2010 and 2025. The nuclear electric propulsion (NEP) system was the front-runner for the shorter mission trips, yet it did not seem realistic to look at total mission trips to Mars below 400 days, especially given the radically high power requirement (120 MW) and IMLEO (1000 t) that would be needed for a fast NEP mission to Mars. Looking at the more reasonable time span of 400-600 day missions, the advanced NTR system was the front-runner, with the NEP system close behind, and lastly the rather impractical chemical system. It should be noted, however, that if longer mission trip times were acceptable, the NEP system would present the lowest IMLEO option given all the systems assessed.[4]

In more recent studies in line with the 2002 'Moon, Mars, and Beyond' initiative, the mission analysis performed has commonly focused on one specific power and propulsion system, going into a bit more detail on mission specifics, hardware, and mass and performance estimates. Three such studies were reviewed that specifically focused on one main architecture that is currently considered feasible for advanced interplanetary travel. These architectures include a Nuclear Thermal Rocket (NTR) system, NEP system, and a Hybrid system that uses one reactor to power both electric and thermal propulsion systems.

A study entitled "Nuclear Thermal Rocket Vehicle Design Options for Future NASA Missions to the Moon and Mars" that was conducted by the NASA Lewis Research Center analyzed a 2010 human mission to Mars. This mission consisted of a 344-day outbound transfer, 1153-day stay at Mars, and a 180-day return. Three NTR burns were performed with an Earth swingby used for the last maneuver in order to reduce energy requirements. Two different reactors were considered, one based on a NERVA reactor, and the second utilizing ternary

carbide fuels. The first had a specific impulse (ISP) of 900 (s), and the latter an ISP of 960 (s). The reactors provided thermal power for the propulsion system, and electric power for any spacecraft needs. This bimodal reactor design functioned by flowing hydrogen coolant through the core to heat the propellant, and then a helium-xenon working fluid to remove heat for power conversion purposes. The results for the NTR spacecraft included an IMLEO of 234 (t) for the NERVA-type reactor, and 207 (t) for the carbide reactor, given four reactors each operating at a thrust level of 15 (klbf).[5]

A team of engineers at NASA's Glenn Research Center conducted the NEP mission analysis study entitled, "High Power MPD Nuclear Electric Propulsion (NEP) for Artificial Gravity HOPE Missions to Callisto." The designed mission was a 4.5-year round-trip crewed journey to Jupiter's moon Callisto, beginning in the year 2041. The vehicle was to be proceeded by both a cargo and tanker vehicle, support a crew of six, provide artificial gravity for most of the mission duration, and be refueled before leaving Callisto to return to Earth. The spacecraft was to be powered by a high temperature gas-cooled fission reactor with a tungsten metal matrix CERMET fuel element. Electrical power was generated using a high power, closed-cycle Brayton heat engine. Hydrogen MPD thrusters provided propulsion with advanced performance parameters including 8000 (s) ISP and 64.5% efficiency. A full mission analysis of this system revealed that the 120-day stay, 2.1-year transfer to and from Callisto would require an IMLEO of 262 (t). This value accounts for an outbound propellant mass of 74 (t), but does not include the return propellant load of 53 (t), which was carried to Jupiter aboard the tanker vehicle.[6,7]

The results of a mission analysis study performed to evaluate the feasibility for a mission to Mars using a Hybrid propulsion system were found in "Mission to Mars Using Integrated Propulsion Concepts: Considerations, Opportunities, and Strategies." Integrated Propulsion

Systems (IPS) is the term used to refer to a Hybrid system, one that uses both NTR and NEP systems for propulsive means. The mission scenario in this study was a manned mission to Mars in which the spacecraft was assembled in Low Earth Orbit (LEO) at about a 300 (km) altitude, and then the reactor engine was turned on to begin the mission. In this particular study, the nuclear and electric engines were both used to spiral out of the Earth's atmosphere until the required Earth escape velocity was reached. The spacecraft then separated into two by means of a tether for on-orbit artificial gravity, and restarted both propulsion systems for simultaneous operation during the remaining voyage to Mars.[8]

The technology assumed in this study consisted of a "Rubbia Nuclear Rocket" and MPD electric thrusters. In the Rubbia nuclear reactor, the heat exchange is essentially reversed from a typical NERVA-type reactor, with fission fragments from subcritical fissions of an isotope of Americium heating the coolant. This allows lower fuel operating temperatures, while enabling higher ISP values to be reached. Four superconductive Magneto-Plasma-Dynamic (MPD) thrusters were assumed for the electric propulsion system. It was assumed in the study that the ISP of the Rubbia systems was 3500 (s) and that of the MPD system was 56000 (s). The mass breakdown for this IPS spacecraft was found to be 378 (t) with an outbound propellant mass of 132 (t) and return propellant load of 92 (t).[8,9]

Study Overview

Study Methodology

Our study attempted to go farther than previous studies, which primarily focused on specific power and propulsion systems applied to a singular mission, by assessing three types of vehicles broken down into eleven different configurations over each of twelve possible mission scenarios. Basic methodology used to perform such an expansive mission trade study includes four major steps:

1. Defining the general mission concept and propagating this to twelve different reference mission profiles
2. Creating ephemeris models
    a. Generating optimized trajectories for each mission profile
    b. Obtaining results of parametric study of ephemerides
3. Developing models for the space power and propulsion architectures
    a. Running the vehicle models with mission trajectory requirements
    b. Performing parametric study of vehicle design attributes
4. Comparing all vehicle configurations in tradespace matrix
    a. Defining measures of effectiveness (MOEs) and scoring algorithm
    b. Assessing all mission architecture blocks in tradespace matrix

The reference missions, or mission profiles, used in this study were built upon missions studied in the past. Though it was desired to encompass a broad spectrum of possible planetary destinations, stay times and transfer durations, this spectrum was derived from missions in previously successful studies. Literature sources were also very useful in confidently making assumptions and ground rules as to trajectory choices, vehicle staging, and planetary escape and capture mechanisms. The choice of mission profiles, however, is inevitably up to the mission planner, with no real wrong or right manner in which to make the choices. Major considerations in designing the profiles were thus focused on designing missions that would be unbiased towards a particular vehicle, and to obtain a set of missions that would adequately represent a subset of realistic mission scenarios for the tradespace. It was essentially the design of the tradespace matrix and designation of appropriate MOEs that will, in the end, determine the utility of the final results.

The next step in the trade study methodology was to set up ephemeris tools to model the trajectories of the chosen mission profiles. The term ephemeris refers to a table of the predicted positions of astronomical bodies such as the planets or moon, and by extension, the predicted positions of artificial satellites.[10] The space vehicles modeled in this study can be seen as these 'artificial satellites,' thus determining their trajectories from Earth to the destination planets depended on complex calculations that took into consideration the orbits of planets at different dates in the future. Two ephemeris codes originally developed by NASA (IPREP and CHEBYTOP) were used in order to model these trajectories with ease. By passing the codes simple inputs based on the reference mission profiles, outputs were obtained that designated the propulsive requirements for the system architectures. Optimization of the transfer time, stay time, and departure date inputs was done so as to minimize these energy requirements.

Modeling the architectures of the space vehicles was the next phase of the study. The main vehicle models created were for NTR, NEP, and Hybrid architectures. These models were then further broken-down into multiple configurations that varied by fuel type for the NTR system and thruster type for the NEP and Hybrid systems. The models were generated with Excel spreadsheets that calculated requirements for power, thrust, propellant load, and vehicle component sizing. The main consideration in these models was to accurately generate mass estimates for each system component in order to calculate IMLEO based on the trajectory requirements input into the vehicle models. Some of the components, such as reactor mass and propellant varied by mission and vehicle type, but other components such as the Transhab had constant mass estimates.[11] Using these spreadsheet vehicle models alone, parametric plots were generated that characterized the performance of each power and propulsion system architecture.

The final phase of the trade study was actually assessing each of the vehicle architectures for each of the mission scenarios. The tradespace matrix, which is seen in Figure 1-1 was defined from the very beginning of the study. It was only after building the vehicle models and assessing vehicle performance for the given mission scenarios, that vehicle attributes could be defined. These vehicle attributes then become the parameters used to assess the MOEs that were established for all of the missions. Finally, the MOEs were rolled up into a single score for each mission architecture so that the architectures could be ranked in the tradespace matrix. This ranking procedure was then used to come up with a final 'best answer' for three distinct categories: each of the 12 mission profiles, each of the three planetary destinations, and for one overall interplanetary mission.

	MARS				Jupiter				Saturn			
	Conjunc.		*Oppos.*		*Conjunc.*		*Oppos.*		*Conjunc.*		*Oppos.*	
	Fast	Slow	Fast	Slow	Fast	Slow	Fast	Slow	Fast	Slow	Fast	Slow
NTR (Graphite Fuel; Thermal Reactor)												
NTR (Composite Fuel; Thermal Reactor)												
NTR (Carbide Fuel; Thermal Reactor)												
NTR (CERMET Fuel; Fast Reactor)												
BNTR (CERMET Fuel; Fast Reactor)												
HYBRID (CERMET; Fast; MPD Thruster)												
HYBRID (CERMET; Fast; Ion Thruster)												
HYBRID (CERMET; Fast;Hall Thruster)												
NEP (MPD Thruster)												
NEP (Ion Thruster)												
NEP (Hall Thruster)												

Figure 1-1. Tradespace Matrix

CHAPTER 2
MISSION PLANNING

Astrodynamics

Essential to a successful mission analysis study is the understanding of astrodynamics fundamentals and how a few specific parameters determine stringent mission requirements. The definition of astrodynamics in the context of this project is the study of the motion of rockets, missiles, and space vehicles, as determined from Newton's laws of motion and universal gravitation. More specifically, it can be seen that astrodynamics deals with the trajectories spacecrafts will assume on interplanetary transfers. The most basic parameters that stream down from astrodynamics calculations will, for example, define the best time for a spacecraft to leave Earth to travel to another destination and how much energy the vehicle will need in order to get there. Due to the highly important yet complex nature of this field of study, a brief overview of astrodynamics topics is discussed herein that will introduce basic terminology and concepts that were integral in the early steps of the mission analysis process.

Orbital Motion

Understanding the transfer methods for interplanetary travel assumes an understanding of orbiting objects. Orbital motion can be described by a family of curves called "conic sections" which represent the only paths possible for the orbit of one body about another. The three types of conic sections include open, closed, and a borderline case. Open conics are those in which the orbiting body repeats its path, and they only consist of circles and ellipses. The orbits of planets around the sun, and satellites around the Earth are all elliptical, with one real and one imaginary focus. The circular orbit is a special case of the elliptical orbit in which the distance from the orbiting body is constant, and the two foci overlap to create one central point of focus. Using the energy equation for all conics found by Equation 2-1, where v refers to the orbital velocity, r to

the distance from the orbiting body, μ to the gravitation parameter (GM), and a to the semi-major axis, the velocity of both an elliptical and circular orbit may be found.

$$\xi = \frac{v^2}{2} - \frac{\mu}{r} = -\frac{\mu}{2a} \tag{2-1}$$

For a circular orbit with radius always equal to a, the velocity is found by Equation 2-2.

$$v_{circ} = \sqrt{\frac{\mu}{r_{circ}}}^{12} \tag{2-2}$$

The borderline case between open and closed conic sections is for a parabolic orbit. Parabolic orbits are rare in nature and an object traveling on one would continue traveling to infinity until eventually coming to rest when all of its kinetic energy was exhausted. The orbital speed required to do just this, overcoming the gravitational field of the orbiting body, is called the 'escape speed'. From the energy equation for a conic section, and the statement that the energy will be equal to zero at a distance of infinity, the escape velocity is given by Equation 2-3.

$$v_{esc} = \sqrt{\frac{2\mu}{r}} \tag{2-3}$$

This equation reveals that the required velocity to escape a planet will be less the farther the spacecraft is from the planet that it rotates. This is representative of why spacecraft designed to leave Earth's atmosphere will first be launched to LEO to be assembled, and then escape the Earth with a much lower velocity requirement.[12]

It is actually the hyperbolic orbit, categorized as an open conic section, which a spacecraft would use to escape from Earth. This orbit differs from the closed orbits because the traveling body does not retrace its path, and from the parabolic orbit because it will have some speed left

over after traveling an infinite distance. A hyperbolic trajectory will only be achieved with a spacecraft that leaves its orbit at a velocity greater than the escape speed. This will result in some residual velocity left over when the spacecraft reaches infinity. This residual speed is referred to as the 'hyperbolic excess speed,' and is found by Equation 2-4, where v_∞ is the hyperbolic excess speed, v_{bo} is the burnout speed, and r_{bo} is the orbiting radius at burnout. This equation was again found via the energy equation for conic sections, where the energy is constant between the end of the burnout and when the spacecraft reaches an infinite distance.[12]

$$v_\infty^2 = v_{bo}^2 - \frac{2\mu}{r_{bo}} \tag{2-4}$$

In the context of interplanetary transfers from Earth, the reaching of infinity is assumed to be the same as reaching the end of the Earth's 'sphere of influence.' Although a body never completely escapes the gravitational field of the Earth, it can be assumed to be nearly zero at some distance from the surface. The sphere of influence (SOI) is said to end when the gravitational influence on the spacecraft is larger due to the sun than the Earth or other orbiting planet. For the Earth, this distance has been approximated as 145 times the radius of the Earth. With respect to the solar system this distance is negligible, but with respect to the Earth it is very distant. It is in fact so distant, that the velocity at the edge of the sphere of influence is assumed mathematically to be the velocity at infinity.[12,13]

Patched Conic Method

A method called the 'patched conic method' combines elements of elliptical, circular, and hyperbolic orbits to describe the orbital motion a spacecraft assumes in order to complete an interplanetary transfer. This method allows one to ignore the influence of the sun while the spacecraft is within the Earth's SOI, to switch to a heliocentric (sun-centered) frame outside of

the SOI, and then to reverse this process upon arrival at the destination planet. The first step in the trajectory design will be to determine the heliocentric transfer orbit.

An ideal minimum energy transfer to the destination planet would be a simple ellipse, commonly termed a 'Hohmann transfer.' This heliocentric transfer assumes that the departure and arrival planets are in circular orbits around the sun with velocity increments tangent to the planetary orbits, and that the velocity changes occur instantaneously. These high thrust velocity changes are commonly referred to as "delta-Vs," and constitute the relative velocities between the respective circular planetary velocities and the perigee and apogee velocity which define the transfer ellipse.[14] For example, the Earth departure delta-V would be the difference between the Earth's velocity relative to the sun, and the spacecraft's velocity relative to the sun as it exits the SOI. The delta-V increments necessary to transfer from the departure planet (perigee) to the arrival planet (apogee) for a Hohmann transfer are given by Equation 2-5 and Equation 2-6, where Δv_p is the velocity increment at perigee of the departure planet, Δv_a is the velocity increment at apogee of the arrival planet, r_1 is the periapsis distance of the Hohmann transfer, and r_2 is the apoapsis distance of the Hohmann transfer.[15] Note that for an interplanetary transfer the large center circle in the picture would represent the sun, and the planets would be represented by the point masses at the outer edges of the blue and red arrows.

$$\Delta v_p = \sqrt{\frac{\mu}{r_1}}\left(\sqrt{\frac{2r_2}{r_1 + r_2}} - 1\right) \tag{2-5}$$

$$\Delta v_a = \sqrt{\frac{\mu}{r_2}}\left(1 - \sqrt{\frac{2r_1}{r_1 + r_2}}\right) \tag{2-6}$$

It is estimated that using a Hohmann transfer for an interplanetary voyage to Mars would take approximately 260 days and would require an outgoing delta-V of 2.98 (km/s) for an

instantaneous thrust acceleration.[13] Although the Hohmann transfer is ideal due to its minimum energy solution, it is not always the most practical transfer method. For instance, once a spacecraft reached Mars after such a transfer, it would have to linger for nearly 6 months before it could return to Earth by means of another Hohmann transfer. Thus less optimal transfers are usually taken despite the corresponding higher energy and delta-V requirements.

The delta-V of all heliocentric transfers will be determined based upon the departure date and the travel time. The future date of departure allows for the determination of the relative positions of the launch planet and the target planet at time of launch. The time of transfer will then determine where the destination planet will be in its orbit when the spacecraft gets there. The path that the spacecraft must follow to successfully intercept the destination planet will determine the energy of the orbit and the delta-V at both departure and arrival. This delta-V will always be the difference between the planetary orbit around the sun and the heliocentric spacecraft speed given by Equation 2-7, where r_p is the radius of the planet's orbit, and ξ_t is the specific mechanical energy of the transfer.

$$v_{v,helio} = \sqrt{2(\frac{\mu}{r_p} + \xi_t)} \tag{2-7}$$

Optimal departure dates based upon the transfer time and stay time at the planet can be determined based on ephemeris data that tracks a planets' synodic periods. This is the time it takes to reappear at the same point in the sky as observed from Earth and relative to the Sun. For instance, the synodic period for Mars is 2.135 years, thus the best launch opportunities that would have minimum delta-V requirements would occur approximately every 780 days.[12,13]

Once the heliocentric delta-V is known, the patched-conic method continues with the determination of the velocities relative to the planets at departure and arrival. The major

assumption that is made at this point is that the heliocentric delta-V is equal to the speed of the spacecraft relative to the planet at the SOI. Using the previously introduced term in the hyperbolic excess speed equation (2-4), the hyperbolic excess speed is obtained by Equation 2-8, where $\Delta v_{heliocentric}$ is the heliocentric transfer delta-V, $v_{v,helio}$ is the velocity of the spacecraft vehicle at escape or capture into the planet, and $v_{p,helio}$ is the velocity of the planet around the sun.

$$v_\infty = \Delta v_{heliocentric} = v_{v,helio} - v_{p,helio} \tag{2-8}$$

Since the hyperbolic escape velocity v_∞ can now be determined, equation (2-4) can be rewritten as Equation 2-9 to determine the speed after injection burn, given the altitude at which the burn takes place. This speed is essentially the perigee burn on the Earth escape hyperbola.

$$v_\infty = \sqrt{v_{bo}^2 - \frac{2\mu}{r_{bo}}} \tag{2-9}$$

Since the elliptical or circular orbital velocity before the burn can be determined given the burn altitude, the actual delta-V experienced by the spacecraft will be that given by Equation 2-10, where $v_{bo,planet}$ was the speed after burn and $v_{orb,planet}$ was the orbiting speed before burn, both relative to the planetary frame of reference.

$$\Delta v_{planet} = v_{bo,planet} - v_{orb,planet} \tag{2-10}$$

It is important to note that although the delta-Vs calculated in the planetary and heliocentric reference frames may be similar, they cannot be assumed equal as significant values may result depending on the specific transfer being used. The delta-V in the planetary reference is that which will be used to assess the amount of propellant needed onboard the spacecraft,

where the thrust maneuver is assumed to occur instantaneously at the burn altitude.[13] A diagram depicting the parameters introduced for the escape hyperbola relative to the Earth can be found in Figure 2-1.

The main difference that will result between the hyperbolic escape from Earth and the subsequent planetary capture, is that the transfer orbit was assumed tangent to the Earth's orbit at departure, but the capture orbit will most likely cross the target orbit at some angle. This angle will be taken into consideration along with the target planet's speed and the spacecraft heliocentric speed to determine the speed at the target's SOI. The speed at the periapsis radius from the target planet will then be calculated based on conservation of angular momentum. Special attention must also be paid to the minimum distance from the orbital plane in which the spacecraft can enter the planet's atmosphere, as entering below this distance will result in collision with the target planet.[12]

Although the delta-V requirements are essentially derived from pre-determined physical laws of nature involving the orbits of planets around the Sun, to a space mission planner they define the 'cost' of the mission. Once the delta-V values are determined from calculations given departure date and transfer time details for a specific mission, these values can then be used to calculate how much propellant would be required given a specific type of propulsion system. The 'rocket equation' is used to perform this calculation, enabling one to determine not only propellant requirements, but essentially the entire spacecraft mass at the launch altitude. In the space business, mass means money, thus the connection can be made between delta-V requirements that stem from orbital mechanics and final monetary cost of any space mission.[14] More specifics related to calculating propellant and system mass based on delta-V requirements

will be found in Chapter 3, which discusses the actual sizing of the spacecraft systems under consideration in this trade study.

Mission Profiles

The difficulty in defining a mission profile is obtaining the seemingly best overall approach given the many variables that play into mission design. Mission characterization involves defining a mission concept which will describe how the mission will work in practice, the mission operations which will detail how people will operate and control the mission, and the mission architecture which links the mission concept to the major mission components.[16] This study was focused on developing mission concepts and mission architectures such that the various power and propulsion systems being analyzed could be compared under different mission scenarios. Mission operations was not a major focus in this study since the trade was essentially made on the capabilities of the power and propulsion architectures to transport humans, and was not concerned with human activities during the transfer periods.

The mission concept was essentially broken down into different mission profiles, each of which characterized the specific parameters of departure date, destination planet, outbound and return transfer times, and planet stay times (or class). The use of planetary swing-bys, and the re-entry method at Earth are two other considerations that typically go into a mission concept but they were not characterized in the mission profiles since all profiles used the same methods in this regards.

The term 'mission architecture' was used in this study to refer to one of the three vehicle architectures (NTR, NEP, and Hybrid) being coupled to a specific mission profile. The motivation behind generating a large number of mission architectures is to obtain a better understanding of the performance of each vehicle under different scenarios. Since it would be inefficient to attempt to model every type of scenario for every vehicle architecture, the mission

profiles were configured in such a way that most of the subset of possible desirable missions would fall into one of the mission categories. This was achieved by setting upper and lower limits on quantifiable mission profile parameters, and then collectively optimizing these parameters for each mission architecture.

The main driver behind assessing vehicle architectures given different mission profiles was to see if one system was decisively superior to the rest for all profiles examined, or if instead different systems were the optimal choice for specific mission profiles. These results would be significant as they would highlight the importance of either focusing development efforts on one vehicle architecture for all possible future manned missions, or focusing first on the mission profile decision and then following with the appropriate vehicle design.

Considerations for Mission Planning

Mission trajectory

The trajectory chosen for each mission profile is dependent on parameters that determine the launch window. These include the departure date, outbound and return transfer times and the stay time on the planet. The latter parameter takes on a significant role in trajectory analysis, often being divided into the two categories of "short-stay" opposition-class trajectories, or "long-stay" conjunction class trajectories.

The opposition-class mission is generally characterized by short stay times on the order of 40-60 days, and round-trip Mars missions that range from 365-660 days. Most opposition-class Mars missions take advantage of a Venus swingby on the return trajectory to Earth, though discussion of this maneuver is briefly withheld. Other characteristics of this type of trajectory include large propulsive energy requirements and the combination of both a short and a long transit leg. Clear disadvantages to this method that have been noted include high variances in

energy requirements given departure date, and large spikes in escape and capture delta-V's due to decreased transit time.[2]

The conjunction-class mission typically has stay-times between 400 and 600 days, and total Mars mission trip times on the order of 900 days. These trips may be the more highly desired of the two trajectory classes, since the stay time on the planet is much longer without a significantly longer transfer time. In fact, relatively short transfer times on the order of 200 days have been examined in previous studies for these mission trajectories. In addition, compared to the high energy requirements of the opposition-class missions, the conjunction class missions typically represent "minimum –energy solutions" for given launch opportunities.[2]

The use of a Venus swingby periapsis burn has been incorporated into methodologies for opposition-class Mars missions, as mentioned previously. This swingby maneuver provides a change in the spacecraft's heliocentric energy, which diminishes the delta-V requirement to enter back into Earth's atmosphere. The maneuver typically requires a very small propulsive burst, but will result in an overall reduction in propellant requirements. Past studies of this trajectory type for Mars missions have indicated that adding a small propulsive maneuver during the swingby increases "mission flexibility," and that a transfer at the periapsis of the Venus orbit is "close to the optimum transfer point." Note that the periapsis burn can be in either the direct or retrograde directions, such that the relative velocity may increase or decrease, respectively.[17]

Mission approach

Two approaches are also recognized for mission design: an all-up mission and a split mission. All-up missions are those in which cargo and crew leave the orbit of the Earth at the same time. In a split-mission design, cargo is flown to the destination planet first, and then is followed by the crewed vehicle. One benefit of this design is that the cargo can be sent on a low-energy trajectory to the destination planet and assure that supplies will be there to greet the crew

when they arrive. In addition, this method will reduce the payload of the crewed vehicle, which already requires more energy due to the need to be sent on a faster trajectory to reduce time in the radiation-filled vacuum of space. On-orbit assembly is a possibility for either approach, and allows for different vehicle components to be launched into LEO on separate heavy lift launch vehicles (HLLV). The assembly could utilize automated rendezvous and dock between subcomponents, or the use of a space station or other docking facility.[2]

The capture methods at both the destination planet and following return to Earth are also a consideration in the mission approach. Both propulsive capture and aerocapture methods have been used in past studies for capture into the destination planet or moon. Propulsive capture imposes a delta-V requirement on the propulsion system, thus necessitating a propellant requirement for the propulsive burn. The aerocapture method instead uses the planet's atmosphere to slow down the vehicle. This flight maneuver uses the friction from the dense atmosphere of the destination planet or moon to slow down the spacecraft, thereby transferring the energy from the high spacecraft speed into heat. This method thus saves on propellant load, yet requires advanced heat shielding to protect the craft.[7] An orbit elevator has also been proposed as a method by which the spacecraft can move in order to reach various orbits once it is already in its destination orbit, without the use of a propulsion system.[6]

Propulsive capture or direct Earth re-entry are the two methods suggested for return to Earth. The propulsive capture, as its name suggests, uses a propulsive burn to capture into an orbit around Earth. The other method, direct Earth re-entry, assumes that the spacecraft skims the desired Earth orbit, without actually capturing into it through any propulsive means. The Earth Crew Return Vehicle (ECRV) would then be released from the spacecraft allowing the crew to descend back to Earth 'Apollo-style', with the remaining spacecraft hardware being

released into space.[18] One of the considerations then in choosing between the methods is whether or not the interplanetary spacecraft should be expendable.

Mission Profile Selection

A primary objective in the selection of specific mission profiles for this study was to choose missions that represent, as much as possible, the entire subset of interplanetary missions that may be desirable in the future. This was accomplished by incorporating different planetary destinations, using the same transfer and capture methodologies for all missions, and by allocating adequate ranges for the mission profile parameters. Through optimization of all mission profile quantifiable parameters, singular data points were generated for each profile, including an exact date of departure, number of outbound and return transfer days, and specific number of stay-time days on the planet. Thus, although seemingly specific missions will be run for the vehicle architectures, each mission will represent a larger subset of possible missions and will reveal the best performance data for each transportation system.

The decisions that were made in the mission design process were influenced by two major sources. The first very influential source was that of the set of literature found on past interplanetary studies. Differences between methodologies arose, such as assuming delta-V values for a mission versus using ephemeris codes to solve for them based on a specified launch window. These literature sources also contained information on NASA DRMs that was particularly useful in the mission planning process since they provided a comprehensive outline of various mission concepts.

The second source that drove mission profile design was that of the ephemeris tools themselves. Since a low-thrust and high-thrust ephemeris tool were both being used, and each tool had some unique capabilities and disabilities, constraints were set from the very beginning on possible mission platforms. For example, either the propulsive capture or direct Earth re-

entry methods could be designated for the high-thrust ephemeris tool, yet the low-thrust tool assumes a capture into Earth orbit, thus only the propulsive capture option could be used if commonality between mission profiles was to be maintained.

Mission trajectory

In order to increase the breadth of the mission profiles, and thereby increase the applicability of this study to future research interests, three planetary destinations were attempted, each with two different stay times and two transfer times. Many advanced propulsion mission studies have been done using Mars as the planetary destination. In terms of present-day space policy and thought, this is directly in-line with the 'Moon, Mars, and Beyond' initiative proposed by George W. Bush in 2002. But there have also been various studies on mission analysis for farther-out missions with destinations including Jupiter's moon Callisto, Pluto's moon Charon, and objects in the Kuiper Belt.[18,19]

For this study, it was decided that Mars would be a logical choice for a planetary destination, and that Jupiter and Saturn would also be investigated in order to test the vehicle architectures against higher-energy requirements. The spacecraft orbit around Mars was a 250 (km) by 33793 (km) elliptical orbit, which is comparable to 1 solar day, and was taken from Borowski's Mars mission study ground rules and assumptions list.[18] The orbits around Jupiter and Saturn will include some basic assumptions. The spacecraft itself will be assumed to be orbiting Jupiter's moon Ganymede, and Saturn's moon Titan, as the spacecraft would not easily find a safe orbit around the planet itself. However, the ephemeris tool input will include the planet as the destination orbiting body and the orbiting distance will be that of the distance from the planet to the orbiting moon. This amounts to the spacecraft seemingly taking on the orbit of the moon around the planet, although it will actually be in a low orbit around the moon, with the spacecraft and moon both being in orbit around the planet. Although some studies model the

three orbit insertion components (propulsive capture at radius of planet's moon, plane change into moon's orbit, and propulsive capture into circular orbit around moon), the results of this study are only able to account for the first component, and assume the other two components negligible.[19] The orbits that will be used in this study include a circular orbit at 998600 (km) from Jupiter, and a 1162000 (km) orbit around Saturn, which again are synonymous with the orbit of the selected moons around their respective planets.

Since both short and long stay times may be desired for future interplanetary missions depending on the operational nature of the mission, both conjunction and opposition-class missions were used for the mission profiles. A range was applied to the stay time so that an optimization of the stay time could be found as part of the overall effort to find the minimum delta-V requirements for each mission. It was decided that the opposition-class missions would have a stay time range of 40-60 days, and conjunction-class missions would have a range of 400-600 days, as these values are considered standard among mission analysis literature sources.[5,12] Note once again that a singular data point will be found for the stay time after optimization, despite the fact that the real CTV would actually be designed with sufficient propellant for a somewhat longer/shorter stay to account for a safety margin.

Although high and low energy missions are already broken down as opposition and conjunction-class in the mission profiles, it was decided that short and long transfer times should also be included due to their own effect on energy requirements and safety concerns. Four of the central issues for mission profile selection are said to be crew radiation exposure, crew time spent in zero g, the component of mission risk that increases with mission duration, and added cost of shortening trip time.[20] Each of the first three of these components condones shortening transfer times, though the last highlights the great expense, both in fuel and in dollars, of shorter

missions. It thus seems reasonable to want to analyze transfer times on both the low and high ends of the spectrum.

Having two data-points for transfer time is also practical from an energy consideration perspective. For instance, since a decrease in transfer time is generally associated with an increase in delta-V requirement, the optimized point could likely be that of the longest transfer time. If this transfer time is longer than that considered acceptable by future mission planners, the dataset for this particular DRM may be deemed useless. It was thus found both fruitful and necessary to include both short and long transfer categories in the breakdown of design reference missions.

The transfer time ranges that were determined for this study's mission profiles were decided by using past studies to determine typical transfer times and by trying to make simplifying assumptions. The first assumption that this study made was to assume that the outbound and return transfer times were equal. This was done to minimize time spent on mission optimization using the ephemeris tools. Secondly, since the transfer times were to be broken down into two groups, it was decided that the Mars transfer ranges would be 100-200 days for the short transfer range, and 200-300 days for the long transfer range, allowing for an even split of 100 days for each. In a study that compared 21 different crew and cargo mission studies, it was found that outbound transfer times ranged from 80 days to 335 days, with return transfers being the same or somewhat quicker.[2] It was thus felt adequate that the profiles covered the 100-300 day transfer range, which equates to nearly 80% of the range covered by numerous other studies.

In regards to the Jupiter mission, Ehricke has been cited as using a 640-day transfer for a Europa mission, but many sources show a more practical 1000-day transfer to another of

Jupiter's moons, Callisto.[9,19] Using the 1000-day transfer as a mid-point, the short transfer range was decided to be 800-1000 days, while the long transfer range would be 1000-1200 days. These categories are applied to both the Jupiter and Saturn mission as no sources were found for crewed mission profiles to Saturn. In addition, research that was done previous to this study showed similar trends for delta-V vs. trip time for Jupiter and Saturn destinations.

Mission approach

The current study serves to assess multiple vehicle architectures under a spectrum of mission profiles for the crewed vehicle component of a split-mission architecture. It is assumed that an unmanned cargo vehicle departs Earth orbit on a minimum energy, one-way trip to the destination planet, carrying science payloads and any other payloads that would be necessary for planetary exploration, but not necessary for the outbound and return trips on the CTV. Proposed additional functions of the pre-deployed cargo vehicle noted in the literature include deploying an unmanned semiautonomous rover to explore the landing site region prior to crew arrival, and deploying navigation beacons to assist in landing the primary cargo payload.[21] Beyond these general assumptions about the cargo vehicle, no aspects of it are modeled or considered in this mission analysis study.

The mission concept used herein assumed that the hardware components of the crewed vehicle were assembled in LEO prior to departure. The components would first have to be launched from Earth on HLLVs, and then assembled by means of an automated rendezvous and dock between elements, or a more complex method involving the space station or other construction facility.[2] After assembly, the crew would be transferred from the International Space Station (ISS) or a similar post to the CTV. Thus missions assessed in this study began from an operational sense at the point were the assembled CTV was ready to leave LEO. In

staying consistent with orbital parameters found in Borowski's studies, the actual LEO altitude the vehicle was assumed to be in was a circular Earth orbit of 407 (km).[18]

Certain aspects of the mission concept that were kept constant for all mission profiles included major CTV components, and planetary and Earth capture methods. It was determined that the CTV would only carry the mass needed for a full two-way trip to and from the destination planet. Although this did require carrying both outbound and return propellant from LEO, the propellant tanks could be dropped upon completion of major burn segments. The propulsive capture method was used for all captures, both at the destination and upon return to Earth to accommodate the capabilities of the ephemeris tools and still maintain the means for an 'apples-to-apples' comparison between architectures. The Earth orbit insertion maneuver occurred at the perigee of a 500 (km) by 71165 (km) orbit, again in accordance with Borowski's standard ground rules. The mission analysis did not consider anything past this point in the mission, though it may be assumed that the crew would depart the ship at this point and perform a r-eentry into Earth's atmosphere in the ECRV capsule.[19]

Mission profile summary

To provide a condensed account of the mission profile assumptions to be used for the reference missions analyzed in this study, a list of the basic mission trajectory and mission approach ground rules is given below.

- Delta-V requirements for each mission were determined through an optimization methodology using high-thrust and low-thrust ephemeris tools
- Outbound and inbound transfer durations were assumed equalMars departure dates ranged between 2030-2035; Jupiter and Saturn dates ranged from 2040-2045
- The following orbits were used for Mars, Jupiter, and Saturn:
- 250 (km) by 33793 (km) elliptical orbit at Mars
- 998600 (km) circular orbit at Jupiter (assume orbiting moon Ganymede)
- 1162000 (km) circular orbit at Saturn (assume orbiting Titan)

- A split-mission scenario was used for all missions; only CTV will be modeled
- Earth Orbit Rendezvous and Dock Vehicle Assembly at 407 (km) occurred after HLLVs transport spacecraft components to orbit
- All CTV propellant for round-trip mission was carried onboard vehicle
- Propellant tanks were dropped after completion of major burn segments
- Propulsive capture method used to capture CTV into planetary orbit
- Earth Orbit Insertion of CTV occurred at perihelion of 500 (km) by 71165 (km) orbit
- TransHab was sized for a crew of 6, with consumables accounting for the total duration of mission

The optimization of the trajectories using the ephemeris tools incorporated the transfer and stay time ranges discussed in the Mission trajectory section. These ranges and their associated design reference missions are given in Table 2-1. The first three categories of "Planet Destination," "Mission Class," and "Transfer Type," all characterize the 12 basic mission profiles. The outbound and return transfer duration and stay time are both given as a range in days, and provide the bounds for the transfer type and mission class, respectively.

Ephemeris Tools

In recognition of the high-thrust NTR architecture and low-thrust Hybrid and NEP architectures modeled in this study, the IPREP and CHEYBYTOP ephemeris tools were both needed in order to model the interplanetary transfers for the missions previously discussed.

IPREP (Interplanetary PREProcessor) is a rapid grid-search optimizer for launch and arrival windows, delta-V, and mass originally created by Martin Marietta Astronautics.[22] It is a commonly used tool for estimation of high-thrust trajectories, thus it was the logical choice to model the trajectories for the NTR architecture in this study. Inputs to the program generally include the order of the planets to be encountered, maneuvers to be performed at each encounter, and the time-of-flight window for each mission segment. IPREP then calculates the delta-V

energy requirements using a patched-conic technique that assumes the planets to be point-masses and finds the position and velocity of each planet from one of the ephemerides. A transfer orbit for each leg of the trajectory is then found by solving Lambert's problem.[23]

CHEBYTOP (Chebyshev Trajectory Optimization Program) is a program built in the late 1960's by the Boeing Company, which provides a two-body, sun-centered, low-thrust trajectory optimization and analysis. Its capabilities extend to preliminary mission feasibility studies such as the one undertaken. Its strengths include requiring a small number of simple inputs and having fast run times for quick interplanetary mission modeling. CHEBYTOP uses the CHEBYCHEV Optimization Method, which is a series of approximations to the control problem that breaks it down into a group of classical calculus optimizations.[24,25] The algorithms used are only relevant to spacecraft with very low thrust-to-weight (T/W) ratios, which makes it an ideal modeler for NEP systems. This code has been used in numerous studies done in the past on low-thrust trajectory systems such as solar electric propulsion (SEP) and NEP for Mars missions and for other planetary destinations. NASA Marshall Space Flight Center (MSFC), for example, used the code to generate thrust-to-weight (T/W) versus delta-V curves for an NEP mission to Pluto.[25] Besides its use for the NEP architecture in this study, it was also used for the Hybrid architecture due to its capability to model high-thrust NTR burns at escape and capture, with an NEP mid-trajectory low-thrust burn.

The transfer methodology used by each of the ephemeris models developed with these codes was slightly different depending on which propulsion system was being modeled. The IPREP code used to model the high-thrust NTR propulsion systems assumes one burn at Earth Escape, a second burn at Planetary Capture, a third burn at Planetary Escape, and finally a fourth

burn at Earth Capture. These burns can be thought of as instantaneous burns for modeling purposes, as is commonly done in traditional delta-V calculations for high-thrust orbit transfers.

The NEP system that was modeled with CHEBYTOP used a spiral trajectory out of Earth's orbit and a spiral capture into orbit at the destination planet. This is due to the fact that a low-thrust engine cannot achieve the necessary escape speeds in a very short amount of time as the NTR systems do. Note that the transfer time designated by the user in the IPREP input file did not account for the number of days needed to spiral out of or into a planetary orbit, but only accounted for the days on the interplanetary trajectories.

The Hybrid system, which was also modeled with CHEBYTOP, assumed an NTR burn to escape Earth's orbit, an NEP burn for the majority of the transfer duration, and an NTR burn to capture into the destination planet's orbit. This same method was then used in reverse to escape from the planet and return to Earth. Even though the Hybrid and NEP systems used the same ephemeris tool, they were indeed modeled in separate ways. Due to features inherent to both the CHEBYTOP and IPREP ephemeris codes and the manner in which the scripts were set up for the ephemeris models generated in this study, the delta-V requirements given by the output files took into account the different trajectory methods used by each vehicle.

Table 2-1. Design Reference Mission Categories

Planet Destination	Mission Class	Transfer Type	Out/Ret Tran. (days)	Stay Time (days)
Mars	Oppos.	Fast	100-200	40-60
		Slow	200-300	40-60
	Conjunc.	Fast	100-200	400-600
		Slow	200-300	400-600
Jupiter	Oppos.	Fast	800-1000	40-60
		Slow	1000-1200	40-60
	Conjunc.	Fast	800-1000	400-600
		Slow	1000-1200	400-600
Saturn	Oppos.	Fast	800-1000	40-60
		Slow	1000-1200	40-60
	Conjunc.	Fast	800-1000	400-600
		Slow	1000-1200	400-600

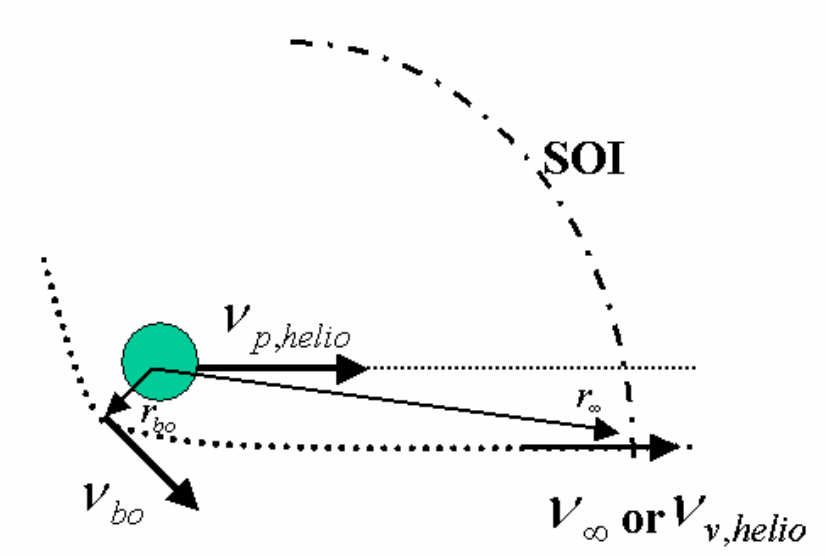

Figure 2-1. Escape Hyperbola

CHAPTER 3
MODEL DEVELOPMENT

Space Reactor Background

Reactor Configuration

All reactors rely on the principle of thermal energy production from the fission process of a fissionable atom such as ^{235}U. This energy production results from the conversion of the kinetic energy of fission fragments and neutrons to heat after slowing down from collisions and interactions with other atoms. This thermal energy is then transferred to a coolant that flows through the reactor core. Space reactors will typically use a lightweight gas such as hydrogen as both the coolant that extracts heat from the reactor, and in the case of a nuclear thermal rocket, the propellant that immediately thereafter is shot out of the rocket nozzle to create momentum.[26] Propellants with low molecular weights are most effective for thermal propulsion as they produce the highest specific impulse.[27] Space reactors that are specifically used for propulsion are known for having high specific impulse and high thrust levels, providing a clear advantage over alternatives such as chemical propulsion.

The actual configuration of a space NTR system is similar to that of a chemical system, except for the reactor heat source. The hardware consists of a reactor, propellant tank, radiation shielding, a feed system, and a nozzle. The major reactor components consist of the radial reflector, reactor pressure vessel, moderator, fuel-element assembly, and control drums. The reflector surrounds the outside of the core and functions to reflect neutrons produced in the chain reaction back into the core, helping to maintain a controlled chain reaction. The pressure vessel is needed in order to maintain reactor pressure and must be made of an aluminum or composite material that will withstand the high radiation, heat flux, and pressures from the reactor. A moderator material is used in a thermal reactor to slow the neutrons produced from a nuclear-

fission reaction to energies in which they are more apt to undergo another fission. The fuel-element assembly contains the actual heat-producing uranium fuel, along with the flow channels for the coolant. Control rods are also found in the core and serve to absorb neutrons to decrease neutron population and maintain the ability to control the reaction rate or even shut down the reactor.[26]

Reactor Fission Spectrum

A major choice in overall reactor configuration concerns the type of fission spectrum it will operate under. It may operate using fast neutrons produced by fission reactions (a fast reactor), or neutrons slowed to thermal energies and thus more likely to produce subsequent fission reactions (a thermal reactor). A fast reactor functions based on a chain of reactions propagated by high-energy fission neutrons. The low probability of fast neutrons producing fission reactions results in a large fuel requirement for this type of reactor. However, highly concentrated fuel will allow a compact reactor, typically of smaller size and mass compared to a thermal reactor. The probability of neutron capture and consequent fission is much higher for thermal energy neutrons that have been slowed by interaction with moderator materials than for fast neutrons. Although thermal reactors are typically larger than fast reactors, they require much less reactor fuel than fast reactors and also a less complicated fuel element and core design.[28]

The reason that both fast and thermal reactors have been considered for space reactors is that they are inherently better equipped for different types of missions. The fast reactors are preferred for long-life, low power operations since the high fissile loading allows high total energy operation. Missions that require large bursts of power but small total lifetime energy may benefit more from a thermal reactor. The relatively long neutron lifetime and large delayed neutron fraction found in thermal reactors would help maintain precise control of burst power.[27]

Nuclear Thermal Power and Propulsion

History of Nuclear Thermal Rocket (NTR) Systems

This history of the NTR engine began in 1953 when the ROVER program began at Los Alamos Scientific Laboratory in order to develop a reactor for the operation of a nuclear rocket. The major reactor series that went through design, build, and test phases during this program included KIWI, Phoebus, Peewee-1, and Nuclear Furnace-1.[28]

The KIWI reactor series holds the accolade of being the first NTR reactor built and tested. It allowed for advances to be made in the areas of instrumentation and control, fuel element design and fabrication, structural design, and testing techniques. The Phoebus reactors that followed had design specifications intended to meet the need of interplanetary propulsion systems, with special focus on manned missions to Mars. The major results from research on this reactor series included control of rocket parameters over a wide range of operating conditions, along with finding that large nozzles for NTR applications was feasible. The Peewee reactor series came next chronologically, and was meant to investigate performance characteristics of a smaller reactor. This was followed by the last stage of ROVER, the Nuclear Furnace series, which was designed to test advanced fuel elements containing composite fuel.[28]

The end of the research-focused ROVER program led to the start of the Nuclear Engine for Rocket Vehicle Applications (NERVA) program, which focused more heavily on concept development. During this 11-year program, the NRX reactor series was developed, incorporating the non-nuclear system components (propulsive components) into the reactor designs developed during ROVER. The NRX-XE' engine was the main focus as vertical downward firing tests of the engine in a simulated space vacuum were conducted. This allowed for investigation of the engine start-up and shutdown characteristics, along with the resulting engine performance parameters. Over the course of this program, more than 20 NTR reactors

were built and tested at the Nuclear Rocket Development Station at Nevada's Nuclear Test Site. Although the NERVA program was canceled in January of 1973 due to a change in national priorities, the most poignant outcome of the work done during ROVER/NERVA was the confidence that an NTR engine could be developed to meet the objectives of structural integrity, restart capability, predictability, control, and reliability.[28]

Fundamental Research

Two of the primary areas of current research for NTR systems are reactor fuels and reactor operational capabilities. Research of space reactor fuels is of high importance due to the fact that the reactor is heating a coolant for propulsive purposes. Increasing the operating temperature of a space reactor fuel thus has implications for overall propulsive performance. Reactor operations are also being analyzed in terms of providing dual-mode functions instead of a single mode, the implications of which may have profound effects on overall spacecraft capabilities. Improvements in the area of fuels research have been consistent since the ROVER years, while dual-mode bimodal reactor configurations have only been studied in recent years. It is important to note that for both areas of research, however, no full-scale hardware testing has been undertaken for nearly 35 years.

The four main types of reactor fuels that have undergone serious consideration for space application include graphite, composite, and carbide fuels for thermal reactors, and fast reactor CERMET fuel. Graphite fuel is the oldest and most mature, as it was studied and used during the ROVER/NERVA programs. The original ROVER engine had rods 54 inches in length, with a mixture of uranium, zirconium, and carbide in a graphite matrix.[29]

Both the composite and carbide fuels were developed based upon experience gained with graphite fuels, yet they only underwent minimal testing near the end of the ROVER/NERVA era. The composite fuel composition differed from the graphite fuel in that it was a 'composite' of the

UC_2 and ZrC used to make up the fuel pellet and coat in the early generation coated-particle matrix graphite form. It was found that the ZrC coating increased both the lifetime and the integrity of the fuel as it protected the fuel from the hot hydrogen propellant. Carbide fuels, on the other hand, eliminated the protective carbide coating required for matrix fuels. Improvements were made with carbide fuels since it was found that the composite fuel coating severely limited the endurance and temperature performance of the fuels.

Since the termination of the ROVER/NERVA programs, many advances in fuels research have been made. Some stem from improvements in other related areas such as materials research, and include an increase in hydrogen turbopump efficiency, improvements in titanium pressure vessel manufacturing techniques, and improvements in nozzle cooling. The term applied to updated NERVA NTR engines that use these latest fuel technologies available is NERVA Derivative Reactors (NDR). NDRs typically have carbon-based matrix fuel elements with graphite moderator and ZrH moderator sleeves in the support structure. Typical chamber temperatures for NDR graphite, composite, and carbide fuels are 2500, 2700, and 3100 (K) respectively, while ISP values are 885, 921, and 1020 (s) respectively.[28]

Bimodal reactor designs, which have been under development only more recently, have consistently been designed based on the use of CERMET fuel. This is primarily a result of both CERMET fuels and bimodal designs being based upon fast fission reactors. CERMET fuel is termed according to its ceramic metallic formulation, and is primarily configured of UO_2 fuel encased in tungsten and tungsten-rhenium alloys.[30] Properties of CERMET fuel include high strength, thermal conductivity, temperature capability and burnup, in addition to giving reactors a long operating life and the ability to restart. It is important to note that use of CERMET fuel and fission reactors is not limited to bimodal reactor configurations.

Bimodal reactors, named appropriately for their two modes of operation, have been kept behind their unimodal counterparts due to the significant costs associated with their testing and production. Their discussion, however, reaches back to the ROVER/NERVA program, during which the potential benefits of such reactors were recognized. The basic reactor design used for that program was assessed for possible modifications that would allow electric power generation. In more recent years, the Air Force Phillips Laboratory has conducted studies on bimodal reactor designs for possible military applications. The DOE Office of Nuclear Energy has since collaborated with the Phillips Laboratory in order to develop bimodal bus designs along with initial performance requirements.[30]

Bimodal reactors have increased complexity in both design and function due to their dual-mode operation. During the power and propulsion modes, the reactor must operate under very different sets of conditions and must perform extremely different functions. In addition to these capabilities, a space reactor is expected to have both high reliability and a long lifetime. The engine must function in cooperation with more hardware than a unimodal engine, given that a power conversion unit and heat radiator are required to produce electric power and get rid of waste heat. While the amount of electric power generated is the important performance parameter in power mode, the thrust-force and specific impulse are the driving parameters in the propulsion mode.

In a typical bimodal reactor design, the core will consist of heat pipes and CERMET fuel with numerous propellant channels. In the propulsion mode, liquid hydrogen may be run through reactor components for cooling purposes, and will then run through the CERMET fuel element one time before expanding out the rocket nozzle. In the power mode, the heat pipes will serve as the energy transport medium from the reactor fuel to the power conversion system. A

small gap between the fuel elements and heat pipes serves to allow for thermal radiation between them, creating the primary energy transfer mechanism for the power mode. A working fluid such as sodium or xenon then runs through the heat pipe, transferring the energy to the power conversion unit.

A reactor design by the Phillips Laboratory uses 93% enriched CERMET fuel with finned heat pipes. The CERMET fuel elements are nine-sided blocks with 52 axial propellant channels. They are 59.5% UO_2 by volume and 40.5% tungsten. The heat pipes provide both energy transport and structural support, which relieves the need for tie-tubes. This reactor design was said to have a 10 (kW) electric power output capability with a 10-year lifetime, and produced 220 (N) of thrust with a specific impulse of 825 (s) for the propulsive mode.[30]

Development of the NTR Model

The NTR architecture, which utilizes a nuclear reactor for thermal propulsion, was one of the three main architectures studied in this project. This architecture was broken down into five systems that all achieve NTR propulsion through different selections of fuel and reactor types. The five NTR systems that were assessed in the tradespace matrix are found in Table 3-3, which categorizes each system according to reactor mode and energy spectrum along with fuel type.

Although the NTR systems were broken down according to characteristics of the space reactor, it is important to understand how the reactor functions within the entire spacecraft. The term ‘architecture’ itself was used in this study to describe not only the reactor, but also each of the subcomponents that makes up the entire CTV that will carry humans to an interplanetary destination. Thus it should be noted that the NTR architectures were all based upon the same basic principles and had almost identical vehicle schematics. The exception to this generality within the NTR architecture group was the one system operating with a bimodal reactor. While unimodal reactors’ main functionality was to provide heat to the hydrogen coolant that is

expelled through the rocket nozzle, the bimodal reactor had a secondary coolant loop that provided electric power to the spacecraft. Within the group of unimodal reactor systems, the only real differences were in the physical makeup and operation of the reactor itself.

The four unimodal reactor systems can all be described using the schematic found in Figure 3-1. The divisions of the entire CTV were broken-down into power, propulsion, and spacecraft categories. This schematic was intended to provide an overview of how the components within these groups interacted, along with a very rough idea of where they were physically located respectively within the space vehicle structure. The solid black lines depict flow of hydrogen propellant from the tanks all the way through its exit from the rocket nozzles. The dotted black lines depict transfer of electricity from the fuel cell power source to the components that require electricity for functionality. The power and propulsion system boxes in the schematic are specific to the NTR unimodal systems, and will thus be discussed in the following section. The general spacecraft components, indicated in yellow, will be discussed later in the text, as their modeling was not dependent on the type of propulsion and power system architecture.

The one NTR system that used a bimodal reactor had a significantly altered architecture schematic as shown in Figure 3-2. As can be seen in the schematic, fuel cells utilized in the unimodal systems are no longer used for onboard spacecraft power needs. In addition, power conversion units, power management and distribution (PMAD) systems, and radiators were all added to accommodate the reactor power generated by the bimodal reactor, and a secondary propellant was added for power conversion purposes. The solid black lines in the figure again indicate propellant flow, while the dashed lines indicate flow in the power distribution process.

Power

One of the ways in which an NTR reactor will differ from a purely NEP power reactor is that the required thermal power will be defined based on the desired temperature and mass flow of the propellant instead of the mission energy requirements. The derivation of this power can be found through both Equation 3-1 and Equation 3-2, where $\dot{m}_{prop\_NTR}$ is the rocket mass flow in (kg/s), T is the thrust in (N), v_{e_NTR} is the exit velocity of the propellant in (m/s), P_{s_prop} is the thermal power in (MWt) for the propulsive mode, and t_{H2} is the temperature in (K). It is interesting to note that the thrust value, which is needed to determine the power requirement, is a parameter that is chosen by the designer. In this study it was chosen to be 15 (klbf), which is on the lower end of typically considered thrust ranges. Thus it can be reasoned that the power is determined by both the designer and the properties of the fuel itself.

$$\dot{m}_{prop\_NTR} = T / v_{e\_NTR} \tag{3-1}$$

$$P_{s\_prop} = \dot{m}_{prop\_NTR} * (0.018061 * t_{H2} - 5.715417) \tag{3-2}$$

After the power required of each type of reactor fuel core for a thrust of 15 (klbf) was calculated, the actual mass of the NTR power and propulsion system had to be determined. The basic components consisted of the reactor, pressure vessel, internal and external radiation shield, and propulsive hardware. The propulsive hardware was further broken down into the three main components of the nozzle, turbopump assembly, and nonnuclear support hardware such as lines, valves, actuators, and instrumentation thrust structures. The data-points for these three propulsive hardware components were taken from an SAIC report for the 'SAIC ELES-NTR'

design. The mass estimates for the three components were 421 (kg), 104 (kg), and 1264 (kg) respectively, which gave a total of 1789 (kg) to be added to the reactor and shielding masses.[31]

The mass of the reactor and pressure vessel were estimated from SAIC plots, which gave mass as a function of power, pressure, and temperature. Linear interpolation tools were developed in order to be able to confidently generate mass estimates based on the characteristic parameters of each fuel. The fuel parameter values that were used for the estimation of the reactor mass included chamber temperature, ISP, and calculated power, all of which are seen in Table 3-2. Although the interpolators required the three inputs of temperature, pressure, and power, the ISP was also needed for the calculation because the mass flow parameter that defined the power requirement was dependent on ISP. Also, the pressure used for all cases was assumed constant at 1000 (psia).

Once the reactor masses had been calculated, the internal and external shield masses were calculated based on these values. It was decided to estimate the shielding masses by using ratios of shielding to reactor mass found from data-points in the literature. It was thus determined from data that characterized a 75 (klbf) Westinghouse/NERVA design, that the internal shielding was to be 26.96% of total reactor mass, and external shielding 80.27% of reactor mass.[28] Calculating the total NTR power and propulsion system mass was then accomplished using Equation 3-3, where f_{Int_shield} was set to 29.6% and f_{Ext_shield} was 80.3%.

$$m_{NTR} = m_{reactor} + m_{propul.} + m_{reactor} * (f_{Int\_shield} + f_{Ext\_shield}), \quad (3\text{-}3)$$

The reactor and shielding masses for each type of fuel, along with the total NTR system mass for each fuel is given in Table 3-3. Note that although only one reactor was used to carry out power and propulsion requirements, an extra reactor system equal in weight to the primary reactor was carried on board for redundancy.

A unimodal NTR architecture uses all of the heat generated from the reactor for heating of the rocket propellant. Any electric power needed by the spacecraft had to come from an alternate source. Due to proven performance on the Space Shuttle, fuel cells were chosen for electric power generation for the NTR unimodal system. Fuel cells are self-contained generators that operate continuously without the need for sunlight. They work by converting the chemical energy of an oxidation reaction to electricity. An added benefit of their use is that they actually produce water as a byproduct, which can the be used for drinking.[16] Two key parameters of fuel cells used in the calculation of their mass were the specific power of 275 (W/kg), and the lifetime estimate of 100 days. The equation used to calculate the mass of fuel cells based on electric power requirement and the mission duration is given by Equation 3-4, where P_e is the electric power in (kWe).

$$mass_{Fuel\_Cell} = (1/.275) * P_e * (mission\_days/100) \quad (3\text{-}4)$$

The bimodal reactor provided both the hydrogen propellant heating and electric power requirement for the spacecraft. Thus, although the actual mass of the bimodal reactor was on average higher than that of a unimodal reactor, no extra mass was assumed for power generation. There was, however, mass associated with the power conversion that is required to convert the reactor's thermal energy to electrical power. The three main components required to fulfill this function include the PMAD system, the Brayton Conversion Unit, and the radiator. The equations defining these component masses can be found by Equation 3-5, Equation 3-6, and Equation 3-7, respectively, where $P_{s,spacecraft}$ is the thermal power requirement needed to satisfy spacecraft electrical power needs in (kW), η_S is thermal to electric conversion efficiency, and $SpMass_{rad}$ is the specific mass of the radiator (kg/kW).

$$mass_{PMAD} = .635 * P_e \tag{3-5}$$

$$mass_{CBC} = 0.875 * P_e \tag{3-6}$$

$$mass_{rad} = ((P_{s,spacecraft})(1-\eta_S)) * SpMass_{rad} \tag{3-7}$$

These equations were derived from both literature data-points and textbook material.[16,32] Further details on these components and their derivations is given in the NEP propulsion section, which focuses more predominantly on the power conversion process.

Propulsion

The NTR propulsion equations were developed based on the principles of the "rocket equation," which take into account both delta-V requirements and the mass of the spacecraft. The ephemeris tool that was used to model the NTR architecture assumed that there was an escape burn at Earth and the destination planet, and also a capture burn at the respective planets. These four high-thrust burns typically last on the order of a few hours and are represented in the equations by four separate delta-V values. The four separate equations that were used to calculate the propellant mass at each of these burns are shown in Equation 3-8 through Equation 3-11, where the exit velocity is given by Equation 3-12, and the mass totals at the beginning of each of the four burn segments are given by Equation 3-12 through Equation 3-16.

$$m_{prop1NTR} = m_{TOT1} * (1 - e^{-\Delta v1 / v_{e\_NTR}}) \tag{3-8}$$

$$m_{prop2NTR} = m_{TOT2} * (1 - e^{-\Delta v2 / v_{e\_NTR}}) \tag{3-9}$$

$$m_{prop3NTR} = m_{TOT3} * (1 - e^{-\Delta v3 / v_{e\_NTR}}) \tag{3-10}$$

$$m_{prop4NTR} = m_{TOT4} * (1 - e^{-\Delta v4 / v_{e\_NTR}}) \tag{3-11}$$

$$v_{e\_NTR} = Isp * g \tag{3-12}$$

$$m_{TOT1} = m_{power/prop\_inert} + m_{spacecraft} + m_{prop1,2,3,4} \quad (3\text{-}13)$$

$$m_{TOT2} = m_{power/prop\_inert} + m_{spacecraft} + m_{prop2,3,4} - m_{prop\_tank1} \quad (3\text{-}14)$$

$$m_{TOT3} = m_{power/prop\_inert} + m_{spacecraft} + m_{prop3,4} - m_{prop\_tank1,2} \quad (3\text{-}15)$$

$$m_{TOT4} = m_{power/prop\_inert} + m_{spacecraft} + m_{prop4} - m_{prop\_tank1,2,3}. \quad (3\text{-}16)$$

The Δv terms in the propellant mass equations signify the delta-V requirements determined by the ephemeris tools, and the $m_{power/prop\_inert}$, $m_{spacecraft}$, m_{prop}, and m_{prop_tank} values are masses in (kg) calculated by the NTR model.

Another important parameter in these equations that is a function of fuel parameters is the ext velocity v_{e_NTR}. It is seen from the exit velocity equation above that this parameter is a function of ISP, increasing for fuels with higher operating temperatures, and thus decreasing the required propellant load. Note also that the delta-V values from the ephemeris model output were used with the assumption of no gravity losses. Therefore, any losses that were not accounted for in the original code, were not accounted for elsewhere in the propulsion models.

The weight of the spacecraft at LEO was also an important parameter in the propulsion model. This can be seen by the dependence of propellant load on spacecraft mass as well. All of the spacecraft components, total propellant, and four propellant tanks were included in the first mass estimate (m_{TOT1}). At the end of each stage, however, the fuel that was spent, along with the mass of the tank, had to be deducted from the mass estimated before the burn. The mass represented in the equations above by the notation $m_{spacecraft}$ comprises that of general components including the communication and navigation systems, along with the TransHab and

ECRV. The $m_{power/prop\_inert}$ notation refers to any components required for power or propulsion including the reactor itself, fuel cells, and power conversion components.

Nuclear Electric Power & Propulsion

History of Electric Propulsion (EP) Systems

The history of electric propulsion (EP) dates all the way back to 1903 when the visionaries in the scientific community began exploring its potential for spaceflight. In that year Tsiolkovsky released his article "Investigation of Universal Space by Means of Reactive Devices," which contained the Tsiolkovsky rocket equation, notably the most fundamental mathematical expression in the field of space propulsion. It was only eight years later that he published an article that mentioned the idea of electric propulsion, saying "it is possible that in time we may use electricity to produce a large velocity for the particles ejected from a rocket device." The combined knowledge of cathode ray tube development at that time, along with his appreciation for the importance of rocket exhaust velocity to space propulsion led to Tsiolkovsky's anticipation of the future of electric propulsion.[33]

Around the same period, Robert Goddard was also investigating electric propulsion ideas as a natural result of his physics work on electricity and his passion for propulsion. His initial musings on the electrostatic acceleration of electrons eventually led to thoughts on the reaction of ions in an electrostatic accelerator, and the neutralization of the charged exhaust with a stream of oppositely charged particles. By 1917 Goddard had developed the world's first documented electrostatic ion accelerator, with the intention that it could be used for propulsion.[33]

It was Hermann Julius Oberth, however, who first declared to the technical community that EP was a serious and worthy consideration for future astronautics. His 1929 text *Ways to Spaceflight* devoted an entire chapter entitled "The Electric Spaceship" to the capabilities and future role of EP in propulsion and attitude control. This book is also what brought EP into the

spotlight for science fiction writers. Unfortunately, after the 1930s this is where EP stayed as scientific advancements halted and efforts eventually switched to chemical rockets that were needed for the second World War.[33]

The following decades after the war did see a renewal in interest in EP research. In 1949 British physicists L.R. Shepherd and A.V. Cleaver declared that ion rocketry was impractical, and in 1951 American astrophysicist Lyman Spitzer found that ion propulsion was perfectly feasible. Ernst Stuhlinger wrote his classic text *Ion Propulsion* on the same subject in 1964. The 1960s in particular saw a growth in coordinated research and development programs addressing EP technology, mostly due to the pervasive upswing of U.S. space ambitions. Following experimental flight tests in the 1970s came the first commercial applications of EP in the 1980s as attitude control thrusters on commercial spacecraft. The early 1990s saw electrothermal arcjet use on many communication satellites, and by 1998 electrostatic ion thrusters had been used on a planetary mission for NASA.[33]

Current activities in electric propulsion are being conducted by NASA and throughout academia and include basic research all the way to flight demonstration. A cooperative agreement between NASA and MIT has allowed for research in the area of Hall thruster modeling to provide a theoretical understanding of the physical processes occurring in this electrostatic thruster type. In the flight arena, NASA currently has one active electrically propelled satellite called Earth Observing-1 (EO-1) that operates with pulsed plasma thrusters. In addition, NASA is currently developing the DAWN asteroid science mission that will use three NSTAR ion engines, and is providing a set of colloid thrusters in support of the ESA Smart2 spacecraft as part of the New Millennium Program. NASA's Project Prometheus, which was canceled due to budget constraints in 2004, aimed to combine space nuclear power with

electric propulsion technologies to allow for sophisticated active/passive remote sensing, greater launch window flexibility, and increased science data rates. The technology areas that were under development for the project's Jupiter Icy Moons Orbiter (JIMO) mission included high power and high ISP gridded ion thrusters, increased thruster lifetime, high power uptake power processing units (PPUs), and radiation-hardened components. Continued research in these areas is essential if advanced robotic and human missions to interplanetary destinations is ever to be accomplished.[34]

Fundamental Research and EP Description

Within the field of electric propulsion, three main subdivisions have arisen: electrothermal electrostatic, and electromagnetic propulsion. In electrothermal propulsion, the propellant is heated by an electrical process and expanded through a suitable nozzle. Three subclasses of this division include resistojets, arcjets, and inductively and radiatively heated devices. In electrostatic propulsion, the propellant is accelerated by direct application of electrostatic forces to ionized particles. The most common thruster type in this class is the ion thruster, though some development work has also been done on field emission electric propulsion (FEEP), which produces minute amounts of thrust. In the third category of electromagnetic propulsion, the propellant is accelerated under the combined action of electric and magnetic fields. Subclasses in this electric propulsion category include magnetoplasmadynamic thrusters (MPDT), Hall-current accelerators, and pulsed plasma devices.[35]

When considering potential EP thrusters for interplanetary, high-energy requirement missions, it is currently only feasible to consider the electrostatic and electromagnetic classes of propulsion. The electrothermal method falls behind the other two classes due to fundamental thermal limitations for exhaust speeds and lifetimes that primarily result from the heating and expansion processes required of electrothermal accelerators.[35] Acceleration of the propellant by

external forces, however, will allow for higher efficiencies and specific impulse values. The specific thruster types within the electrostatic and electromagnetic categories that were considered in this study include ion, MPD, and Hall thrusters.

Ion thrusters

One of the electrostatic devices capable of satisfying the acceleration levels described above is the ion thruster. It functions by accelerating a beam of atomic ions with a suitable electric field and then neutralizing it with a flux of free electrons. Positive atomic ions are liberated from the propellant source and accelerated by the electrostatic field created with strategically placed magnets. These atoms are then combined with the electron source outside of the grid to produce a net zero charge stream with speed determined by the net potential drop over the distance between atom release and the neutralization plate.[35]

Although the ion engine is one of the most complex within the group of EP engines, they also have undergone the most research and development over the years. They are appealing for space travel due to past demonstration of long lifetime, high efficiency, and high specific impulses. For the purposes of this study, the lifetime was assumed to be 20000 hours, the ISP was estimated at 6000 (s), the thruster efficiency at 90%, and the thrust per thruster at 1 (N) with xenon as the propellant choice.[26,35] Disadvantages with this thruster include the indicated low thrust density, high system complexity, and high PPU specific masses. This technology has been demonstrated on over a dozen U.S. and Soviet flight tests dating back to 1962. The first operational use of ion engines was in 1994 for the Japanese ETS-6 and COMETS satellites, and was followed by use on a commercial satellite bus in 1997 and the interplanetary Deep Space NASA mission in 1998.[35] Future research on these systems will most likely focus on developing higher power capabilities, decreasing the mass of high power PPUs, and developing extremely small propellant feed systems.[36]

MPD thrusters

Despite having considered only one electrostatic thruster in this study, both the MPD and Hall thruster engines were considered from the electromagnetic group. This follows appropriately from the fact that electromagnetic acceleration presents many possibilities for implementation given that the applied fields and internal currents may be steady, pulsed, or alternating over a range of frequencies. There are also a variety of propellant types, electrode configurations, and means for injection and ionization of atoms that are available when using these electromagnetic thrusters.[35]

An MPD thruster is configured with a central coaxial geometry cathode, an annular anode, and an interelectrode insulator. In this thruster type, gaseous propellant flows into the upstream part of the channel whereby the atoms are ionized with a uniform electric arc, compressed into a hot plasma just beyond the cathode tip, and expanded out the thruster as plasma exhaust. These thrusters are capable of high specific impulses, moderate efficiencies, and high thrust. The parameters assumed for this study include a lifetime of 2400 (h), an ISP of 5000 (s), an efficiency of 65%, and a thrust of 100 (N).[9,26,35,37] It is to be noted however, that megawatt power levels and the subsequent propellant flow rates for MPD thrusters have not yet been tested and are both technological and economic problems.[35] A major objective for MPDT research is the achievement of thrust efficiencies greater than 50% with non-condensable propellants while operating the thrusters below the plasma instability threshold.[35]

Hall thrusters

Electromagnetic Hall thrusters rely on use of the same-named "Hall effect," which refers to the potential difference on opposite sides of a thin sheet of conduction material through which electric current created by a magnetic field applied perpendicular to the Hall element is flowing. In this type of thruster, propellant is accelerated by an electric field in a plasma discharge with a

radial magnetic field. Channel and field geometries lock the plasma electrons into nearly collisionless cross-stream drifts, leaving the positive ions to accelerate downstream under the applied electric field.[35] This thruster device is sometimes thought of as a cross between an electrostatic and electromagnetic accelerator.

Although Hall thrusters have a relatively high specific impulse and thruster efficiency, they have a low thrust output per thruster, and past testing has shown life-limiting erosion and unstable and oscillatory plasma discharges to be of concern.[34] The assumed performance parameters used in this study include a lifetime of 8000 hours, a specific impulse of 400 (s), a thruster efficiency of 62%, and a thrust of 0.4 (N).[38] Research interests for Hall thrusters include using krypton as propellant, increasing the lifetime to greater than 8000 hours, and eliminating the erosion in the plasma discharge chamber.[34]

Despite knowledge of current performance parameters including ISP, efficiency, and thrust for each of the EP thruster types under consideration, the type of missions that the thrusters are being applied to requires some assumptions on the future state of the technologies. Advanced interplanetary missions will have very high delta-V and burn time requirements that may be feasible for these EP systems on paper, but have not actually been tested experimentally. As alluded to earlier, testing of these thrusters at high powers and for long-life durations will, in itself, be a demanding task. However, as the missions being studied have departure dates on the order of 2030 for Mars and 2040 for Saturn and Jupiter, a “leap of faith” will have to be taken by assuming that the technologies will be available to satisfy the mission requirements. The assumptions made in this study also included the thrusters being able to operate at very high power with PPUs that can process power coming from megawatt-level nuclear reactors, and thrusters that can burn for considerably long times. It is suspect that these capabilities will

improve over the next 20-40 years and the performance parameters will most likely increase along with them.

Development of the Nuclear Electric Propulsion (NEP) Model

The NEP architecture was broken-down into three systems based on the type of NEP thruster being used. This was different than the breakdown for NTR systems, which varied by reactor fuel type. Since the propulsive performance of NEP systems was primarily dependent on thruster type and this performance can vary greatly between different thruster options, this was the primary focus. The reactor needed for an NEP system was unimodal in the sense that it only needed to generate power (in contrast to the usual connotation of 'unimodal' as only producing propulsive heat). It was thus not extremely important what type of reactor was used since the masses of all reactor types were only slightly different and the reactor mass was merely a small fraction of the total mass of the CTV.

The thruster types chosen for analysis in this trade study included MPD thrusters, ion thrusters, and Hall thrusters. Each of these thruster types would provide different ISP, efficiency, and overall performance capabilities to an NEP spacecraft, thus it was paramount to properly explore the breadth of NEP systems by assessing each of these thruster options.

The schematic shown in Figure 3-3 depicts the spacecraft components that together make-up the NEP vehicle architecture. It is apparent in this diagram that the reactors served only as power generation for the spacecraft subsystems and electric propulsion mechanism. While the blue components are part of the power generation subsystem and the yellow components comprise the set of common vehicle components, the pink components now represent the electric propulsion subsystem. In an NEP system, electric thrusters provide the sole means of propulsion and require both liquid propellant and electric power for functioning. The arrows in the

schematic are divided between the solid black arrows that depict a coolant or propellant flow, and the dashed black lines that indicate flow of power to each system.

Power

The considerations for determining the reactor mass for the NEP power reactor were much different than those for sizing the different NTR reactors. Since space reactor fuels provided the trade within the NTR architecture, the different mass sizes of each of the NTR reactors was pivotal to the results since mass was based upon fuel choice. In addition, the NTR reactors provided the propulsive energy for the spacecraft, making fuel parameters such as temperature and ISP important variables in an overall comparison of NTR systems.

In the case of the NEP power reactor, the only parameter that went into the NEP architecture model based on the reactor was that of the reactor mass. In addition, only one reactor was needed for all of the NEP systems, since the NEP trade was essentially on the type of electric thruster being used. The propulsive properties of the EP thruster were what differentiated these systems, and thus the mass of the reactor simply became another term to lump into the total mass carried along with the spacecraft.

It was thus decided to label the NEP power reactor as a fast reactor, without specification to its specific fuel form. This generalism was used so that various data-points from literature sources could be used to develop an equation to be used in calculating reactor mass based on the power requirements calculated by the NEP model. Three NEP power reactor descriptions were taken from previous NEP mission analysis studies, and their main descriptive parameters were compiled in Table 3-4.[32,37,39]

Although each of the three reactors from these studies had slightly different fuel forms, they were all fast reactors, as expected for an NEP system. As discussed previously, fast reactors are ideal for NEP systems since they can provide long-duration steady power. The mass and

power data-points corresponding to these three reactors included the total mass of the power reactor, pressure vessel, and internal and external shielding. By plotting each of the points on the curve seen in Figure 3-4, a trendline was used to calculate Equation 3-17, where the mass in (kg) is dependent on the electric power requirements Pe in (MWe) of the CTV.

$$Mass_{reactor\_NEP} = 53.939 * Pe^2 + 976.12 * Pe + 2814.9 \quad (3\text{-}17)$$

The reactor masses were thus calculated separately for each mission since the calculated power requirements varied for each mission. It should also be noted that the ISP was assumed for the NEP reactor to be 925 (s), since this is the same ISP as the CERMET fast reactor used in the NTR model.

In order to better understand the flow of power and the associated losses from the reactor to the thruster, a pictorial representation of this flow, along with parameter descriptions, is found in Figure 3-5. Because the Brayton power conversion unit was indiscriminate of the final destination of its electric power, it provided the function of converting all thermal power generated by the reactor to electric power for spacecraft needs. The PMAD system, which consisted of cabling, fault protection, and switching gear, then directed the power to the appropriate spacecraft loads.[16] Losses were found in the Brayton Conversion Unit, PPU, and electric thrusters, as shown and described in the power and efficiency diagram. Some of the major equations used to describe the power and efficiency calculations visualized in the flow diagram are given by the thermal power Equation 3-18, and the electric power Equation 3-19, where the power for propulsive needs is given by Equation 3-20, and the overall system efficiency is given by Equation 3-21

$$P_s = P_{s,prop} + P_{s,spacecraft} \quad (3\text{-}18)$$

$$P_e = P_s * \eta_s = P_{e,prop} + P_{e,spacecraft} \quad (3\text{-}19)$$

$$P_{e,prop} = P_{pp} + P_{th} \tag{3-20}$$

$$\eta_T = \eta_s * \eta_{pp} * \eta_{th} \tag{3-21}$$

Propulsion

The size of the propulsion system was dependent on two main factors: the energy requirements for the mission, and the remaining spacecraft vehicle mass. The energy requirements for the NEP spacecraft consisted of a delta-V value for the outbound and inbound transfers and the burn time of the thrusters during these transfers. It is important to note that this was the only architecture that required spiral trajectories out of the Earth and destination planets' atmospheres. This was necessary due to the need for the spacecraft to pick up speed in order to escape from the atmosphere of each respective planet. Although the propellant was sized according to the total requirements of both the transfer and spiral durations, the crew would only be on the CTV for the transfer duration as it was assumed that they were transferred to the spacecraft after it picked up the necessary speed for escape. This was important so that the requirements for transfer time given in the mission profiles would not have to include the rather long spiral times required by the NEP system. This drawback to the NEP system was not neglected as it was accounted for in the final tradespace analysis.

In addition to energy requirements, the sizing of the system propellant was also dependent on the weight of all the components it had to propel through space. This weight included the communication and navigation components, TransHab and ECRV, truss structure, power reactor, Brayton Conversion Unit, radiators, and the propulsive thrusters and PPUs. More simply put, enough propellant had to beonboard to carry the rest of the spacecraft weight to its destination. It must not be forgotten that the weight of the unused propellant itself also played into the weight equation since it too was carried onboard the spacecraft until it was used.

The two main mass estimates needed to size the propellant mass for outbound and return journeys were the IMLEO (m_{TOT1}) and the initial mass at departure from the destination planet (m_{TOT2}). The propellant loads required to carry these masses were divided into two separate equations (Equation 3-22 and Equation 3-23) since the outbound and return burns are two distinct entities.

$$m_{prop1} = m_{TOT1} * (1 - e^{-\Delta v1 / v_e}) \tag{3-22}$$

$$m_{prop2} = m_{TOT2} * (1 - e^{-\Delta v2 / v_e}) \tag{3-23}$$

This allowed for the second propellant load equation to be calculated assuming a smaller mass due to the first propellant load being burned off, and from dropping its associated propellant tank. The initial mass quantities at initiation of the two main burns are given in Equation 3-24 and Equation 3-25, where it can be seen that the propellant and total mass equations are interdependent.

$$m_{TOT1} = m_{NEP\_inert} + m_{prop1,2} \tag{3-24}$$

$$m_{TOT2} = m_{NEP\_inert} - m_{prop\_\tan k1} + m_{prop2} \tag{3-25}$$

The term m_{NEP_inert} used in the mass equations represents the total spacecraft mass minus the propellant, an equation for which is given by Equation 3-26, where the terms represent the mass of the power reactor, propulsion hardware, communication and navigation components, and TransHab, ECRV and structural truss masses, respectively.

$$m_{NEP\_inert} = m_{power} + m_{pp+th} + m_{comm,nav} + m_{Transhab,ECRV,truss}\ ^{15} \tag{3-26}$$

As the mass sizing of the power reactor and its associated pressure vessel, shield, and feed system have been previously discussed, and sizing of the spacecraft communication and

navigation systems is to follow, only the sizing of the propulsion system will be discussed herein.

The mass estimates for the PPU and thruster hardware were taken from both text and literature sources that had specific mass (kg/kWe) values for ion, MPD, and Hall thrusters. The MPD thruster and PPU combined specific mass was the lowest of the three, at 0.6 (kg/kWe). This parameter was mostly due to the very high power levels processed in this simple and robust thruster device, and has made MPD thrusters highly desirable for interplanetary missions.[26,35] The specific mass estimate for the Hall thruster system was based off of both an advanced thruster and advanced PPU design. The High Voltage Hall Accelerator (HIVHAC) Development Program predicted a possible future thruster specific mass of 1.3 (kg/kWe), while PPU specific masses ranged from a progressive 5 (kg/kWe) to a very advanced 2 (kg/kWe).[37,38,40] Given the distant departure times of the reference mission profiles under consideration in this study, the advanced PPU specific mass was assumed, for a total PPU and thruster specific mass of 3.3 (kg/kWe). Although ion thrusters are known to require very heavy PPUs (~10 (kg/kWe)), a similar technology advancement was assumed for the ion system and a value of 4 (kg/kWe) was used for the PPU specific mass.[35] Combined with a literature data-point of 1.2 (kg/kWe) for the ion thruster itself, a total specific mass of 5.2 (kg/kWe) was assumed for the thruster and PPU combination.[37] The equations for the combined PPU and thruster mass for the MPD system is thus given by Equation 3-27, the Hall system by Equation 3-28, and the ion system by Equation 3-29, where the term $P_{e,prop}$ is the electric power supplied to the EP thrusters.

$$mass_{pp+th} = 0.6 * P_{e,prop} * (1 + burn\_duration / lifetime) \quad (3\text{-}27)$$

$$mass_{pp+th} = 3.3 * P_{e,prop} * (1 + burn\_duration / lifetime) \quad (3\text{-}28)$$

$$mass_{pp+th} = 5.2 \ * P_{e,prop} * (1 + burn\_duration / lifetime) \quad (3\text{-}29)$$

Although these specific mass estimates alone provided the sizing for the thrusters based upon satisfying the mission energy requirements, they do not account for the functional lifetimes of the thrusters that may limit the duration of their use. Thus contingency weight had to be added for thruster hardware for missions that required burns greater than the lifetime of the thruster selected. The burn durations for the NEP system were defined as the spiral out/in times, along with burn times between planets. This duration is not the same as the crewed mission duration, which would include the transfer times and stay time on the destination planet. Given this assumption, thrust correction maneuvers needed during crew stay at the destination planet were assumed supplied via alternate methods such as reaction control systems.

The mass estimates for the xenon and liquid hydrogen propellant tanks differed based on the propellant, not the thruster, and were approximated with textbook equations.[16] The tank estimates for the ion and Hall thrusters thus used the same equation since both required xenon propellant, while the MPD thruster used a tank equation based upon hydrogen propellant.[26] The differences in the densities of the propellants led to a different required volume per unit mass, and thus different propellant tank volumes and masses. Textbook sources gave Equation 3-30 for MPD tank mass, while the equation for the xenon propelled ion and Hall thrusters was given by Equation 3-31.

$$mass_{\tan k\_H2} = .287 * mass_{prop} \quad (3\text{-}30)$$

$$mass_{\tan k\_Xe} = 52 + 0.075 * mass_{prop} + .154 * mass_{prop}^{2/3} \quad (3\text{-}31)$$

For both equations, the term $mass_{prop}$ represented the total amount of propellant used for the mission.[16,32]

The power conversion, power management, and heat dissipation system masses were not dependent on the thruster used, thus common equations could be used for all thruster models. Due to the lack of mass approximations for the PMAD component in textbook material, three data-points from the literature were used to approximate the PMAD mass equation. Microsoft Excel was used to derive a logarithmic approximation to the data-points' trend line, a plot of which can be seen in Figure 3-6. Issues arose for power requirements less than about 1000 kWe due to the nature of the logarithmic function, thus a regressed linear function was used for lower power requirements. The formula for PMAD mass is given in Equation 3-32, which shows the calculation based on the electric power requirement P_e in (kWe).

$$mass_{PMAD} = 7772.7 * Ln(P_e) + 1067.5(\ for P_e > 1000);.635 * P_e(\ for P_e < 1000) \quad (3\text{-}32)$$

In the calculation for the Brayton Unit, a specific mass of 0.875 was used and was taken from a literature data-point for a similar NEP crewed vehicle.[32] The Brayton Unit, or CBC, mass is given by Equation 3-33.

$$mass_{CBC} = 0.875 * P_e \quad (3\text{-}33)$$

The mass of the radiators was determined by a straightforward equation depicting the radiator mass needed to rid the system of excess heat due to losses. The value for the specific mass of the radiators was estimated to be 1.5, which is slightly more conservative than a text estimate of 0.1-0.4 kg/kW, and in close approximation to the Brayton to radiator mass ratio from the previously mentioned literature source.[16,32] The equation used for the radiator mass estimate is seen in Equation 3-34, where $SpMass_{rad}$ is the specific mass value of 1.5 for the radiator.

$$mass_{rad} = (P_{s,prop} * (1 - \eta_{th} * \eta_{pp} * \eta_S) + (P_s - P_{s,prop})(1 - \eta_S)) * SpMass_{rad} \quad (3\text{-}34)$$

An additional equation that was used to estimate the mass for the truss structure for the entire spacecraft was Equation 3-35, where again, $mass_{inert}$ refers to the entire spacecraft mass not including propellant.

$$mass_{truss} = 10\% * mass_{inert} \tag{3-35}$$

In addition to sizing the NEP system components, the propulsion equations also derived the required thermal and electric power for the spacecraft, along with the thrust required by the EP thrusters. One important point to note is that the thermal power generated by the reactor was converted to electric power and then split between the propulsion system that operates the thrusters, and the components requiring constant power. These components included communication and navigation systems along with the TransHab module. This effect is shown through the thermal power equation, Equation 3-36.

$$P_s = \left(\dot{m}_{prop} * (Isp * g)^2 \Big/ 2 * \eta_T \right)_{prop} + (P_{s,COMM,NAV,Transhab}) \tag{3-36}$$

The total electric power requirements for these two separate entities combined is given by Equation 3-37.

$$P_e = P_s * \eta_s \tag{3-37}$$

The thrust variable T is then based only on the thermal power devoted to the propulsion system, $P_{s,prop}$, as seen by Equation 3-38.

$$T = 2 * \eta_T * P_{s,prop} \Big/ Isp * g \tag{3-38}$$

Knowing the value of the thrust is only significant for calculating the number of thrusters that would be needed for a particular EP system given by the simple relation in Equation 3-39, where the term in the denominator indicates the characteristic thrust per EP thruster.

$$\#\_thrusters = \frac{T}{T\_thruster} \tag{3-39}$$

It should be clear from inspection of the analysis performed to develop the NEP propulsion equations, that thruster-specific parameters played a major part in determining spacecraft performance. The EP thruster efficiency, specific impulse, and thrust per thruster had a large impact on power and thrust requirements, overall system efficiencies, and wet and dry mass estimates for the spacecraft. These thruster characteristic parameters were even used as inputs in the ephemeris models, which determined the energy requirements for the system. The specific mass, fuel, and lifetime parameters for each thruster were the main drivers for the mass estimates of the actual thruster and PPU hardware, along with the propellant. The parameters used for the ion, MPD, and Hall thrusters in this study are briefly summarized again in Table 3-5.

Hybrid Power and Propulsion

Background

Up until this point, Hybrid vehicle architectures have only been minimally analyzed through paper studies. One such study indicates that an integrated nuclear thermal and nuclear electric propulsion system would grant the ability to obtain from two systems much more than one can obtain from a single technology.[6] A NASA presentation on 'Bimodal Nuclear Thermal Rocket Propulsion for Future Human Mars Exploration Missions' gives pictures, schematics, and explanation of how a bimodal nuclear thermal reactor could apply electrical power production to a secondary electric propulsion system. The basic methodology is that the bimodal nuclear thermal rocket (BNTR) would produce short bursts of high thrust for escape mechanisms,

followed by a long power generation phase wherein the electric thrusters would be operational.[41] It is the hope of mission planners that a Hybrid spacecraft would combine the benefits of both NTR and NEP to increase overall performance for challenging interplanetary missions.

Development of the Hybrid Model

The Hybrid vehicle architecture schematic was devised as a cross between the NTR bimodal system and the NEP system. As can be seen in Figure 3-7, the schematic for the Hybrid system maintained the power and propulsion subsystems seen previously in the NTR bimodal schematic, along with the electric propulsion subsystem seen in the NEP schematic. Dashed lines in this schematic refer to power generation flow, while the solid black arrows refer to propellant or coolant flow.

The unique vehicle design in the Hybrid schematic allowed for the reactor to provide power for the spacecraft needs and the necessary thermal energy and electric power for two modes of propulsion. The location of the two propulsion systems relative to the TransHab was indeed intentional, as the reactor system would most likely reside at the opposite end of the TransHab, while the EP system would be on the same end. The two thrust mechanisms would also therefore produce thrust in opposite directions relative to the spacecraft itself, requiring realignment of the vehicle before changing propulsive mode.

Power

The same 'bimodal' NTR reactor that was used for thermal power generation for the NTR bimodal architecture was also used for the three Hybrid architectures. A bimodal engine was required for this architecture in order to provide thermal propulsion for the NTR engines and electric power for the EP thrusters and other spacecraft functions. The bimodal reactor utilized a fast fission spectrum and CERMET reactor fuel. An assumption of two reactors onboard the spacecraft was used just as for the other architectures. In order to estimate the total reactor mass,

a dependence on the electric power requirement was used just as it was for the NEP system. This estimate was found by using the same equation for reactor mass as the NEP system, but adding an additional weight to account for NTR reactor fuel and propulsive hardware. The bimodal engine at 5272.3 (kg) was designed to have an electric power output of 25 (kWe). An NEP reactor operating at 25 (kWe) would have a calculated mass of 2839.3 (kg). This difference between the two of 2432.9 (kg) was thus assumed to be the "additional" NTR weight added to the calculated weight of the reactor based only on the NEP reactor mass. The NEP reactor mass equation for one reactor is shown below in Equation 3-40, and was updated to account for the additional mass needed for the Hybrid reactor.

$$Mass_{reactor\_Hybrid} = (53.939 * Pe^2 + 976.12 * Pe + 2814.9) + 2432.9 \quad (3\text{-}40)$$

Propulsion

The equations that defined the EP thruster sizing, along with the parameters for the EP thrusters, were the same as those used for the hybrid architecture. The EP aspect of the Hybrid vehicle was identical to the NEP architecture with all three types of EP thrusters assessed. Although the vehicle had an NTR engine, all configurations utilized the bimodal CERMET reactor, thus the trade was solely on EP thruster type, not on NTR fuel type as it was for the NTR architecture.

The equations that changed compared to the NEP system were those for the propellant sizing. The Hybrid propulsive equations represented operationally both NTR and NEP delta-V requirements, in which one NTR delta-V burn occured for planetary escape and was then followed by a long-duration NEP delta-V burn that allowed for capture. The first three of the four tanks associated with the four delta-V maneuvers was dropped after its respective burn segment. For instance, the mass of the propellant required for the second burn used the IMLEO

mass minus the propellant burned in the first NTR segment along with the tank that housed that propellant. These tanks were non-recoverable and inevitably became space 'junk.' The equations that defined the propulsive mass requirements for the Hybrid architecture's four burns are given by Equation 3-41 through Equation 3-44, where the mass equations at initiation of each burn are given by Equation 3-45 through Equation 3-48.

$$m_{prop1NTR} = m_{TOT1} * (1 - e^{-\Delta v1 / v_{e\_NTR}}) \tag{3-41}$$

$$m_{prop2NEP} = m_{TOT2} * (1 - e^{-\Delta v2 / v_{e\_NEP}}) \tag{3-42}$$

$$m_{prop3NTR} = m_{TOT3} * (1 - e^{-\Delta v3 / v_{e\_NTR}}) \tag{3-43}$$

$$m_{prop4NEP} = m_{TOT4} * (1 - e^{-\Delta v4 / v_{e\_NEP}}) \tag{3-44}$$

$$m_{TOT1} = m_{NTR\_inert} + m_{NEP\_inert} + m_{prop1,2,3,4} \tag{3-45}$$

$$m_{TOT2} = m_{NTR\_inert} + m_{NEP\_inert} + m_{prop2,3,4} - m_{prop\_\tan k1} \tag{3-46}$$

$$m_{TOT3} = m_{NTR\_inert} + m_{NEP\_inert} + m_{prop3,4} - m_{prop\_\tan k1,2} \tag{3-47}$$

$$m_{TOT4} = m_{NTR\_inert} + m_{NEP\_inert} + m_{prop4} - m_{prop\_\tan k1,2,3} \tag{3-48}$$

Note that the propellant mass subscripts indicating NEP or NTR burns are not included in the second set of total mass equations, but are instead merely indicated by the number, or order, in which they occur.

Common Vehicle Subsystems

TransHab

Every vehicle system that was analyzed for the advanced interplanetary missions in this study had a crew living module called the 'TransHab'. This term, commonly found in mission

analysis literature, was coined for the actual structure that was still in the design phase when research efforts ended in 2001. The TransHab was the first space inflatable module designed by NASA, conceived as a technology capable of supporting a crew of six on an extended space journey. The space habitat had an endoskeletal design, with a light and reconfigurable central structure and deployable pressure shell. The shell was elaborate in that it was made of several layers, could contain water or hydrogen for radiation shielding, and had an outer layer a foot thick. Recommendations drawn from the research completed during this NASA program included having a three-level internal layout with isolated crew quarters at the center, and exercise and hygiene stations situated on different levels from the public functions in the kitchen, dining and conference areas. Unfortunately budget cuts along with reported values of $100 million to build the structure led to the project's demise.[41] After the four-year research period between 1997 and 2001, Bigelow Aerospace purchased the rights to the patents developed by NASA and is currently continuing development of a similar structure for future commercial space applications.[11]

The ECRV was an additional habitation environment designed to be attached externally to the TransHab for a majority of the mission duration. In a hypothetical mission, when the CTV is being assembled in LEO prior to flight, the crew will be transferred from the launch vehicle to the CTV via the ECRV. The TransHab will then be inflated and flooring and partitions deployed so the crew may move from the ECRV into the TransHab for the remainder of the trip. The ECRV will also likely be the capsule the crew will use to aerobrake into the Earth's atmosphere after the interplanetary voyage. This would follow the propulsive capture of the entire CTV back into LEO and disengagement of the ECRV from the main space vehicle.

A vital consideration for the future design and sizing of the TransHab will be radiation shielding. It has been noted by several literature sources that the hazards of space radiation create the primary restraint on crewed interplanetary space missions. This is a problem that has not yet been resolved by nature due to the many complexities space radiation presents. Future crewmembers will be exposed to many types of radiation (ionizing and non-ionizing), which fluctuate considerably over time and location. This implies that different crew procedures and levels of protection will be needed over the course of a mission. More research will have to be done on the shielding properties used for protection, as human-rated structures must be approached with a very radical design perspective.[42] For example, some studies have proposed surrounding the crew module with hydrogen propellant tanks for radiation protection. Although the hydrogen-containing materials would be good radiation absorbers, the aluminum tank structure would actually produce dangerous secondary radiation particles. There is also uncertainty in the biological response to high-charge radiation. Currently, no exposure limitations have been set for deep space missions, and recommendations simply rely on exposure limits for operations in LEO.[43]

Some work has been done in the past to try and model how much and what type of radiation could be expected on interplanetary missions. The two main forms of ionizing radiation that are estimated include the constant, but low intensity galactic cosmic radiation (GCR), and the low frequency, but high intensity solar particle events (SPE). One study reported that with 1280 (kg) of polyethylene TransHab shielding for a Mars journey, 13.38 (cSv) of radiation dose equivalent was detected for SPE and 17.65 (cSv) for GCR for each one-way 180 - day transfer. The surface habitation on Mars resulted in 28.05 (cSv) for GCR and 2.23 (cSv) for SPE.[44] The lower rate of exposure on Mars was a result of the natural radiation shielding from

the Martian atmosphere. Although this study found a total radiation dose equivalent rate under the NASA LEO limit of 50 (cSv/year), the rate of exposure during the transfer period would indeed have been over the limit if it had been received for an entire year. A long duration transfer would have led to 63.5 (cSv/year) exposure, which is a significant violation of the current limit.

Although radiation shielding would be a significant factor in the design and development of the TransHab, it was deemed too difficult to account for shielding mass for all of the reference missions run in this study. It was assumed therefore that the 1900 (kg) that was assumed for the TransHab shielding weight, in addition to other materials such as wastewater and propellant tanks, would provide the necessary shielding for the trip. The breakdown of the TransHab-related masses thus became quite simple and was modeled from previous mission analysis sources. The module itself had a mass of 21000 (kg), the 6 crewmembers and their belongings equated to 600 (kg), and the ECRV was set at 5100 (kg). The consumables were dependent on the length of the mission (including stay time at planet), and were sized at 2.45 (kg) per person per day for food and water.[18] The breakdown of masses for the TransHab components can be found in Table 3-6.

The power requirement for the TransHab was also an important parameter to consider when generating the total operating power requirements of the spacecraft. The actual value of constant power that must be provided for the crew module so that everyday living and working needs can be satisfied was a difficult value to estimate, especially given the scarcity of information in the literature. In the lecture notes of G.L. Kulcinsky, however, a value of 100 (kWe) was given for a “manned outpost” on the surface of Mars.[45] It was believed that this

would be a reasonable estimate for the TranHab since it would require similar power needs to a planetary ground station.

Spacecraft Functional Components

The remaining spacecraft components that are common to each of the space architectures were those that provided for various communication and navigation functions to get the spacecraft to its destination and back. These system components were broken down into the following groups: command and data handling (C&DH), tracking, telemetry and command (TT&C), attitude determination and control system (ADCS), the reaction control system (RCS), and truss structure used to link all spacecraft hardware. The C&DH subsystem distributed commands and accumulated, stored, and formatted data from the spacecraft. The TT&C subsystem linked spacecraft with ground or other spacecraft by receiving commands and sending status telemetry. The ADCS provided stability and orientation in the desired directions during a mission despite external disturbances. The propulsive RCS subcomponent was linked to the ADCS by performing the thrust actions that were needed by the spacecraft as determined by the ADCS.

Although the general functions and equipment needed by these subcomponents was important to understand from the systems engineering perspective, the two most important parameters in the spacecraft model development were the mass and power estimates for the components. It was again difficult to estimate the size and power of these subcomponents given the limited number of papers found in the literature that went to similar depth-levels for spacecraft sizing, yet one paper provided values for a reasonable estimation. For the purposes of this study, the ADCS was estimated at 70 (kg), the C&DH at 35 (kg), and the TT&C at 205 (kg). The total power required was taken from the same reference, which designated the "communication loads" as requiring a power of 5 (kWe).[37] The RCS mass was taken from two

data-points, one from an NTR study, and the other from an NEP study. The NTR study showed an RCS mass that was 5.7% times that of the propulsion propellant mass, the NEP study gave a value of 6.9%, and one textbook suggested a range from 3-10%.[16,18,37] It was thus decided to set the RCS mass to 6% of the propellant mass required by the main propulsion systems for a given architecture. Since the RCS would only require a minimal amount of power at various small time increments over the course of the duration of the flight, it was decided to neglect its power requirement when sizing the overall power of the nuclear reactors. The structure of each spacecraft was based on the total mass of the system, scaling with system mass. A common estimate which was used to size the truss structure mass was 10% of the overall spacecraft mass.[16] A summary of the mass breakdown between common subcomponents is given in Table 3-7.

Analysis Tools

ModelCenter Software

The main analysis tool used in this study was Phoenix Integration, Inc.'s ModelCenter. This tool created a visual environment for process integration and employed complex design exploration techniques, making it ideal for performing trade studies and exploring a design space.[46] One major benefit to this tool was that it reduced both the time to run individual programs and the possibility for human errors that lead to costly mistakes. In addition, ModelCenter offered powerful and timesaving design tools that included parametric plots, optimization tools and linking of models. Each of these assets together provided the ability to conduct a large trade study within a reasonable time period.

The Analysis Server, a product by the same company, was used in conjunction with ModelCenter in order to be able to convert codes being used into reusable components that were directly accessible within ModelCenter. The Analysis Server was a flexible, Java-based software

server that allowed applications to be wrapped for integrated engineering processes. The 'wrapped' components, which are termed FileWrappers, are built from the FileWrapper utility, which was designed to automate the execution of analyses based on file I/O programs. The FileWrapper components thus had the ability to automatically edit the appropriate input files, run the code's executable, and parse the output file whenever it is executed. A template file, which is a copy of the input file in standard format, had to be created for use with a FileWrapper component, as the FileWrapper loads the template file and substitutes any user-inputs into it.[46]

Incorporation of Models into ModelCenter Framework

ModelCenter was used in this study by wrapping individual Excel worksheets and ephemeris codes into ModelCenter system models that allowed for user inputs, automatic passing of data from one worksheet to another, optimization and converging of parameters, and finally parametric analyses.

Ephemeris models

The IPREP and CHEBYTOP ephemeris codes were used to generate the NTR and the Hybrid and NEP ephemeris modeling tools, respectively. This was accomplished through the use of ModelCenter in conjunction with Analysis Server. The IPREP and CHEBYTOP executables were first input into the models by generating FileWrappers and input templates that the Analysis Server used to connect with the ModelCenter files. An example of the FileWrapper and templates created for the three propulsion system-specific ephemeris models is given by the CHEBYTOP Hybrid model files found in Appendix C: ModelCenter Template and Filewrapper. Creating these FileWrappers allowed the execution of IPREP and CHEBYTOP to be done using components within their respective ephemeris models, with input and output variables appearing in easy-to-use lists within the ModelCenter GUI.

The IPREP component was able to run an entire two-way mission in one sweep, but the CHEBYTOP component had to be run twice within the NEP and Hybrid models to simulate the outbound and return transfers, and was thus input as two separate components in each of the models. The data for the apogee and perigee variables for each destination was held within an Excel worksheet in each of the three models so that selection of planetary destination would allow the correct orbit parameters to be passed to the IPREP or CHEBYTOP components. A tool to aid in converting a date input by the user to a Julian date required by the executable was also incorporated as an Excel component.

For the two models that used the CHEBYTOP components, an additional Excel component was added that uploaded the thruster-related parameter values upon user selection of a thruster type. These parameters included the assumed values for thruster efficiency, ISP, and thrust force per thruster for the selection of Hall, ion, or MPD thruster type. Once all of these components were incorporated into the model, input variables that included departure date, stay time and transfer time were incorporated into the user interface and then linked to the appropriate variables in the model components. Key output parameters that were desired from the models included the delta-Vs, electric thruster burn times, and NEP spiral times. A screenshot of the ModelCenter NEP ephemeris model's graphical user interface (GUI) is given in Figure 3-8.

ModelCenter's Darwin optimization tool was also incorporated into each of the three ephemeris models. This genetic algorithm-based tool with fully featured GUI was integrated as a trade study plug-in within ModelCenter. The genetic algorithm method is based on probabilistic rules with evolution achieved through application of probabilistic operators that mimic biological genetics.[46] The goal that was achieved by using this optimizer within the ephemeris model was to minimize the overall mission delta-V for a given mission profile. Since

each mission profile was designed with ranges on the parameters for departure date, stay time, and transfer time, these variables became the design space for the optimization. The lower and upper bounds for these parameters became inputs that could be manually set by the user depending on the mission profile under review. Execution of this tool enabled the energy requirements to be minimized based on manipulating each of the four variables in the design space to find the very best answer given the specified mission profile requirements. Attempting to perform such an optimization manually would have undoubtedly required many hours of running the ephemeris model trying to make improvements one variable at a time. A screenshot of the Darwin Optimization tool GUI is shown in Figure 3-9.

Vehicle architecture models

Incorporating the vehicle architecture models into ModelCenter was much more straightforward than the ephemeris models since only Excel models that were fully self-generated were used. This involved using the Excel component tool to insert the various Excel models needed for each architecture, and then using the linking tool to link parameters within the model. The NEP and Hybrid architectures both had two main Excel worksheets incorporated into their ModelCenter models. The first was the main propulsion and power model that sized the reactor, while the second was a thruster selector tool. This latter worksheet allowed the user to select the desired thruster type from the ModelCenter GUI, automatically updating the appropriate propulsive parameters characteristic to that thruster in the sizing model.

The NTR model was slightly different in that its secondary Excel worksheet was a reactor fuel selector, which would input the fuel parameters for the fuel selected into the main NTR propulsion and power model. A screenshot of the NEP model showing the input parameter and output parameter lists, along with a block component input and output diagram is shown in Figure 3-10.

Mission architecture models

The term ‘mission architecture’ was used in this study to refer to a vehicle architecture performing a mission profile. From the modeling perspective this would equate to combining the architecture’s ephemeris model and its power and propulsion model. The mission architectures were then developed into their respective ModelCenter models, and were created by combining both the ephemeris and main architecture model. This allowed a user to then run an entire mission, deriving the IMLEO and other output parameters by simply inputting the mission profile scenario and fuel or thruster type.

Some difficulties were encountered, however, when trying to incorporate certain levels of automation into the models, which would have been timesaving mechanisms for the user. For instance, the ephemeris model’s Darwin optimizer tool that manipulated departure date, transfer and stay time in order to minimize delta-V energy requirements would not function properly within the larger mission architecture ModelCenter model. This was due to the fact that the term it was trying to optimize was being passed to the power and propulsion model, and was no longer an output parameter of the ephemeris model as required. This finding affected the planned methodology for the data analysis process. It was decided to maintain use of the ephemeris ModelCenter models for optimization purposes, record all optimized departure dates, transfer and stay times in a database, and manually enter these parameters into the mission architecture models to run the full-scale models. When the mission architecture models were run, the optimized delta-V energy requirements were automatically generated in the ephemeris model and passed to the power and propulsion model. Figure 3-11 provides a visual of a mission architecture model GUI that shows these user inputs, the two models incorporated into the larger model, and the desired output parameters.

Validation of models

Following completion of the mission architecture models it was decided to attempt to validate the models by comparing the IMLEO results from alternate sources to the results of the mission architecture models developed in this study. One literature source for each of the three main architectures was used for comparison. Attempts were made in each case to try and model a very similar mission to that presented in each study, though lack of specific mission analysis data such as the energy requirements used for sizing was recognized as a weakness in the validation methodology.

The NTR architecture model was validated using the results from a very detailed Pratt & Whitney Rocketdyne NTR model. This model was built upon numerous smaller models, high-level analysis and very thorough attention to reactor design and development details.[47] All of the fuels analyzed in the NTR model studied in this paper were also analyzed by the P&W model, thus it was decided to compare the IMLEO results for both models at the 15 (klbf) thrust setting. One of the main differences between the models, which may have some effect on the validation results, is that the P&W model assumes 1, 2 or 3 engine configurations wherein each engine provides the indicated thrust. The NTR architecture model developed in this study assumed only one engine was providing the thrust, yet an extra engine's weight was included in the model for redundancy purposes.

The mission that was analyzed for the NTR validation was a round-trip Mars mission with these specific delta-V energy requirements:

- TMI (Trans-Mars Injection)=3.60 (km/s)
- MOC (Mars Orbit Capture)=1.44 (km/s)
- TEI (Trans-Earth Injection)=1.09 (km/s)
- EOC (Earth Orbit Capture)=0 (km/s)

By running the NTR architecture model with the above energy requirements for each of the fuel selections (graphite, composite, carbide, and CERMET), a comparison of IMLEO estimates was made with the P&W model. The results from both models, along with the percent error between the two sets of results, can be found in Table 3-8. The percent error data-points ranged from 0.4% for the graphite model up to 8.63% for the CERMET model, with the lowest error cases pertaining to the more researched graphite and composite fuels. Considering the differing assumptions that most likely went into development of each of the two models, along with a vast difference in development time for the models, these comparison results provided strong support for validation of the NTR model.

The NEP literature source used in validating the NEP architecture model analyzed a 2033 Mars crewed round-trip mission that used MPD thrusters and a fast power reactor. The exact delta-V values used in the study were not given, thus a mission was set up in the NEP ephemeris model to generate approximate values for the energy requirements. A known difference between the paper-study analysis and the approximations used herein was that an Earth flyby was used in the paper-study versus the direct Earth re-entry assumed in the ephemeris model. To account for this difference, it was decided to match the propellant mass of 276 (kg) given in the literature study in order to determine the correct delta-V for the return trip. Using an outbound delta-V of 19.3 (km/s) and return delta-V of 19 (km/s), a transfer time of 275 days, and MPD thruster selection, the resulting IMLEO from the NEP architecture model was found to be 598.8 (MT). The literature source quoted an IMLEO of 560.7 (MT).[32] The NEP model thus gave a 6.8% higher estimate of the IMLEO than did the source, a rather reasonable value given the assumptions and approximations that had to be made to compare the two estimates.

A study on hybrid vehicles was also used in an attempt to validate the Hybrid architecture model. The mission was again a round-trip crewed Mars mission with a short stay. Similar to the previous validation methodology, a longer stay-time was assumed. This assumption was made since energy requirements were not explicitly cited in the paper-study, and the ephemeris model gave far less demanding energy requirements for a longer stay-time on the surface of Mars. The outbound and inbound NTR delta-V requirements were found to be 3.17 (km/s) and 0.22 (km/s), respectively, while the NEP requirements were 14 and 11.8 (km/s). The literature source cited an IMLEO of 298 (MT) for the hybrid vehicle with MPD thrusters, and the Hybrid architecture gave a result of 275 (MT), a difference of only 7.7%.[6]

The validation results presented for each of the three architecture models satisfied the objective of comparing the results seen in a literature study for each vehicle type, to those generated by the models developed in this study. The outcome was highly satisfactory in that the models created herein did a relatively good job of predicting the same results as professional mission analysis results done by experts in each particular power and propulsion field. These results were important since they provided credibility to the predictive nature of each of the individual architecture models. This was crucial for conducting a meaningful trade study of all three architectures, since they were compared directly against each other to determine the best performing vehicle architecture.

Table 3-1. NTR Architecture Systems

NTR System	Reactor Mode	Energy Spectrum	Fuel Type
1	Unimodal	Thermal	Graphite
2	Unimodal	Thermal	Composite
3	Unimodal	Thermal	Carbide
4	Unimodal	Fast	CERMET
5	Bimodal	Fast	CERMET

Table 3-2. Fuel Operating Parameters

	Chamber Temp. (K)	ISP (s)	Power (MWt)
Graphite	2500	875	306.6
Composite	2700	925	316.6
Carbide	3100	1000	342.0
Cermet	2700	925	316.6

Table 3-3. NTR Reactor Mass Sizing

* prop. hardware added to total	Reactor (kg)	Intern. Shield (kg)	Extern. Shield (kg)	Total (kg)
Graphite	3665.0	988.4	2,942.0	9384.4
Composite	3062.3	825.9	2,458.2	8135.3
Carbide	3404.0	918.0	2,732.5	8843.5
Cermet-uni	1059.1	285.6	850.2	3983.9
Cermet-bi	1680.8	453.3	1,349.2	5272.3

Table 3-4. NEP Power Reactor Descriptions

Power (MWe)	Mass (kg)	Type	Spectrum
5	9044	Liquid-metal	Fast
1	3845	Particle bed reactor	Fast
10	17970	Li-cooled pin type	Fast

Table 3-5. EP Thruster Characteristic Parameters

Type	Efficiency	ISP (s)	Thrust (N)	Spec_Mass (kg/kWe)	Fuel	Lifetime (days)
Ion	0.90	6000	1.0	5.2	Xenon	850
MPD	0.65	5000	100.0	0.6	Hydrogen	350
Hall	0.60	2500	0.4	3.3	Xenon	100

Table 3-6. TransHab Mass Breakdown

Component	Mass (kg)
Module	21000
ECRV	5100
Crew/Suits	600
Consumables	14.7/day

Table 3-7. Common Subcomponent Mass Breakdown

Component	Mass (kg)
ADCS	70
C&DH	35
TT&C	205
RCS	6%*mass_prop
Structure	10%* total mass

Table 3-8. NTR Model Validation Mass Estimates

	P&W Mass (kg)	Models Mass (kg)	% Error
Graphite	239000	238042	0.40%
Composite	200000	211738	5.87%
Carbide	180000	195854	8.81%
Cermet	170000	184666	8.63%

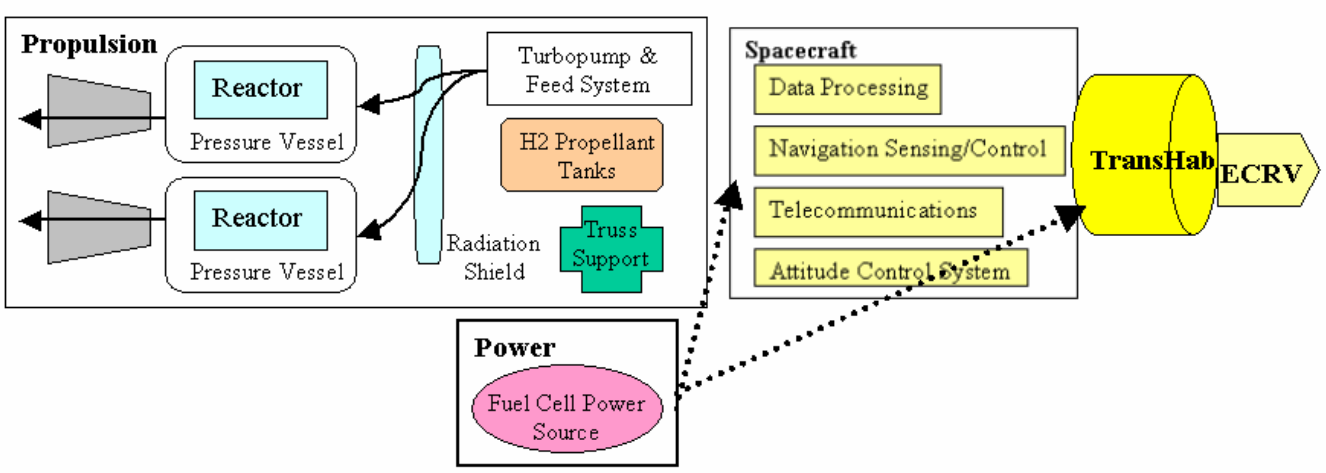

Figure 3-1. NTR Unimodal Vehicle Architecture Schematic

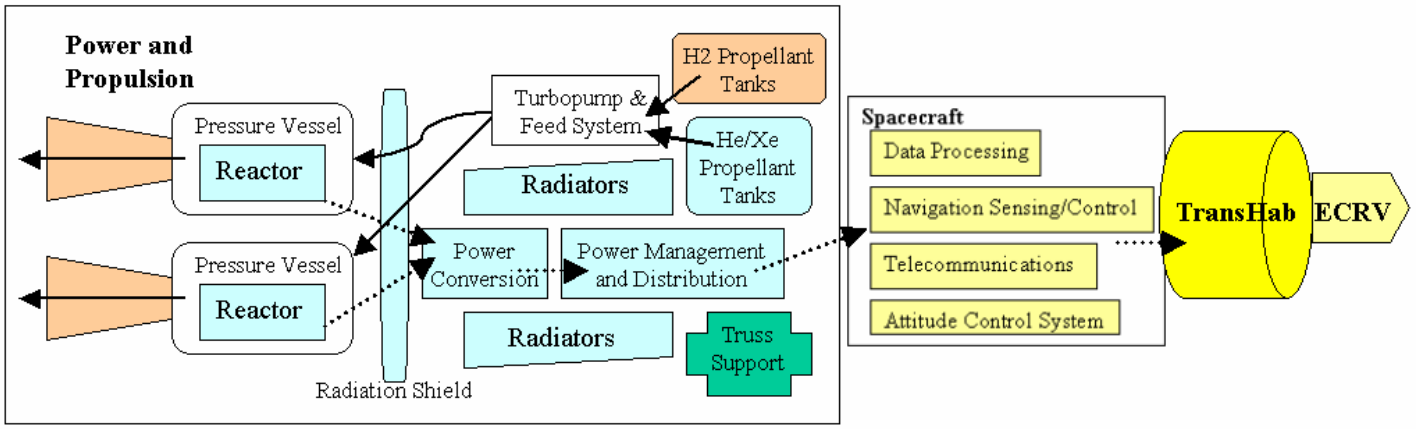

Figure 3-2. NTR Bimodal Vehicle Architecture Schematic

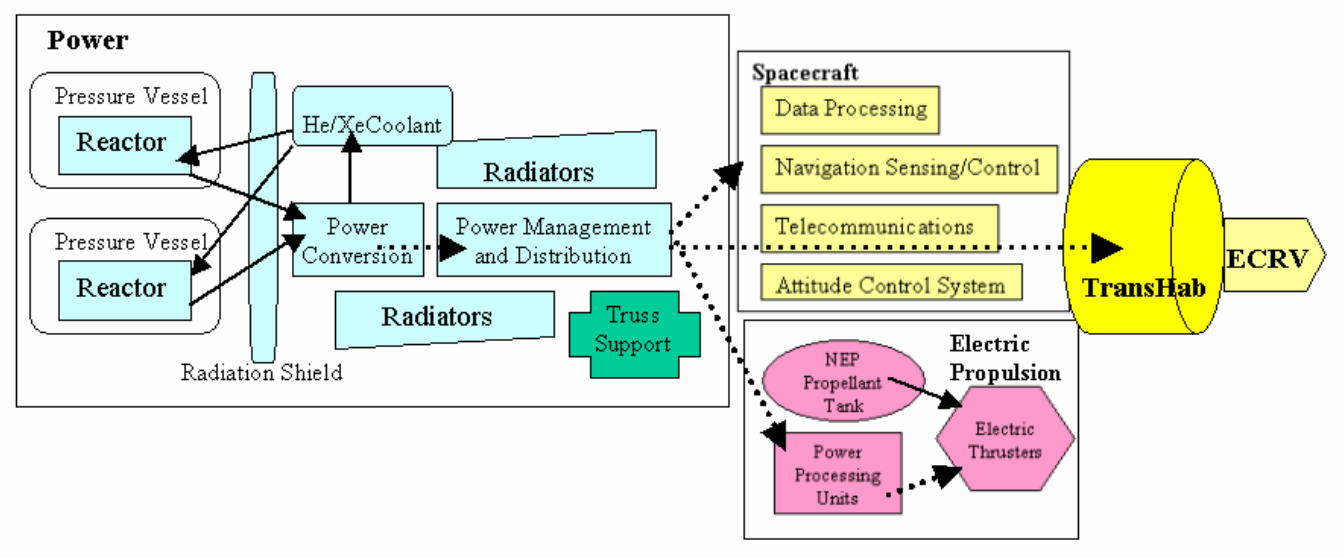

Figure 3-3. NEP Vehicle Architecture Schematic

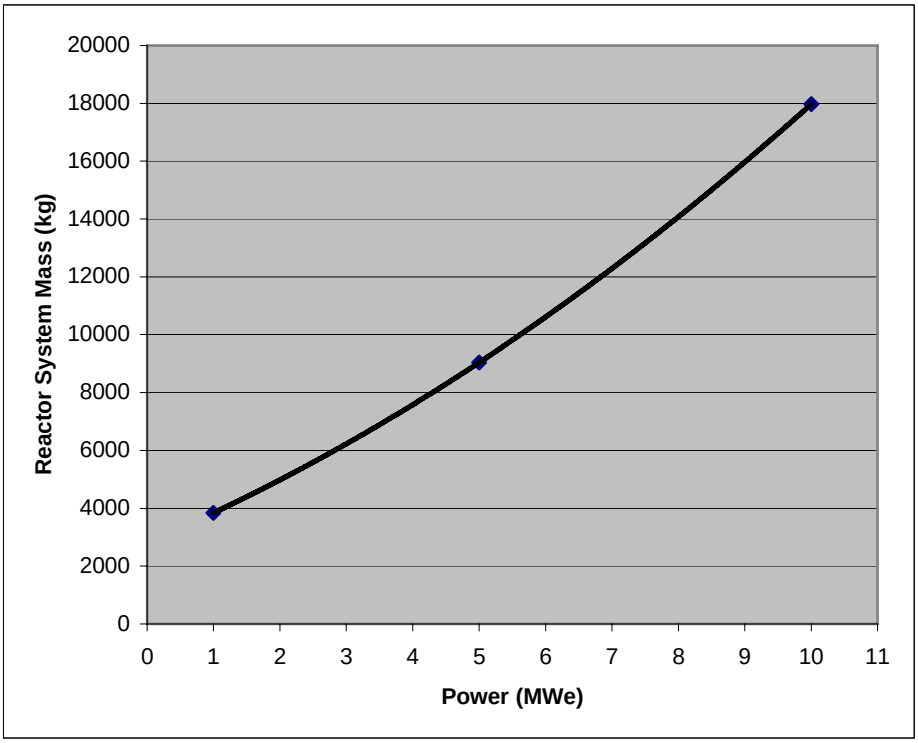

Figure 3-4. NEP Reactor Mass vs. Power

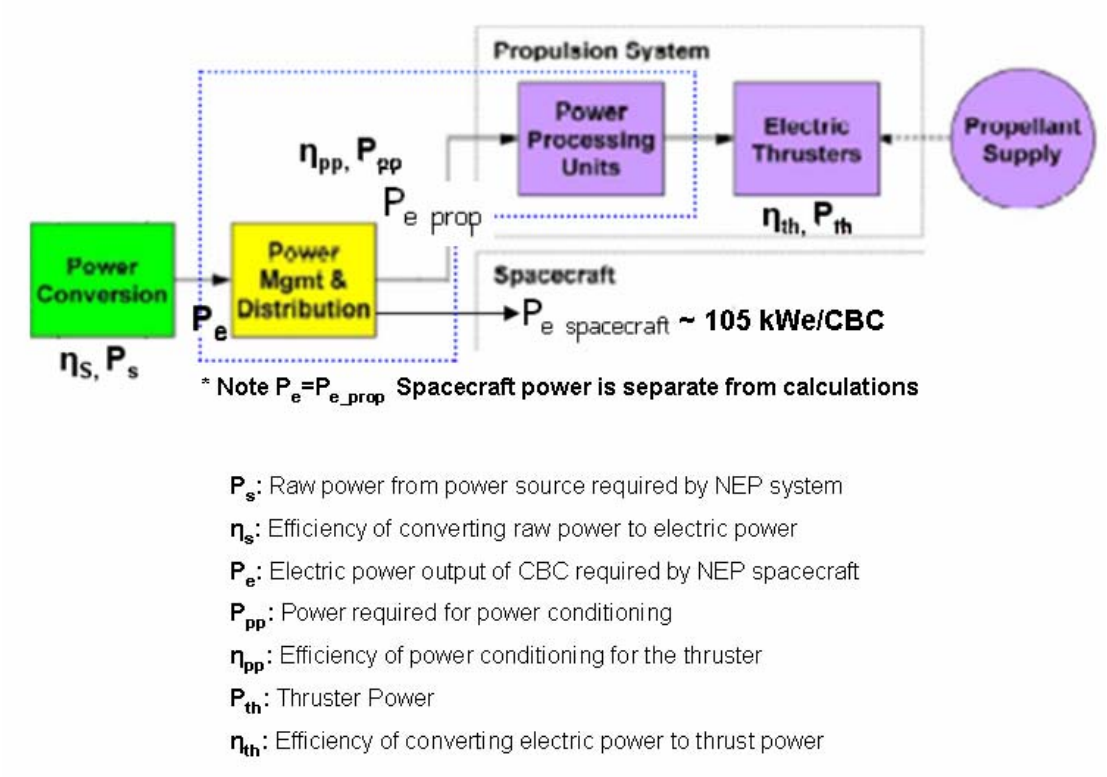

Figure 3-5. Power and Efficiency Flow Diagram

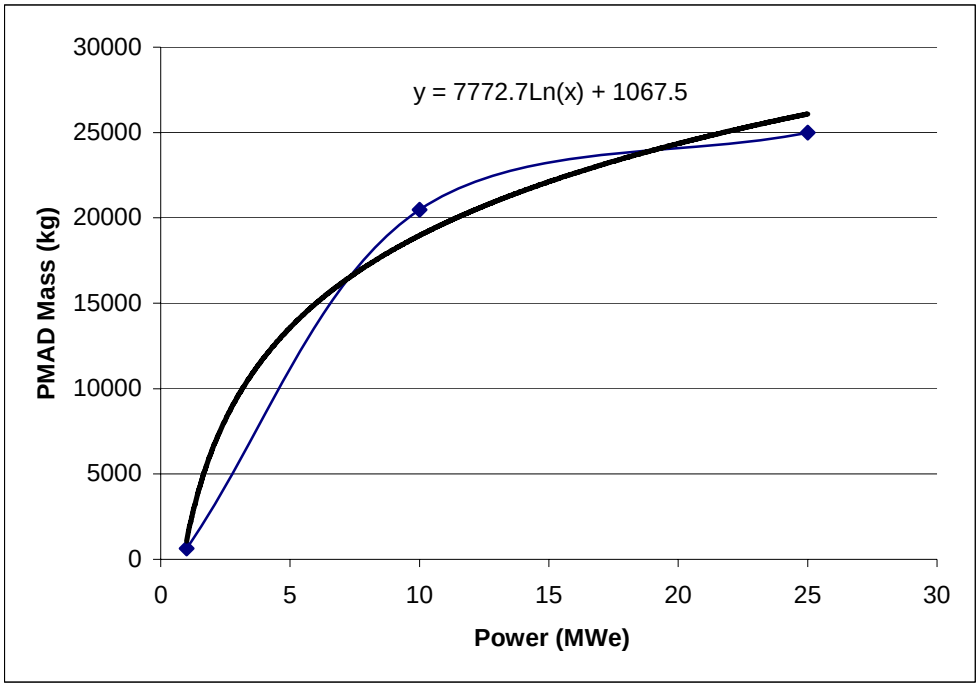

Figure 3-6. PMAD Mass Sizing Equation

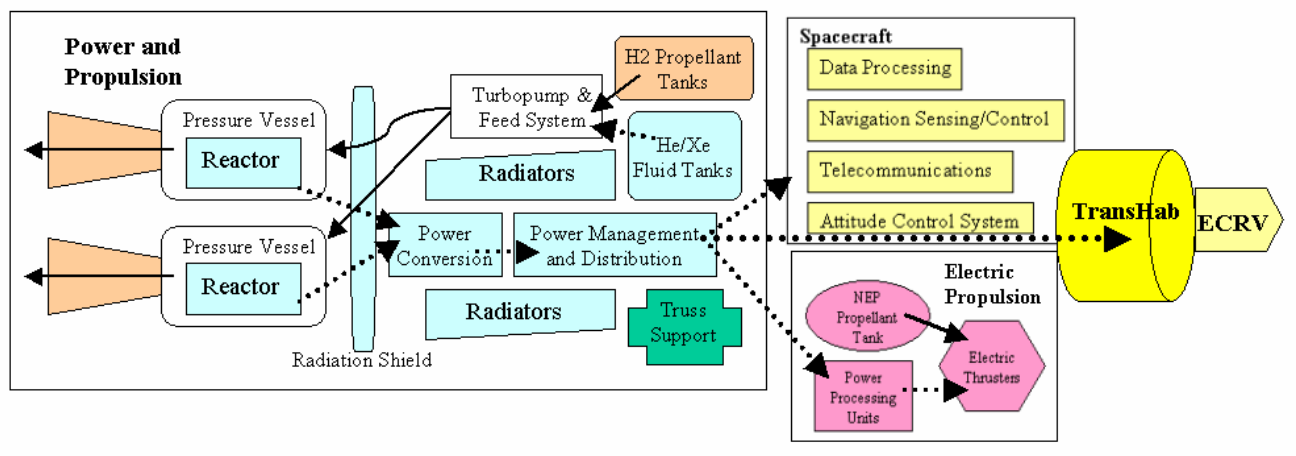

Figure 3-7. Hybrid Vehicle Architecture Schematic

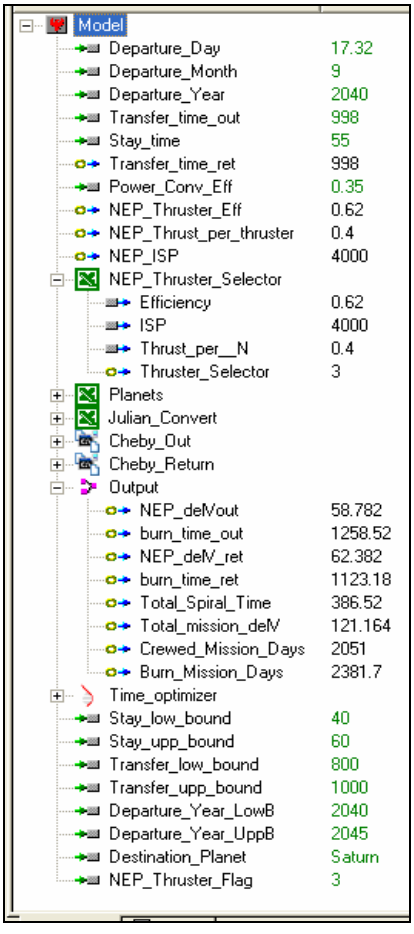

Figure 3-8. NEP Ephemeris Tool GUI

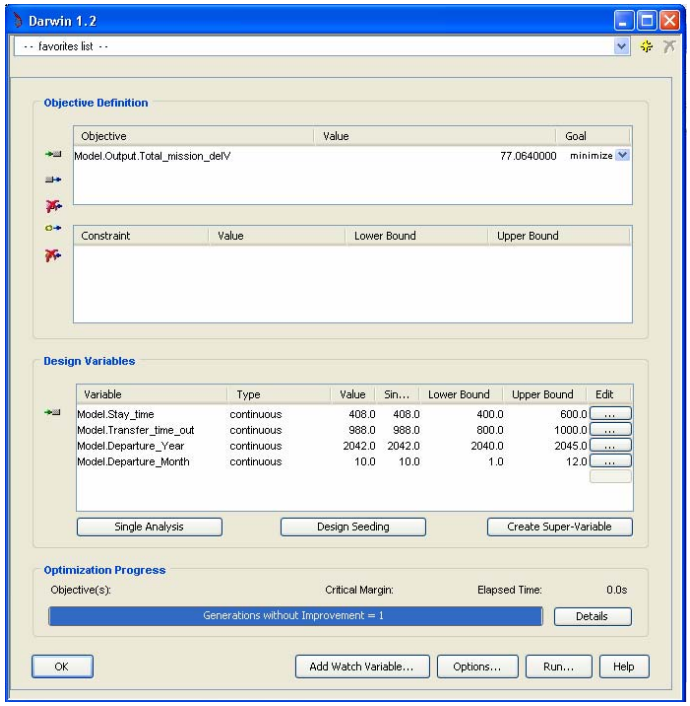

Figure 3-9. Darwin Optimization Tool GUI

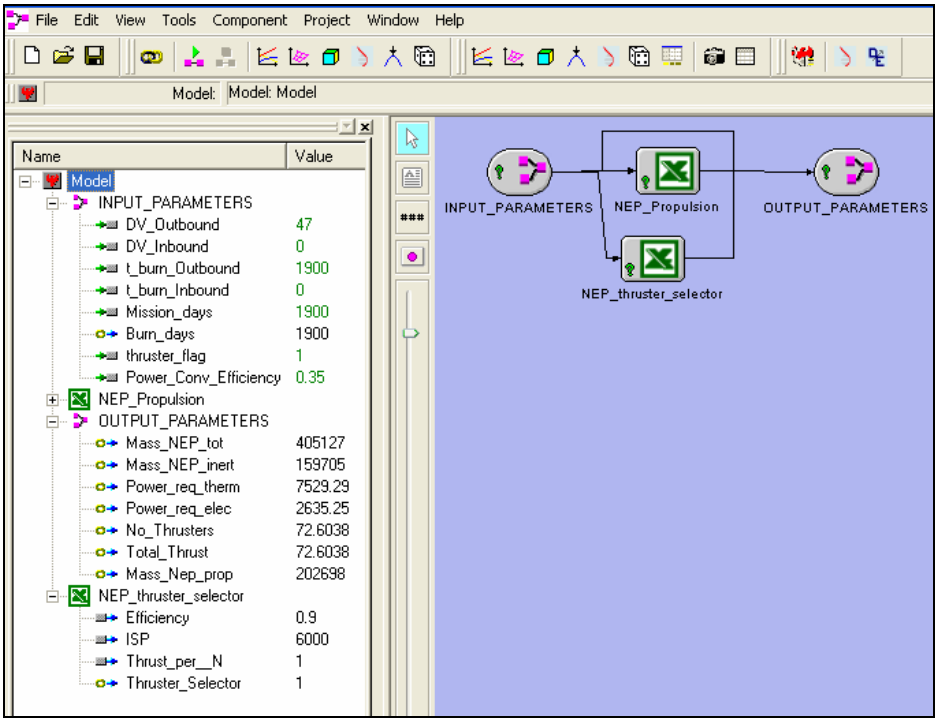

Figure 3-10. ModelCenter Screenshot

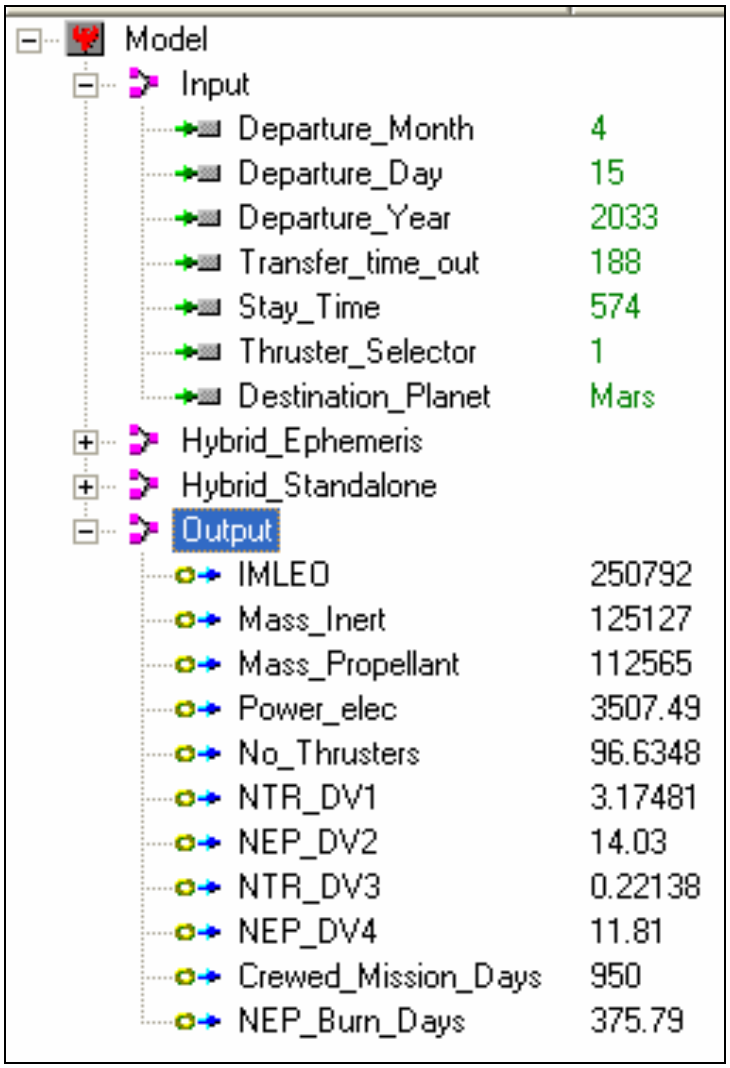

Figure 3-11. ModelCenter Mission Architecture GUI

CHAPTER 4
TRADE STUDY RESULTS

Due to the breadth and depth of this mission analysis trade study, the data analysis phase of the investigation was divided between three main areas: ephemeris analysis, vehicle architecture analysis, and tradespace assessment. The ephemeris analysis utilized the ephemeris tools in order to model the energy requirements for the three major vehicle systems based upon departure dates and mission duration. The vehicle architecture analysis determined performance parameters of the power and propulsion systems for these missions. The tradespace assessment then used these results to assess the entire tradespace matrix based on pre-determined MOEs.

The ability to create the parametric and carpet plots that were needed for the data analysis and tradespace analysis to follow were done using the time-saving functionality inherent to ModelCenter. ModelCenter's data analysis toolbar was used to set various parameters for plotting, producing multiple charts for different types of interpretation. Figure 4-1 shows the actual ModelCenter Toolbar with intuitive buttons for each data analysis option, along with four examples of plots that can be generated, including carpet, contour, surface, and statistical dependence plots.

Ephemeris Analysis

One of the key steps in performing mission analysis is using ephemeris tools to determine system energy requirements for a desired mission. Although the energy requirements for the specific reference mission profiles were needed to assess the tradespace matrix, it was desired to first derive some more general ephemeris results from the models created in this study for the NTR, NEP, and Hybrid vehicles.

The single most important parameter to be obtained from the ephemeris models was the delta-V value, which is essentially a requirement on how much energy will be needed by the

propulsion system. This requirement will determine how much propellant must be carried on board in order to get the useful hardware to its destination in space. The analysis to follow will allow one to see how this delta-V parameter is dependent on other variables such as stay time, transfer time, and departure date, the effects of which are determined by celestial mechanics.

The following plots attest to the capabilities of both the ephemeris models developed for this study using legacy NASA codes, and the ModelCenter software tool used to run the ephemeris models. Their presentation is separated between departure and duration categories, which refer to whether the delta-V parameter was plotted against the departure year and month, or versus transfer and stay time.

NTR

Departure

The LEO departure date is one of the major factors in determining delta-V values with ephemeris models. This is why the departure year, month, and day were all used in the process of trying to find the optimal time to leave the Earth. The idea of the synodic periods for each planet can be visualized in Figure 4-2 as a wave-like pattern is seen for the delta-V values over a range of 15 years. The peaks and valleys of each curve represent the cyclical nature of the location of the Earth relative to each destination planet over time. It can be seen that the number of cycles is directly proportional to the distance from Earth, giving more minimum-energy opportunities to Mars, and less to Saturn. Note that the data seen in this plot, and similar ones to follow, assumes a transfer time of 200 days for Mars, and 1000 days for both Jupiter and Saturn, with a 500-day stay at all planets.

Contour plots were also created to assess how the delta-V energy requirements were affected by both departure month and year. Figure 4-3 shows the dependence of the energy requirement on both of these parameters, where the color legend in the upper right-hand corner

relates delta-V values in units of (km/s) to the colored lines seen on the plot. This plot indicates that any year and month between the two green curves in the upper left-hand area would be the optimal time of departure. The range of values for delta-V based on all results is between 39.1 and 109.8 (km/s), though changing the stay and transfer time would certainly provide flexibility in further optimizing these results.

The Saturn and Jupiter contour plots could not be created for the NTR model using the IPREP ephemeris code. Consistent with prior knowledge of this code, the simulations seemed to break down at these more distant planets and years, specifically with Saturn, and at years after 2042. This also meant that the optimizer tool could not be used to optimize the Jupiter and Saturn reference missions, thus they had to be estimated using a manual optimization process.

Duration

In addition to departure date, the transfer time and stay time play a major part in determining energy requirements. Delta-V versus transfer time curves were plotted for all destination planets across a range of 200 to 1200 days, fully encompassing the ranges allowed for the reference missions. It can be seen in Figure 4-4 that the requirements for the Mars missions actually get more difficult after 300 transfer days, and the Jupiter and Saturn requirements get less difficult after approximately 400 days. This observation can again be related to the distance of each planet from the Earth and/or the sun. Note that the departure year used for the Mars analysis was 2031, while that for Jupiter and Saturn was 2041.

The delta-V values were also plotted against stay time to see how this parameter affects requirements. It can be seen from Figure 4-5 that each planet's curve has two valleys and one peak. This seems to support the idea of using conjunction and opposition-class missions since the valleys correspond relatively to the 40 to 60-day stay opposition-class missions, and the longer 400 to 600-day stay of the conjunction-class missions.

Next, the energy requirements for each planet were assessed separately using a surface plot to see the affects of both transfer time and stay time on delta-V. Figure 4-6 shows the results given a transfer time range of 100-300 days, and a 400-600 day stay time range. It appears the NTR system would have a very difficult time completing this mission at low transfer times that also have a short stay time, but will have a much simpler mission at all other transfer and stay times.

Jupiter's surface plot shows a delta-V assessment given transfer times of 1000 to 1200 days and stay times between 400 and 600 days. This plot, seen in Figure 4-7, shows much more variation in energy requirements across the transfer and stay time ranges along with a more even influence of either independent parameter on delta-V.

Saturn's contour plot in Figure 4-8 reveals much smoother curves than that of Jupiter's when plotted over the same transfer and stay time ranges. However, similar patterns are seen between the areas of maximum and minimum delta-Vs. Jupiter's optimum point for the specific departure date used is around 900 days for the transfer and 500 days for the stay time. Saturn's optimal mission profile is around 1150 transfer days and 500 stay days for the same departure date as Jupiter.

NEP

Departure

The NEP mission profile analysis plots were obtained just as they were for the NTR ephemeris model, with expected variations to be seen due to the different type of propulsion system. The delta-V versus departure year plot seen in Figure 4-9 shows both similarities and differences compared to the comparable NTR plot. A similar synodical pattern is seen in the Mars curve, which has exactly six peaks, just as in the NTR curve. The Jupiter and Saturn curves, however, appear somewhat different, as only one peak and valley can be seen for each.

This may be due to the fact that the NEP system has less propulsive power and will be accelerating much slower to its destination, thus increasing the periods of the curves of these more distant planets.

The contour plot of delta-V vs. departure month and year for Mars is shown in Figure 4-10. It can be seen that the optimal departure is in the early months of 2031 and a bit later in the year 2033, representing the Earth-Mars 2.13 year synodic period. The delta-V values range from 40.2 to 99.7 (km/s) at these departure dates.

The departure contour plot for Jupiter can be seen in Figure 4-11. This plot shows a much larger relative area of optimal energy requirement as compared to the Mars plot. This is in agreement to the earlier finding that there are more cycles over time in the Jupiter and Saturn curves versus Mars for the same range in years. This plot serves to portray the 1.09 year Earth-Jupiter synodic period, as similar delta-V minimums and maximums are repeated just over every 12 months. However, it is apparent from the high delta-V results ranging from 73.6 to 133.4 (km/s), that further optimization of mission parameters would be needed to make this flight practical.

The Saturn contour plot in Figure 4-12 shows the trend seen in the Jupiter plot even more clearly as much less variation is seen for delta-V requirements over the range in dates plotted. Most of the plot reveals an area of optimal departure dates, while only the lower left-hand corner shows departures dates of high delta-V. Again, the synodic cycle of 1.03 years can be seen as the delta-V values repeat just about every year. The delta-V values for the Saturn mission are the highest, ranging from 126.4 to 169.6 (km/s).

Duration

The dependence of delta-V on transfer time for the NEP missions can be seen in Figure 4-13. In comparison to the NTR plot, this plot shows fewer peaks in delta-V across the spectrum

of transfer days. The Mars delta-V again sees a large increase after 400 transfer days, but the Saturn and Jupiter missions don't seem to be optimal until after their first peaks around 650 transfer days.

Figure 4-14 shows a plot of delta-V versus stay time. Although the NTR plot showed one prominent peak for each of the three curves, the NEP plot shows somewhat different profiles. Mars still has a central peak, but a much lower delta-V valley in the upper stay time range. Jupiter has two separate peaks in the NEP plot, and Saturn has a flattened spectrum with one low peak and one shallow valley.

The surface plot in Figure 4-15 shows the Mars delta-V profile for the 100 to 300- day transfer time range and 400 to 600-day stay time range. A more gradual slope downward as transfer time increases can be seen in this plot versus that for the NTR system.

Jupiter's contour plot, which is seen in Figure 4-16 has more variation than found in the Mars plot. It only shows a small area of minimum delta-V, primarily for missions with both long transfer and stay times.

Saturn's contour plot, seen in Figure 4-17, is similar to Jupiter's in that it has a peak area protruding close to the center of the 3-D mapping. It does, however, show a more sharply negative slope with larger regions of both optimal and poor delta-V requirements.

Hybrid

Departure

Although the Hybrid vehicle does utilize NTR bursts at the beginning of each of its escape and capture maneuvers, the longer EP burns result in Hybrid ephemeris results similar to those seen in the previous NEP analysis section. For instance, Figure 4-18 shows a cyclical delta-V pattern for Mars with six peaks, just as in the NEP plot. Jupiter's curve is also familiar, showing

mostly a low valley region between two peaks, while the Saturn curve is primarily flat, not having any apparent cyclical pattern.

Looking at Figure 4-19, the contour plot of delta-V vs. departure month and year for a Mars mission shows optimal departures according to the 2.13 year synodic period near the beginning of 2031 and 2033. This was the same trend found for the NEP vehicles, as could be expected. The range in delta-V values for the Hybrid system is between 37.9 and 127.5 (km/s), which has both higher and lower limits than the smaller NEP range, which was between 42.6 and 102.6 (km/s).

The contour plot for a Jupiter mission, shown in Figure 4-20, also gives more desirable delta-V values than the NEP vehicle. The delta-V range for the Hybrid system is between 52.8 and 146.8 (km/s), while that for the NEP system was between 113.6 and 171.1 (km/s). Just as in the NEP case, the Hybrid ephemeris plot shows that an optimal departure can be obtained for at least one month out of every year in the period between 2040 and 2045.

Saturn's contour plot, shown in Figure 4-21, reiterates the fact that there is little fluctuation in delta-V over the five-year time period analyzed. The optimal departure time for the Saturn missions is actually around mid-year each year between 2040 and 2045, being at a minimum delta-V between the 4^{th} and 8^{th} months. The range given for delta-V does not vary much from the NEP results, fluctuating between 120.0 and 158.2 (km/s) compared to the NEP range of 126.4 to 169.6 (km/s).

Duration

The Hybrid results for delta-V vs. transfer time, found in Figure 4-22, seem to provide the same general results as the NEP duration plots. The Mars curve shows a minimum energy region before 400 transfer days, and only returns to these optimal delta-V values around 650 transfer days. Despite small disturbances in slope, both the Jupiter and Saturn curves show a

continually downward trend in delta-V values until around 900 days, at which point the slopes begin to flatten out.

Comparing delta-V vs. stay time results found in Figure 4-23 with the comparable NEP plot also shows very similar results between the two. The same patterns are seen for each curve, with the Mars delta-V curve dipping between 400 and 600 days, the Jupiter curve having two peaks at either end, and the Saturn curve being relatively flat.

The effects of transfer and stay time on delta-V for a Hybrid mission to Mars can be seen in Figure 4-24. A more variable dependence on stay time can be seen for this Hybrid vehicle compared to the NEP vehicle. This is shown in the red delta-V area found in the first half of the stay time range. The NEP and Hybrid vehicle plots also have the similarity that both show a minimum delta-V at high transfer and short stay times.

Figure 4-25 shows much more variation in delta-V with changing stay and transfer times as compared to the Mars mission. This Jupiter mission shows high delta-V values at low transfer and high stay times, but seems to find optimal delta-V values above transfer times of 1000 days. In comparison to the NEP Jupiter mission, this delta-V plot again has much more variation and also has a wider range of opportunities for optimal mission delta-Vs.

The Saturn plot shown in Figure 4-26 reveals a surface plot with only minor folds. It is generally of a downward slope from low to high transfer times, and is much more dependent on transfer time than stay time. This is shown as the optimal delta-V areas are at higher transfer times given any stay duration.

Vehicle Architecture Analysis

Parametric performance plots of the vehicle models over a range of delta-V requirements were also found in this trade study in order to assess the overall capabilities of the vehicles. IMLEO sizing plots based on delta-V values were used to reveal the response of each system

model across a range of energy requirements. In this way, the system performance was revealed for any possible mission that would fall into the range of the energy parameter plotted, dismissing temporarily the focus on the specific design reference missions. In addition, these parametric plots may serve as points of validation for the system models to be compared against other models in previously completed or future studies.

Parametric plots tailored to the design of each specific vehicle architecture were also generated in order to draw upon parameters that best characterize each system. For example, trades within the NTR category were on fuel type, while the trade was on electric thruster type for the NEP and Hybrid vehicles. The NTR results also include a plot of burn time, as this is a calculated value in the NTR vehicle model. Burn time, however, is an input to the NEP model, and was thus included as an independent variable in an IMLEO plot. The plot that was unique to the Hybrid model was an IMLEO surface plot that had both NTR and NEP delta-V requirements as independent variables. It was hoped that the results provided through the fuel and thruster trades, along with the vehicle-specific plots, help further reveal the capabilities of each of the vehicle configurations.

NTR

The main point of departure between the 5 NTR configurations was the type of nuclear fuel used in the reactor. The NTR vehicle architecture model was used in this analysis to assess any difference the different fuel types actually made on the overall size of the vehicle. Figure 4-27 reveals that there is little difference in the IMLEO between the fuel types for a total mission delta-V less than approximately 6 (km/s). This value, however, would still be less than the minimum required for a typical Mars mission.

Above this delta-V value, it appears the CERMET fuels perform the best until the carbide fuel outperforms the CERMET around a delta-V of about 10 (km/s). This finding is most likely

due to the heavier weight of the carbide fuel negating its performance at low delta-Vs, but then its superior propulsive properties showing its benefits given higher mission energy requirements. The relatively low propulsive performance parameters of the graphite and composite fuels make these vehicles the heaviest for all delta-V values above 6 (km/s). A sharply increasing slope in the IMLEO curve for graphite is evident around 11 (km/s) and for composite fuel around 12 (km/s), thus it is expected that they would reach their delta-V limits soon after.

The IMLEO values for each fuel were also found for a singular mission to Mars that had a total delta-V of 8 (km/s). This allowed for the opportunity to view the IMLEO of each fuel type side-by-side, as seen in Figure 4-28. The IMLEO is broken down between the propellant mass and the inert mass to give an idea of the split between the two, and to compare the relative amount of propellant to total IMLEO between fuel types. For instance, it can be seen that the graphite vehicle has a higher relative amount of propellant mass to total IMLEO than does the carbide fuel, evidence of the better fuel performance of the carbide reactor.

Since the NTR model also calculated the burn time of the NTR at each of the escape and capture maneuvers, these values were plotted versus fuel type in Figure 4-29. The delta-V values used to estimate these burn segments were for an optimal Mars mission, with an Earth escape delta-V of 3.6 (km/s), planetary capture of 1.4 (km/s), planetary escape of 0.85 (km/s), and Earth capture of 1.46 (km/s). These burn times were directly calculated from the value of propellant for each burn, which is a function of delta-V, thus the relative heights of the bars are consistent with those seen in the previous figure of IMLEO versus fuel type. Although trajectory equations often use the assumption of instantaneous velocity changes at each burn, these results reveal that the NTR systems actually take between 0.5 and 3 hours for the completion of a single burn, with total mission burn times under 5 hours.

One of the other utilities of the vehicle models was in assessing the breakdown of IMLEO between all of the major vehicle components. As seen in Figure 4-30, the breakdown of the NTR graphite vehicle model for a singular Mars mission is in the following proportions: the reactor mass is 6% of IMLEO, fuel cell mass is 1%, TransHab and consumables are 16%, propellant is 55%, truss structure is 4%, RCS is 3%, and propellant tanks are 15%. Note that the reactor mass is actually a small percentage of the total IMLEO, and that the real effect of changing fuel type is in how the fuel performance affects the sizing of the propellant mass. In addition, this percentage actually represents the weight of two reactors, where only one is being used for propulsion, with the second for mere redundancy.

NEP

One of the dependent parameters unique to the NEP vehicle architecture model was the required thermal power. In the NTR and Hybrid models the maximum power was decided by the parameters of the fuel for the thermal rocket propulsive mode, and all were on the order of 320 (MWt). The actual thermal power required for the NEP system was much lower since it was only needed to provide electric power that drove the much lower-thrust electric thrusters. Figure 4-31 shows the required thermal power in (kWt) that is converted from the electric power requirement, and plots this power versus total mission delta-V. A spread in power requirements between the thruster types can be seen above approximately 15 (km/s). The ion thruster maintains a modest positively sloped curve, while the Hall and MPD thrusters show a sharp rise in delta-V beginning around 30 (km/s). The MPD and Hall thruster curves continue to overlap until about 37 (km/s) at which point the Hall curve shows an even more drastic increase in slope.

An examination of Figure 4-32 shows agreement between the effect of delta-V on IMLEO and on the power requirement, as similar trends can be seen. Above 30 (km/s), the IMLEO also begins to increase dramatically for the MPD and Hall thrusters. This serves to show how the

mission energy requirements based on trajectory not only affect the mass of the system, but also the power reactor requirements. It also asserts that the NEP vehicle model begins to fail first for the Hall and MPD thrusters, followed by the ion thruster system, as mission demands increase.

A specific Mars mission was also assessed for the NEP system in order to compare mass estimates based on the thruster selected. The opposition-class mission used for these data-points was based on transfer delta-Vs of 20 (km/s) each, and a burn time of 500 days in each direction. Figure 4-33 shows the very large difference in IMLEO between thruster types for a Mars mission of total delta-V equal to 40 (km/s). This is consistent with the previous plot, which asserts that the IMLEO spikes upwards for the Hall and MPD systems at large delta-V requirements. It also provides a glimpse of the results to be found for the tradespace matrix, which had missions to Jupiter and Saturn that both required much higher delta-V's than the case shown here.

In addition to the IMLEO dependence on delta-V, it was also desired to assess the level of dependence the IMLEO parameter had on the thruster burn time. For the NEP system, less thrusters and less propellant were needed to complete the same delta-V burn if it could be accomplished over a longer period of time. ModelCenter was thus used to generate a surface plot of the IMLEO versus burn time and delta-V, which can be seen in Figure 4-34. For the specific mission modeled in the run, it is found that the IMLEO has a 68% dependence on delta-V and a 32% dependence on burn time. These results are portrayed through the plot and attest to the significant dependence on burn duration for success of an NEP mission.

Lastly, a vehicle mass breakdown based on a Mars mission was generated for the NEP architecture using the more efficient ion thrusters. From Figure 4-35 it is found that the reactor comprises 5% of the total IMLEO, the thrusters are 9 % of the total, thermal components are 9%,

TransHab and consumables are 6%, propellant is 57%, truss structure is 5%, RCS is 3%, and propellant tanks are 6%.

Hybrid

The Hybrid vehicle architecture was expected to perform similarly to the NEP architecture due to the nature of the trade on electric thruster type. Confirmation of this is seen in Figure 4-36, which shows that the thruster curves for IMLEO versus delta-V have the same trends that they did for the comparable NEP plot. The ion thruster outperforms the MPD and Hall thrusters by a significant margin. The main difference, however, is that at the same delta-V values, the Hybrid plot gives IMLEO values around two to three times those of the NEP system. This is confirmation that, in order for the Hybrid system to be competitive, it must have significantly lower delta-V requirements placed on the electric thruster system. This relief may be granted by having the NTR engines onboard, taking responsibility for a portion of the total mission energy requirements.

A Mars conjunction-class mission was set up for the Hybrid vehicle in order to compare the IMLEO values of each thruster for a specific mission. The outbound and return NEP delta-Vs were 14.0 and 11.8 (km/s), while those for the NTR were 3.17 and 0.22 (km/s). Figure 4-37 reveals a gradual increase in mass for the mission when going from ion thrusters, to MPD, and then to Hall thrusters. Compared to the NEP results, it is found here that this mission was accomplished with less mass for all three thruster cases. It can be seen from both the NEP and Hybrid plots, however, that there is a relatively even split between propellant and inert mass for the ion system, but there is a higher proportion of propellant mass for the Hall thrusters, and a smaller proportion for the MPD thrusters in the Hybrid cases.

This effect of the NTR and NEP engine requirements on Hybrid vehicle performance can also be seen through the surface plot found in Figure 4-38. This plot shows the IMLEO of an ion

thruster Hybrid vehicle plotted against both NEP and NTR delta-V requirements. It was found by repeating this analysis for vehicles with MPD and Hall thrusters that the dependence on the NTR system did decrease. For example, the mission analyzed gave a 39% dependence on NTR delta-V vs. 61% dependence on NEP delta-V, while giving a 34% dependence for MPD vehicles and 33% for Hall thruster vehicles.

A breakdown of IMLEO mass for a typical Mars mission is given for the Hybrid system in Figure 4-39. This mission is seen to be less demanding for the Hybrid system than for the NEP system, as a lower overall IMLEO is found. The difference results in lower propellant mass and lower thruster and thermal mass percentages, but generates higher percentages for the propellant tanks and TransHab.

Tradespace Assessment

The utility of a tradespace assessment is in being able to take a set of systems that could all be used to satisfy a given scenario or objective, and determine which system will best achieve the desired end-result. The culminating phase of this study was thus to assess the mission architecture tradespace matrix in order to determine the best vehicle systems for the reference mission profiles. In order to accomplish this, all of the mission architecture models had to be run. This entailed optimizing the delta-V for each mission profile using the ephemeris models, and then running the vehicle architecture models with these optimized energy requirements. A metric had to then be derived to draw a connection between the vehicle architecture results and the overall ability of the vehicle system to satisfy the mission objectives. This metric can be seen as a way to 'wrap' all of a vehicle's attributes and performance parameters into one package that more simply represents the ability of the system to achieve the desired goal. This package was represented via a score that was used to rank each system in the desired categories.

In deriving a score to use for the tradespace assessment, it was important to first establish the measures of effectiveness. These MOEs serve as the standard for identifying successful solutions, as they can only be measured against the accomplishment of a mission.[48] Since they are often determined by the end-user of the proposed systems, MOEs can be seen as a 'wish-list' of the desired system attributes. For instance, two different systems may be suggested to best fulfill a mission given two different sets of MOEs, since a different type of system performance may be desirable based on the attributes established in each set. Deciding which system will best support a mission thus depends to some degree on the priorities of those who will use the system.

Although the MOEs are seen from the stakeholder's perspective as qualitative attributes, a quantifiable figure of merit was still needed in order to provide an assessment of the MOEs. This is where the real systems engineering task arose, as separate metrics had to be created using quantitative Measures of Performance (MOPs) to assess each MOE. The score associated with each MOE was then used in a metric to derive one score that determined the overall effectiveness of each system in completeing the assigned missions. These numerical scores were then translated into a relative assessment of the systems, relieving an outsider's concern for the internal details of the solution.[48] This allowed for a straight-forward assessment of the power and propulsion architectures based upon pre-determined needs, giving big-picture results of how well each system performed.

Methodology

Mission architecture analysis

The term 'mission architecture' has been previously defined as the application of a vehicle architecture configuration to the completion of a reference mission profile. Although the capabilities of both the ephemeris models and the vehicle architecture models has been previously explored, a discussion of their use in modeling specific missions has been saved until

this point. It was the assessment of the mission architectures that was needed to generate the performance parameters required for assigning scores in the tradespace matrix.

The first step in analyzing each mission architecture was to generate optimal delta-V energy requirements from the ephemeris models. This optimization was achieved through the use of the Darwin optimizer tool, which optimized a mission given a range on departure year and month, transfer time, and stay time at the planet. These ranges came directly from the reference mission profiles found in the tradespace matrix. It was pivotal that the optimal mission be found for each propulsion and power system so that one system would not have an unfair advantage over the other when comparing their results in the tradespace analysis. This is in essence why three ephemeris models were created for each of the three main vehicle architectures, since the models had to be able to handle the specifications of each unique system.

Due to the inclusion of the Darwin optimization tool in the ephemeris models, the mission optimization procedures became somewhat automated, reducing overall analysis time. The first step after opening one of the ephemeris models and inputting the destination was to update the stay time, transfer time, and departure month and date upper and lower bounds. These appeared as inputs in the ModelCenter GUI that employed simple pull-down selection menus so as to warrant off careless mistakes in inputs. The next step was to run the Darwin utility component that appeared as an icon in the ModelCenter viewing window. Once the utility stopped running after an optimization time of approximately 3-4 minutes, the output section in the GUI contained the resultant delta-V value of the optimal mission given the parameters that were set by the user. The snapshot tool was then selected and a listing in a cell-structured format similar to Excel was brought up on the screen allowing simple highlighting of the desired cells. The parameters that were selected to be included in the mission architecture database included the optimized

departure month and year, stay time, transfer time, delta-V, and also the burn time and spiral time for the electric thruster systems. This procedure then had to be repeated for the remaining mission profiles. Note that the same optimized mission profile parameters were used for all configurations within the NTR, NEP, and Hybrid systems since energy requirements did not vary based on fuel and thruster type.

The set of optimized mission requirements for each of the 12 missions corresponding to each of the 3 vehicles were then put into the appropriate vehicle model, and were run for all configurations. Since the optimization steps had been previously completed, each of the missions took only seconds to run. The immediate result to be noted was whether or not the vehicle was able to complete the mission under the 1000 (t) IMLEO limit discussed in the next section. If it did not, all other results were discarded. Missions that did satisfy this requirement resulted in recording of the vital vehicle parameters.

Determining MOE scores

In order to be able to assess which system best satisfied each mission, a metric able to handle the mission architecture results had to be defined. The MOE scores were used to rank the vehicles for each mission, for each planet, and for overall interplanetary travel. The 132 MOE scores appearing in the tradespace matrix were thus used to find the best system for each of the 12 mission profiles, for each of the 3 planetary destinations, and for one general interplanetary mission. These categories were broken down in order to represent different levels of flexibility in system design based on the required missions that engineers may need to design for in the future.

Although multiple missions were analyzed in the tradespace matrix, the same five MOEs were used to assess the systems for each reference mission profile. Based upon the capabilities

of the engineering models developed for this study, along with important measures of success found in past mission analysis studies, the MOEs were established as:

1. Mission completion
2. Launch costs
3. Crew safety
4. Vehicle complexity
5. Mission control operational costs

By designating these five attributes as the MOEs, they alone were used to determine the relative effectiveness of each system in satisfying the requirements of each mission scenario.

The first MOE, 'Mission Completion,' was a simple assessment of whether or not the vehicle architecture model was able to run given the ephemeris energy requirements. For some of the more energy-intensive missions, it was expected that the less powerful propulsion systems, notably the NEP systems, would not perform adequately. This could be seen by running the model and seeing if the IMLEO 'blows up,' or stated mathematically, goes towards infinity. As most interplanetary mission analysis done in the past has reported IMLEO estimates in the range of 100 to 500 (t), it was decided to set a modest cutoff limit of 1000 (t) for a vehicle to be considered to have completed the mission. Although the other MOE scores were based upon a percentage out of 100%, the score for MOE_1 was simply either a '1' for a system weighing less than 1000 (t), or a '0' for a system weighing greater than 1000 (t). Note that a '0' would nullify the results from the remaining four MOEs for that specific mission architecture, giving a 0% as the total MOE score.

The second MOE was 'Launch Cost', an attribute that was entirely based upon the IMLEO of the system to complete a mission. This was decided given the fact that most of the cost of

launching a spacecraft into orbit is based upon the mass of the useful spacecraft hardware and propellant that must get to orbit. Total launch cost estimates have been given around $2000/kg, where the actual launch vehicle launch cost will be about 60% of this value.[48] In order to generate a MOE_2 metric that gave a score as a percentage, a ratio of the IMLEO to the maximum possible IMLEO of 1000 (t) was used. This metric can be seen by Equation 4-1, where *IMLEO* is given in units of kilograms and is thus divided by 1000 in order to provide a ratio to the 1000 (t) limit.

$$MOE_2 = 1 - \frac{IMLEO/1000}{1000} \tag{4-1}$$

The third MOE of 'Crew Safety' was focused on how long the crew would remain in the transfer orbit within the tight constraints of the TransHab and subject to large radiation doses. A metric for crew safety was derived based upon the actual number of transfer days the crew was subject to ($transfer\_days$), the minimum number of days the model allowed for ($transfer\_\min$), and the range of transfer days the model considered ($transfer\_range$). This metric is given by Equation 4-2, where the minimum transfer was set as 100 days for Mars and 800 days for Jupiter and Saturn, and the range was 200 days for Mars and 400 days for Jupiter and Saturn.

$$MOE_3 = 1 - \frac{transfer\_days/transfer\_\min}{transfer\_range} \tag{4-2}$$

The least quantifiable MOE was the fourth in the list: 'Vehicle Complexity.' The complexity of the vehicle really came down to the choice of fuel for the NTR configurations and the electric thruster type for the NTR and Hybrid configurations. The complexity of these systems was thus given by the relative technology readiness level (TRL) of the different fuel and thruster types, as perceived by this researcher. The TRL was assessed based upon a

comprehensive understanding of past research and development, and current versus expected performance parameters of all the fuel and thruster options. A qualitative assessment of the TRL for each of the 11 systems was then equated with a percentage, resulting in each of the scores found in Table 4-1. Note that the Hybrid configuration scores were based upon the product of the BNTR CERMET fuel score and the electric thruster type score.

The final MOE established was 'Mission Control Operational Costs.' Just as the 'Launch Cost' MOE had to be related to something other than a dollar amount, the mission control costs also had to be related to a figure of merit from data analysis results that would relate to cost in the real world. It was decided to use the duration (in days) of the mission for this figure of merit. For each day that the spacecraft was being operated, mission control had to be available to control this operation and assess spacecraft health. The number of mission days included the days of interplanetary transfer, the stay time in which the spacecraft was in orbit at the destination planet, and for the case of the NEP vehicles, the duration of spiral escape and capture. This MOE is also significant to mission planners because although lower IMLEOs may be achieved from higher efficiency engines, these same engines may have to be in operation longer, equating to increased hardware and maintenance costs. The metric for this MOE is given by Equation 4-3, where $mission\_\max$ is an estimated value of the maximum possible duration of a mission, and was determined to be 2000 days for a Mars mission and 4000 days for a Jupiter or Saturn mission.

$$MOE_5 = 1 - \frac{mission\_days}{mission\_\max} \tag{4-3}$$

Tradespace Mission Architecture Results

In order to be able to perform the analysis of the tradespace matrix previously discussed, all of the parameters that were needed for the MOE metric had to be appropriately book-kept.

Ephemeris parameters that were included in the database for each of the 132 mission architectures included delta-V, transfer time, stay time, burn time, and spiral time. The major performance parameters from the vehicle architecture models that were also included were the IMLEO, propellant mass and operating power. All of these results can be found in Appendix B: Tradespace Mission Architecture Results.

The only vehicle performance parameter that was plotted based on the mission architecture analysis results was the IMLEO. It was felt that the IMLEO was the one true performance parameter that could be directly compared between systems and would provide useful information. For instance, the thrust to weight parameter that is typically used to define propulsion system performance could not be used to determine the best system out of the three main architectures since it was already known that electric thrusters provided a much smaller thrust to weight than thermal rockets. On the other hand, the ISP, or measure of thrust efficiency, is much higher for the electric propulsion systems than for the thermal rockets. Thus, on a parameter -to-parameter level, it is only truly useful to get a glimpse of the overall system performance by comparing the direct weight differences of the systems by their IMLEO values.

The results of running each of the mission architectures in the tradespace matrix revealed the result that none of the three architectures could complete the Jupiter or Saturn missions under the designated IMLEO limitation of 1 million (kg). Within the Mars reference missions, only the Hybrid vehicle with ion thrusters could complete an opposition-class mission, doing so with an IMLEO of 472 (t). Nine of the eleven vehicle configurations were able to complete the fast transfer conjunction-class Mars mission, and all eleven vehicles completed the slow transfer conjunction class-mission. Since the only significant results come from a comparison of

completed Mars missions, the results from these missions are presented side-by-side in Figure 4-40.

In examining this figure, it is seen that there is very little difference between the slow and fast transfer conjunction IMLEO results for the NTR configurations. This results from the very similar delta-V energy requirements for both missions, despite the longer transfer times allowed for the slow transfer missions. The Hybrid and NEP configurations are much more affected by the transfer durations, as shown by the much higher IMLEO values for the fast transfer conjunction missions. It can be seen in the figure that two of the NEP configurations couldn't even complete these missions with a reasonable mass. Only the Hybrid ion vehicle could complete the opposition slow transfer mission. These results reinforce the idea that NEP and Hybrid vehicles will be much more affected by transfer time as compared to NTR vehicles due to their much lower thrust capabilities.

Tradespace MOE Results

After the mission architectures were run, the MOE scores were compiled for the tradespace matrix. These scores all appear in Table 4-2. The mission architectures that have a 0% MOE score are those that could not be completed, as previously mentioned.

The MOE scores for the completed Mars missions, which represent the overall capability of each vehicle configuration to complete the desired mission, can be seen plotted in Figure 4-41. The scores for these missions range from 40.67% for a Hybrid ion vehicle opposition-class mission, to a high of 68.67% for a BNTR CERMET vehicle conjunction-class mission. Although the IMLEO results for the NTR configurations were similar, the MOE scores are much higher for the faster transfer missions, as compared to the slower missions. This contests that other important concerns besides IMLEO, such as the amount of time astronauts spend in space, become important factors when assessing mission architectures. The Hybrid and NEP results

reveal that the fast transfers are better for the ion thruster systems, but MPD and Hall configurations would perform better for slow transfers. It can also be seen that the Hybrid ion configuration is robust, in that it completes the most missions, but the NTR vehicles have higher scores for specific missions.

Based upon these MOE score results, the systems were ranked in order of decreasing performance from 1 to 11. Table 4-3 gives the rankings for each vehicle based on each of the four Mars missions. The Hybrid ion configuration has been given the rank of '1' for the opposition-class mission since it was the only vehicle that successfully completed this mission. For the conjunction-class missions, it is seen that the NTR CERMET, carbide, and composite configurations rank higher than the Hybrid ion configuration.

Since there were no Jupiter or Saturn missions completed, the planet-specific and overall rankings were exactly the same, with the overall rankings being the same as those for the Mars missions. Table 4-4 gives these results, wherein the MOE scores across the board were averaged and then ranked. It can be seen that the Hybrid ion vehicle takes the highest ranking, followed closely by the CERMET, carbide, composite, and graphite NTR configurations, respectively. The NEP configuration with ion thrusters obtained the next highest ranking, followed by the Hybrid and then the NEP MPD and Hall thruster configurations.

By comparing the results from the mission-based and overall rankings, it can be gleaned that the same vehicle configuration will not necessarily excel for all types of missions. Although the Hybrid ion configuration received the top ranking for overall Mars missions, it would probably not be desirable to focus on this one vehicle for all types of Mars missions. It is clear that most of the NTR configurations actually outperform the Hybrid ion vehicle for the Mars conjunction-class missions, with the fast-transfer missions revealing much higher MOE scores

for the NTR systems. This seems to provide motivation for focusing more on specific missions to be performed, versus a specific vehicle to be used, when trying to determine the best power and propulsion system for interplanetary travel.

When examining these results it should be remembered that many of the vehicle configurations, most notably those with EP thrusters, were designed based on projected future operating parameters. These vehicles were compared to NTR configurations given current operating parameters that have already been proven in full-scale testing. In addition, all of the vehicle models in this study were very sensitive to ISP or efficiency values due to the nature of sizing propellant mass based on the rocket equation. It can thus be seen that the highest-ranking Hybrid ion vehicle may have appeared elsewhere in the ranking list if its ion thrusters were simply assigned less optimistic parameter values. This highlights one of the major difficulties in giving an honest comparison between power and propulsion systems, as preliminary system definition and vehicle design play a major role in how the results will stack up.

Table 4-1. MOE_4 TRL Score

System/Technology	MOE_4 Score
NTR/Graphite fuel	0.90
NTR/CERMET fuel	0.80
BNTR/CERMET fuel	0.80
NTR/Composite fuel	0.85
NTR/Carbide fuel	0.80
NEP/Ion	0.70
NEP/MPD	0.60
NEP/Hall	0.50
Hybrid/Cermet+Ion	0.8*0.7= 0.56
Hybrid/Cermet+MPD	0.8*0.6= 0.48
Hybrid/Cermet +Hall	0.8*0.5= 0.40

Table 4-2. Tradespace MOE Scores

Destination	MARS				Jupiter				Saturn			
Stay	Conjunc.		Oppos.		Conjunc.		Oppos.		Conjunc.		Oppos.	
Transfer	Fast	Slow	Fast	Slow	Fast	Slow	Fast	Slow	Fast	Slow	Fast	Slow
NTR (Graphite)	66.65%	54.38%	0%	0%	0%	0%	0%	0%	0%	0%	0%	0%
NTR (Composite)	67.63%	55.40%	0%	0%	0%	0%	0%	0%	0%	0%	0%	0%
NTR (Carbide)	68.01%	55.81%	0%	0%	0%	0%	0%	0%	0%	0%	0%	0%
NTR (CERMET)	68.45%	56.24%	0%	0%	0%	0%	0%	0%	0%	0%	0%	0%
BNTR (CERMET)	68.67%	56.49%	0%	0%	0%	0%	0%	0%	0%	0%	0%	0%
HYBRID (ION)	60.06%	54.81%	0%	40.67%	0%	0%	0%	0%	0%	0%	0%	0%
HYBRID (MPD)	52.69%	54.79%	0%	0%	0%	0%	0%	0%	0%	0%	0%	0%
HYBRID (Hall)	44.78%	52.29%	0%	0%	0%	0%	0%	0%	0%	0%	0%	0%
NEP (ION)	56.78%	52.01%	0%	0%	0%	0%	0%	0%	0%	0%	0%	0%
NEP (MPD)	0.00%	47.27%	0%	0%	0%	0%	0%	0%	0%	0%	0%	0%
NEP (Hall)	0.00%	42.17%	0%	0%	0%	0%	0%	0%	0%	0%	0%	0%

Table 4-3. Tradespace Mission-Based Rankings

Destination	MARS			
Stay	Conjunc.		Oppos.	
Transfer	Fast	Slow	Fast	Slow
NTR (Graphite)	5	7	-	-
NTR (Composite)	4	4	-	-
NTR (Carbide)	3	3	-	-
NTR (CERMET)	2	2	-	-
BNTR (CERMET)	1	1	-	-
HYBRID (ION)	6	5	-	1
HYBRID (MPD)	8	6	-	-
HYBRID (Hall)	9	8	-	-
NEP (ION)	7	9	-	-
NEP (MPD)	-	10	-	-
NEP (Hall)	-	11	-	-

Table 4-4. Tradespace Planet-Based and Overall Rankings

Destination	Mars
NTR (Graphite)	6
NTR (Composite)	5
NTR (Carbide)	4
NTR (CERMET)	3
BNTR (CERMET)	2
HYBRID (ION)	1
HYBRID (MPD)	8
HYBRID (Hall)	9
NEP (ION)	7
NEP (MPD)	10
NEP (Hall)	11

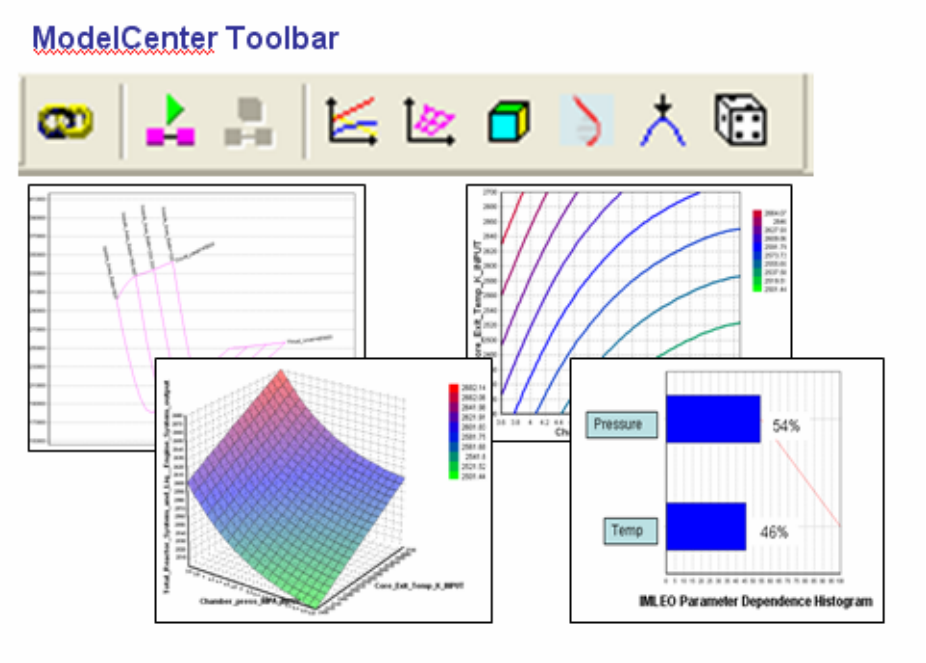

Figure 4-1. ModelCenter Parametric Tools

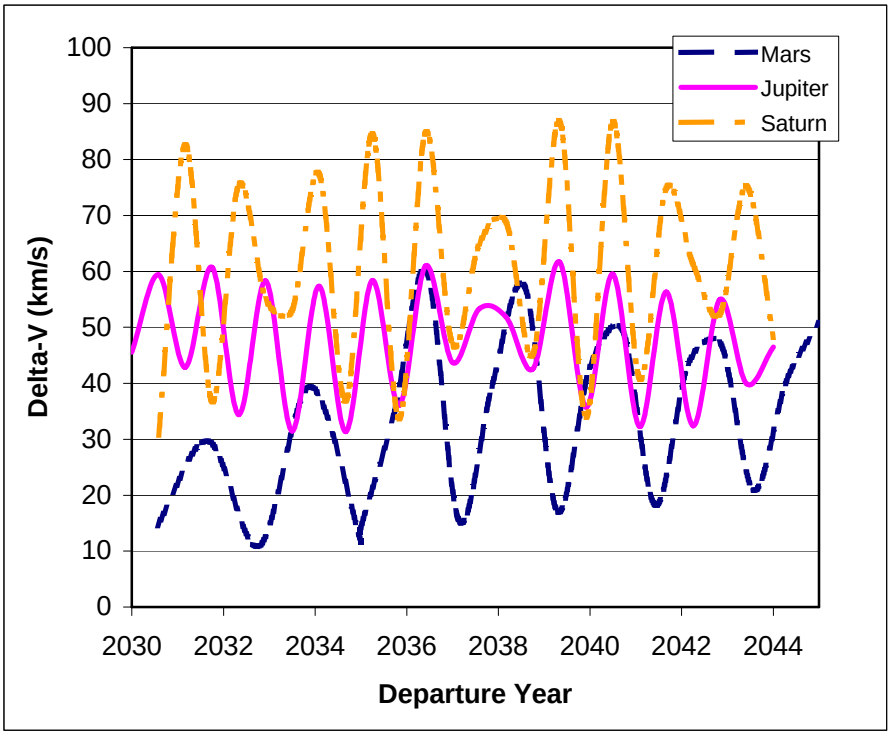

Figure 4-2. NTR Delta-V vs. Departure Year

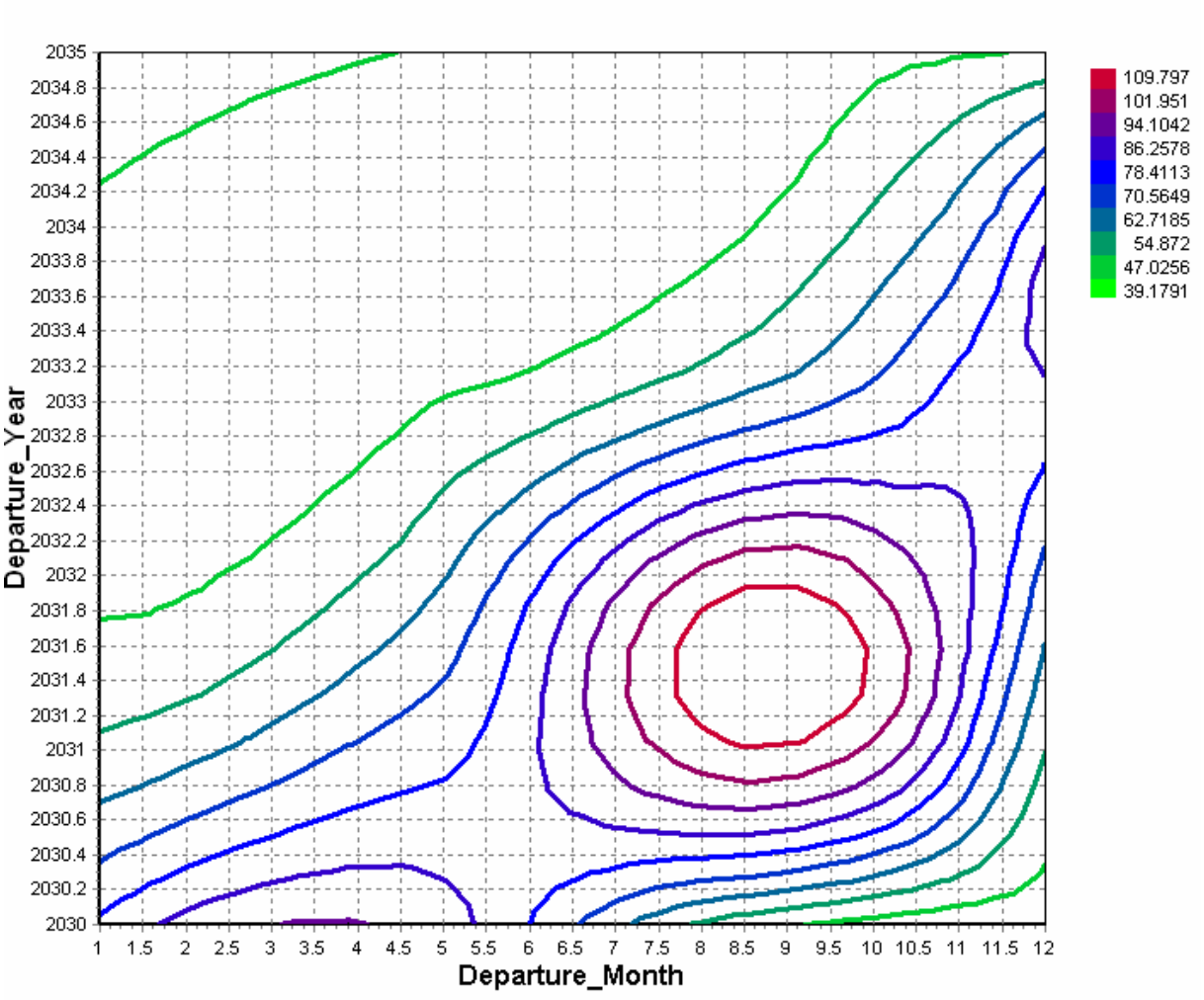

Figure 4-3. NTR Mars Delta-V vs. Departure Year and Month

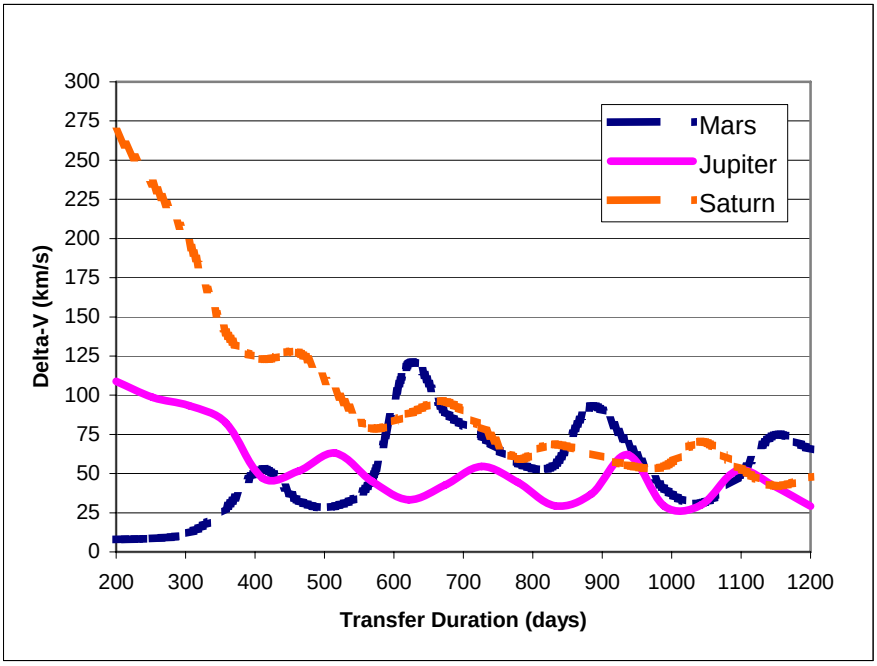

Figure 4-4. NTR Delta-V vs. Transfer Time

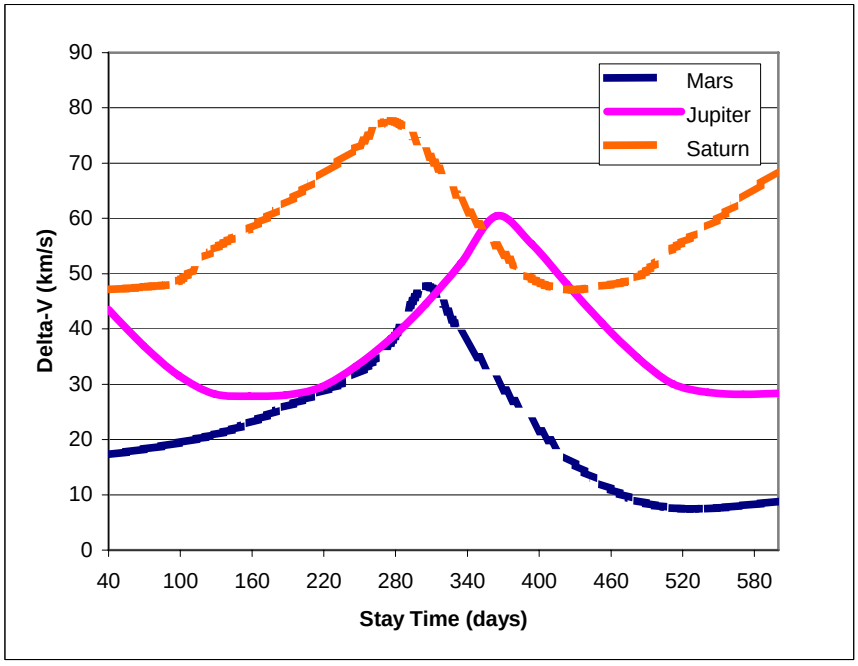

Figure 4-5. NTR Delta-V vs. Stay Time

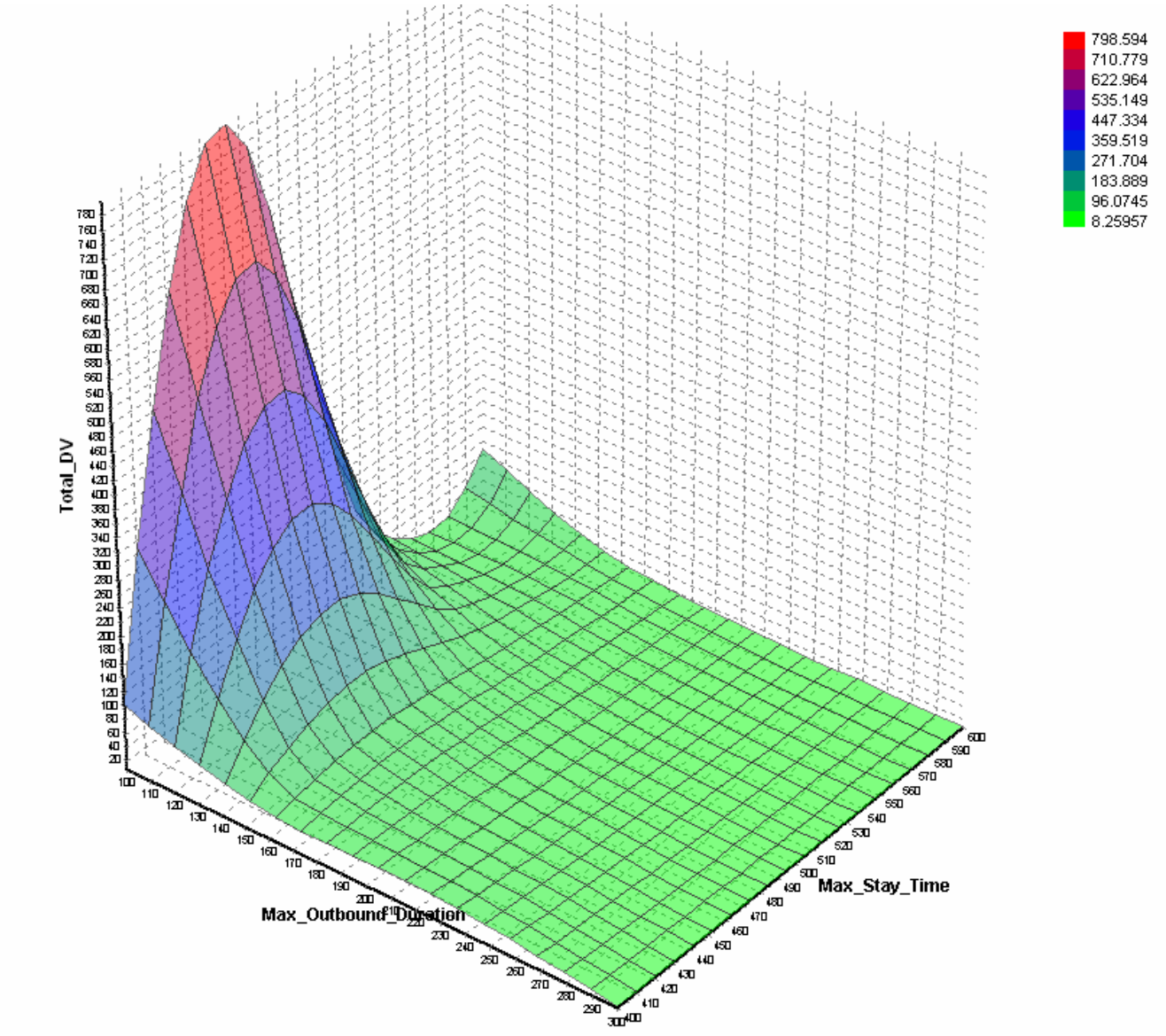

Figure 4-6. NTR Mars Delta-V vs. Transfer and Stay Time

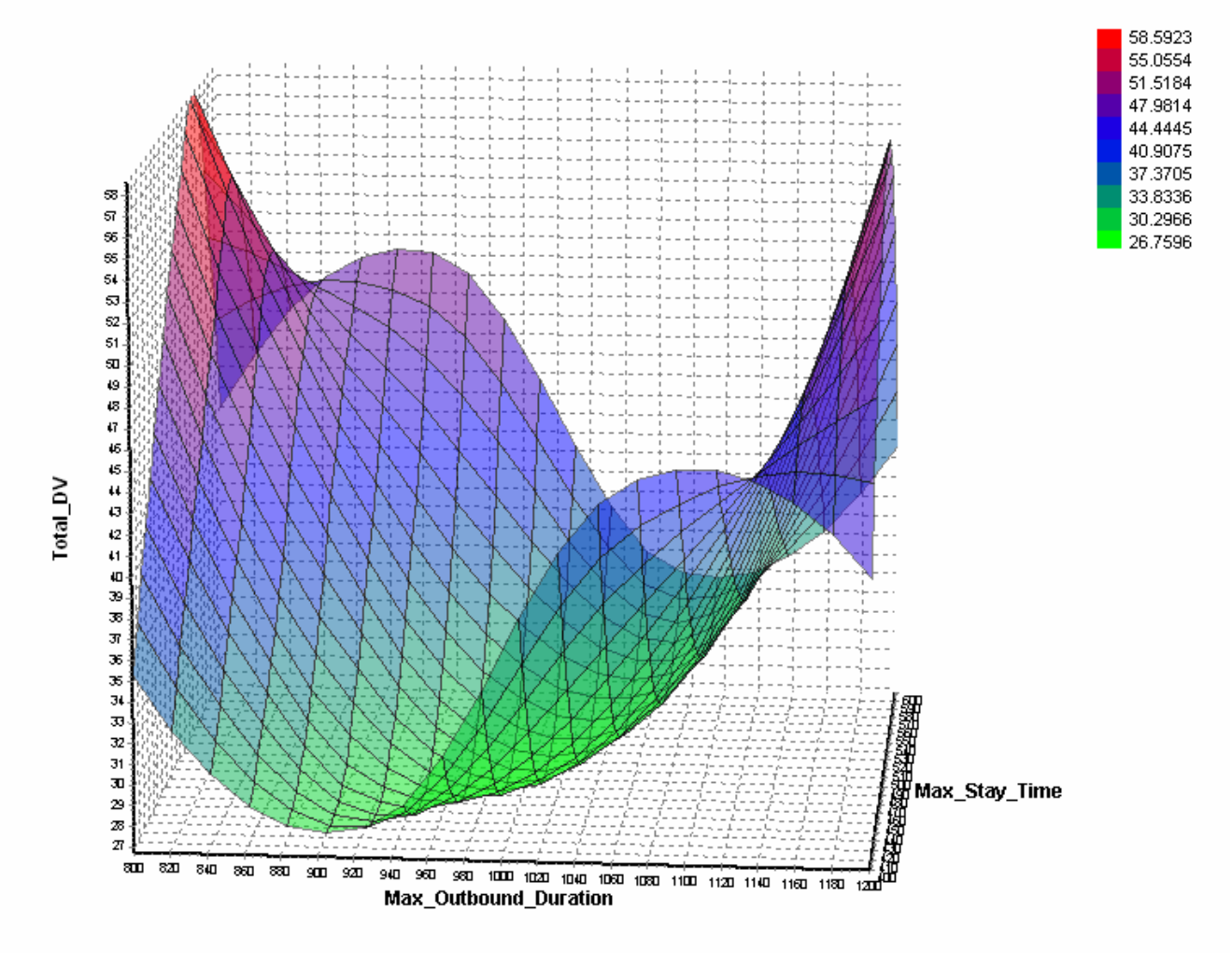

Figure 4-7. NTR Jupiter Delta-V vs. Transfer and Stay Time

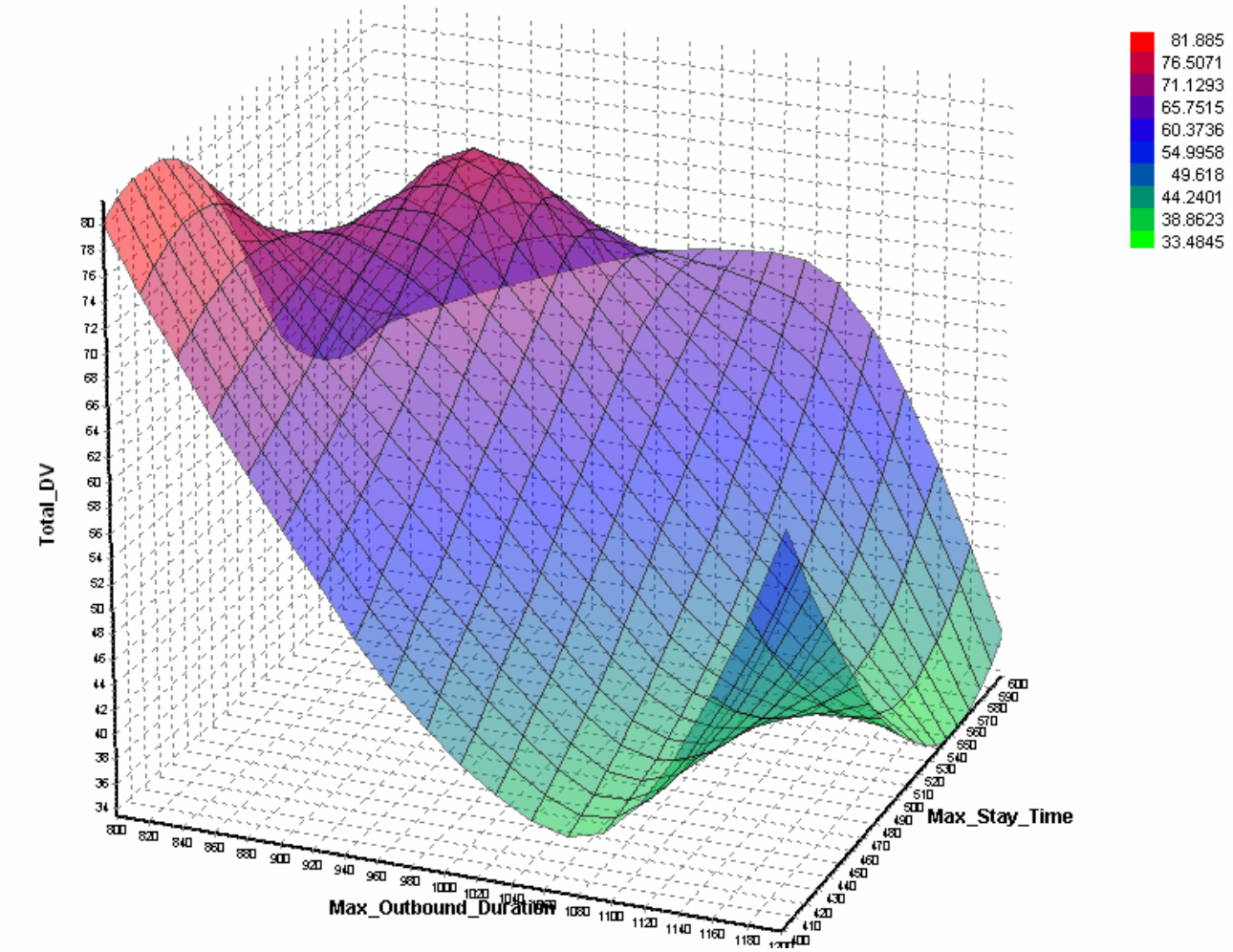

Figure 4-8. NTR Saturn Delta-V vs. Transfer and Stay Time

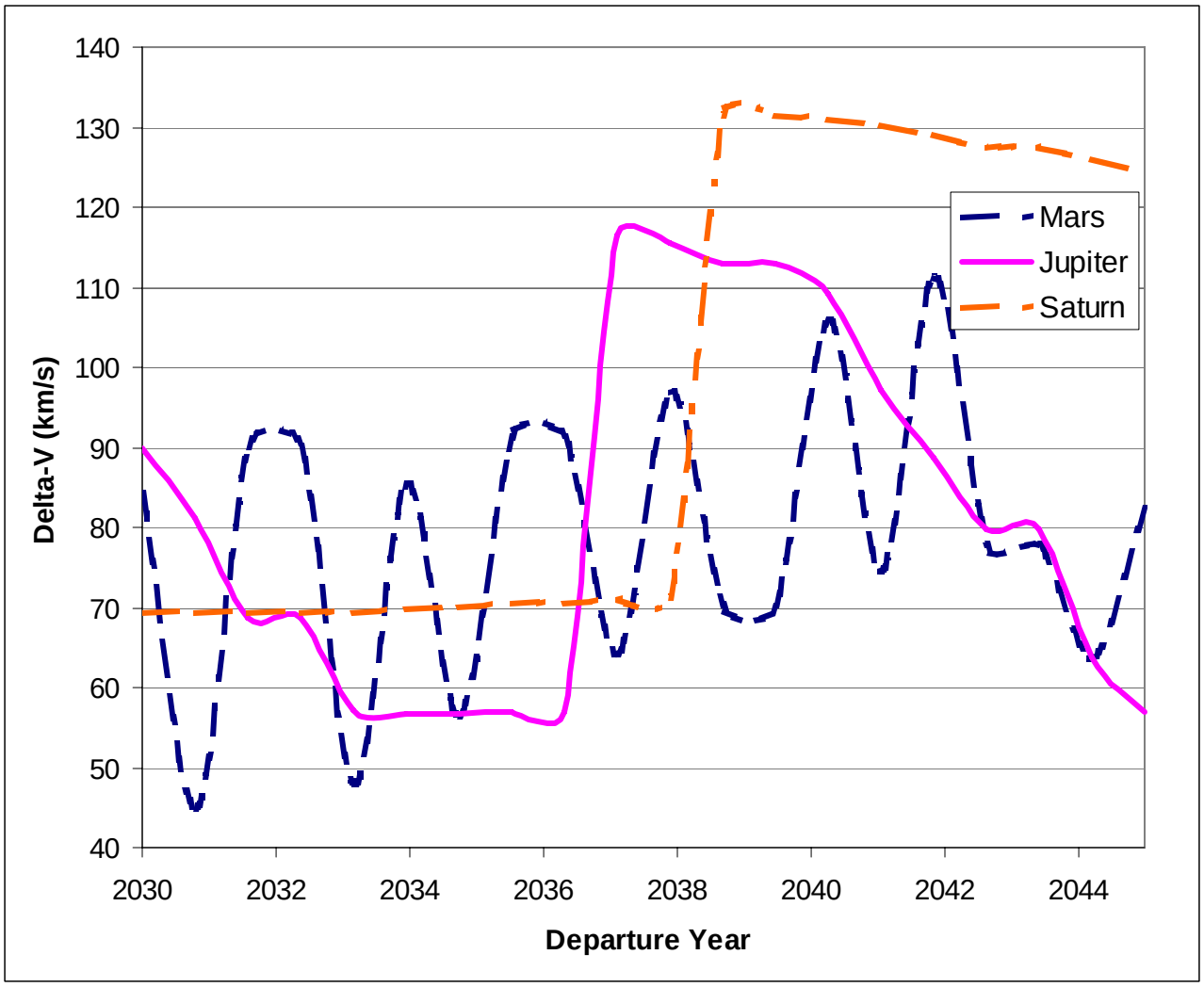

Figure 4-9. NEP Delta-V vs. Departure Year

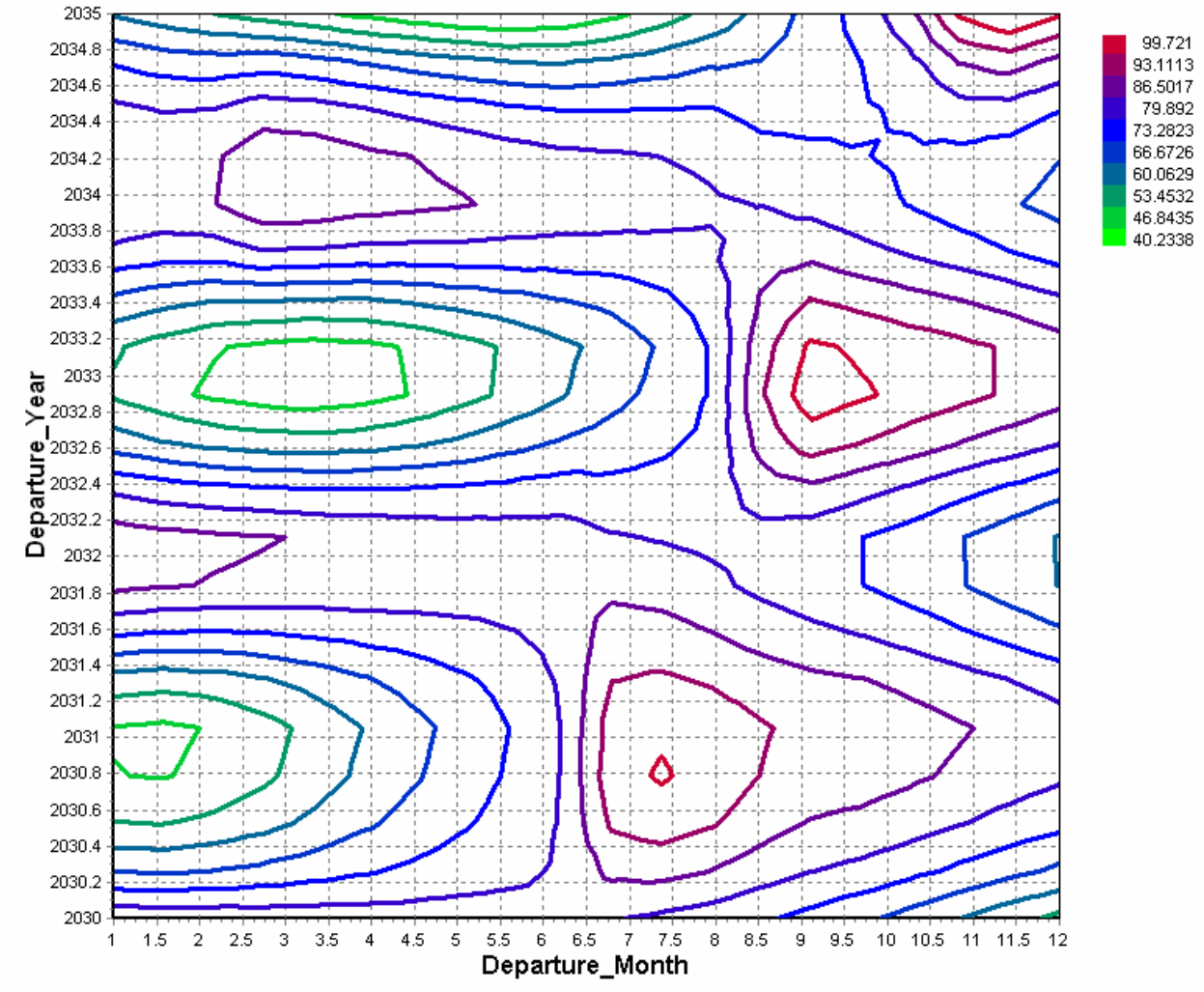

Figure 4-10. NEP Mars Delta-V vs. Departure Year and Month

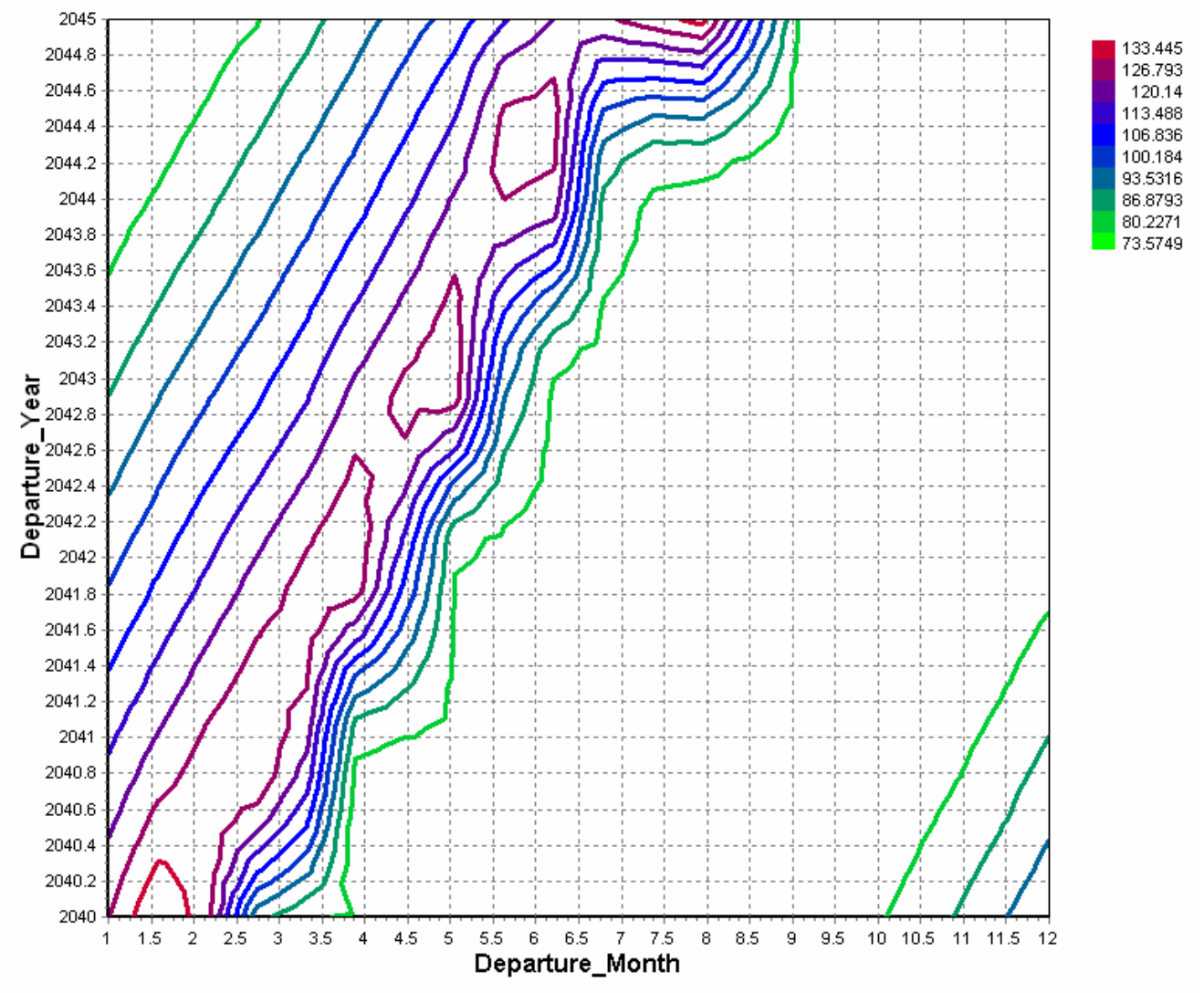

Figure 4-11. NEP Jupiter Delta-V vs. Departure Year and Month

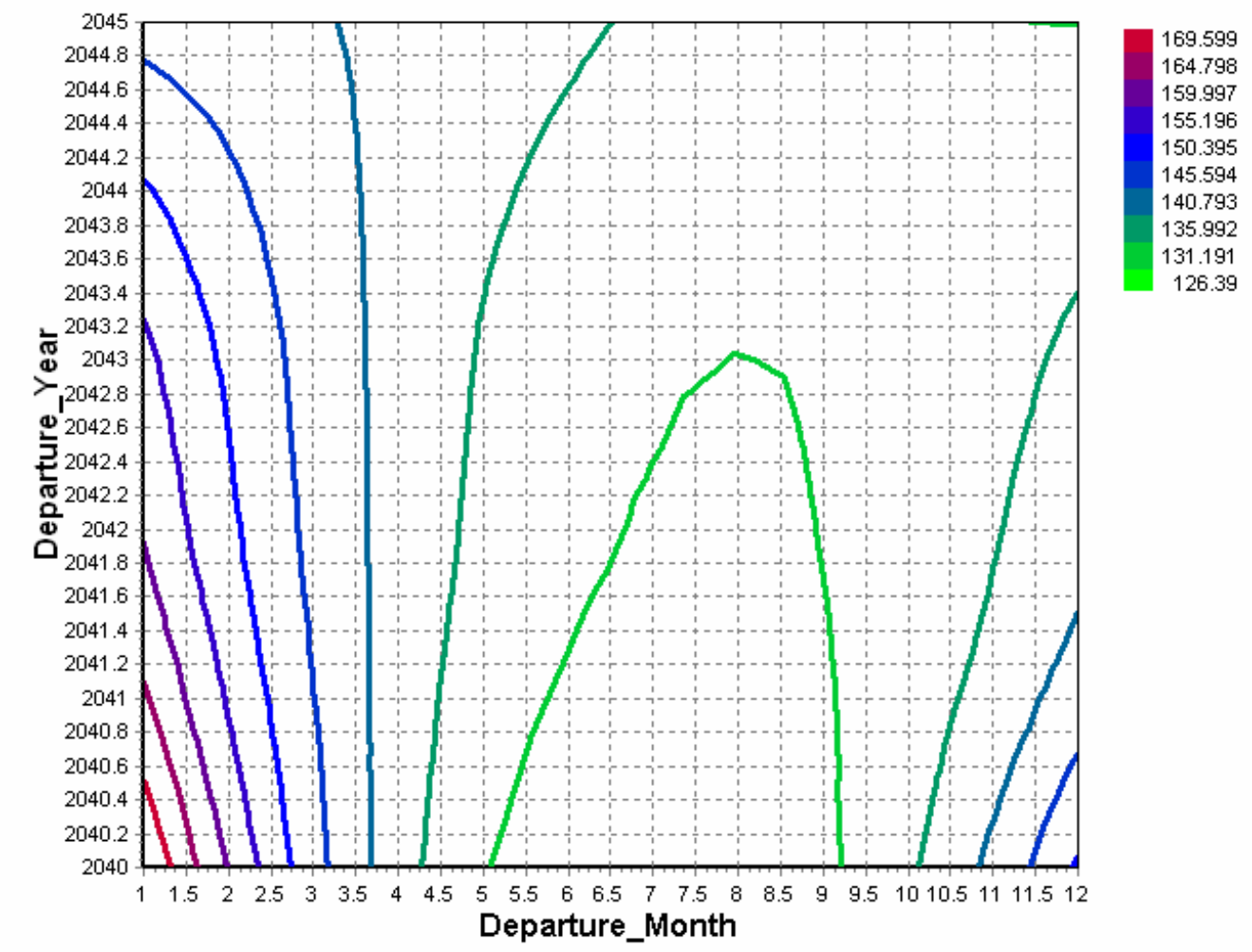

Figure 4-12. NEP Saturn Delta-V vs. Departure Year and Month

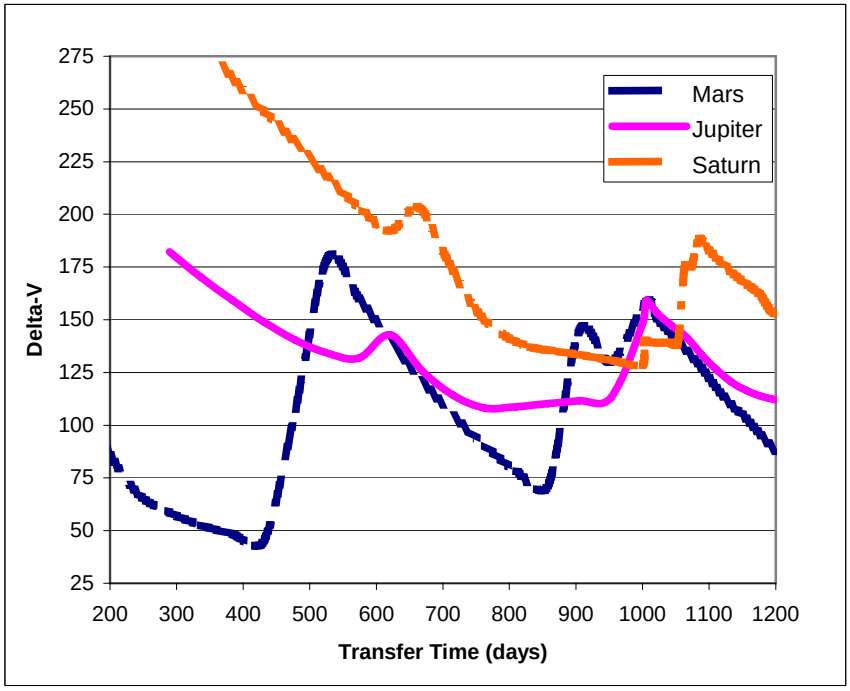

Figure 4-13. NEP Delta-V vs. Transfer Time

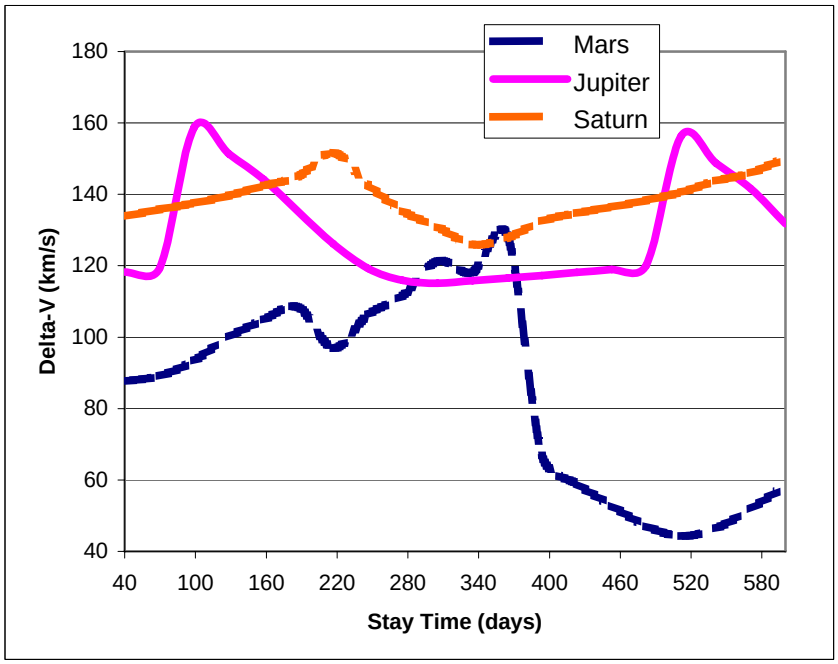

Figure 4-14. NEP Delta-V vs. Stay Time

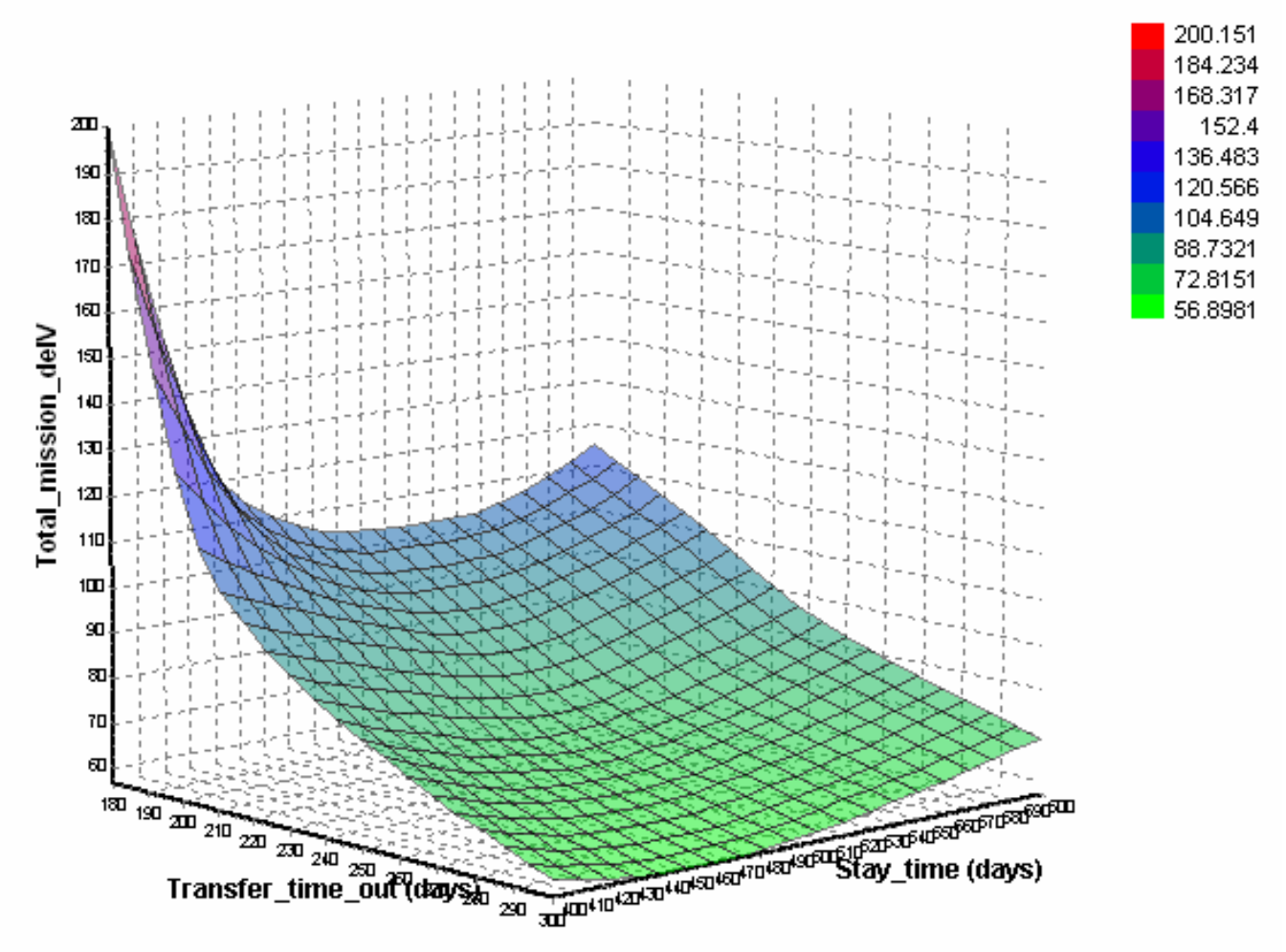

Figure 4-15. NEP Mars Delta-V vs. Transfer and Stay Time

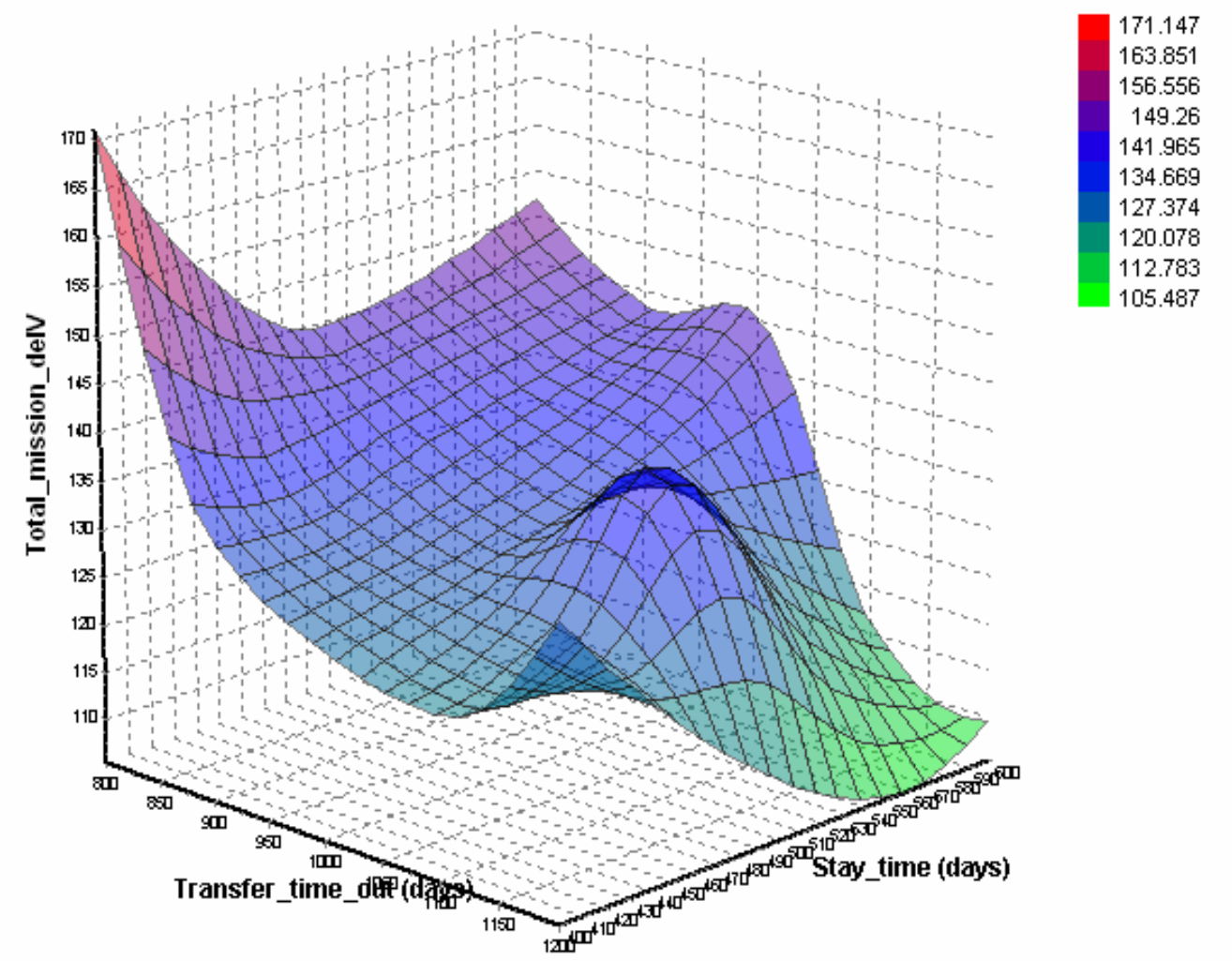

Figure 4-16. NEP Jupiter Delta-V vs. Transfer and Stay Time

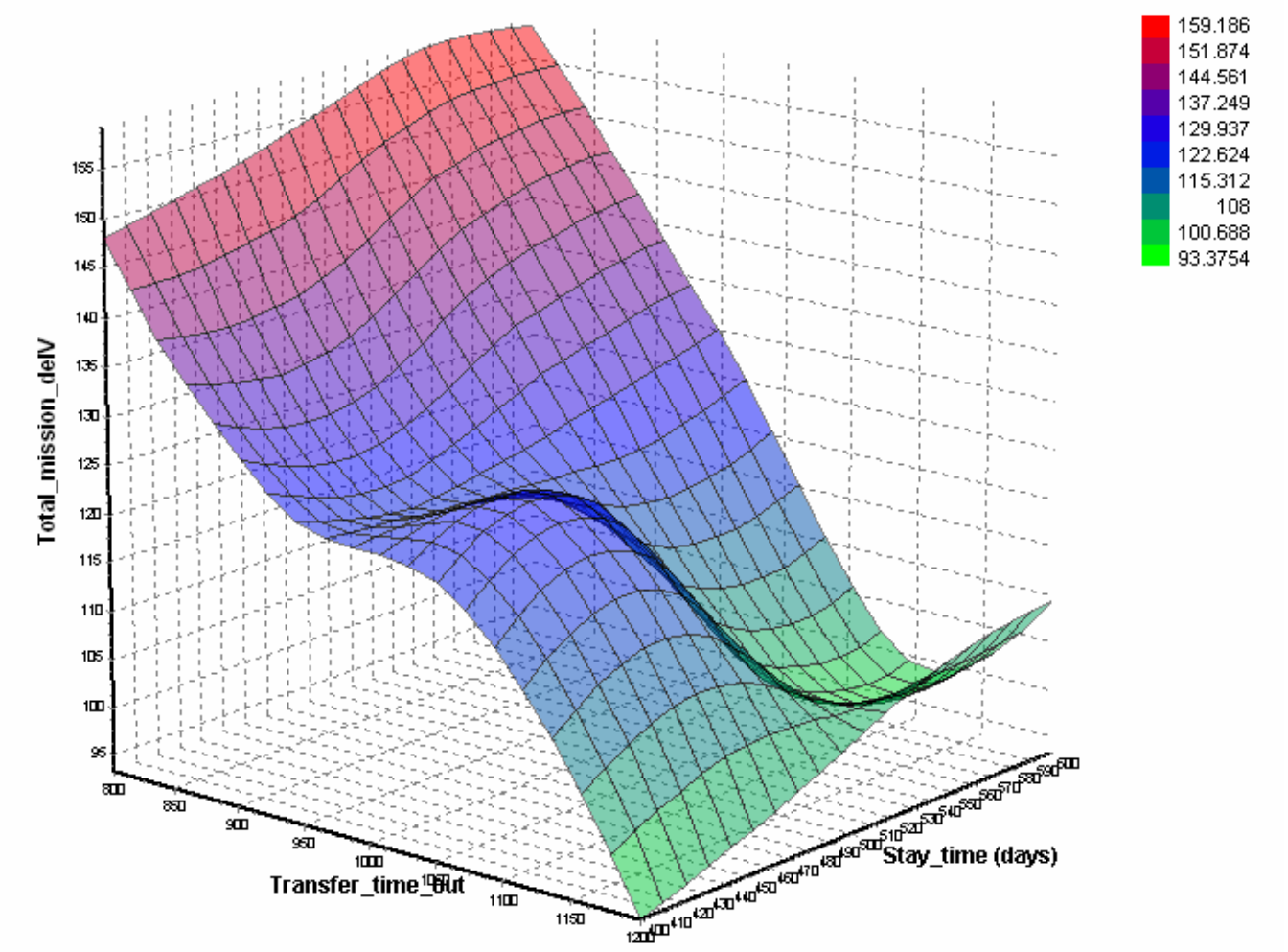

Figure 4-17. NEP Saturn Delta-V vs. Transfer and Stay Time

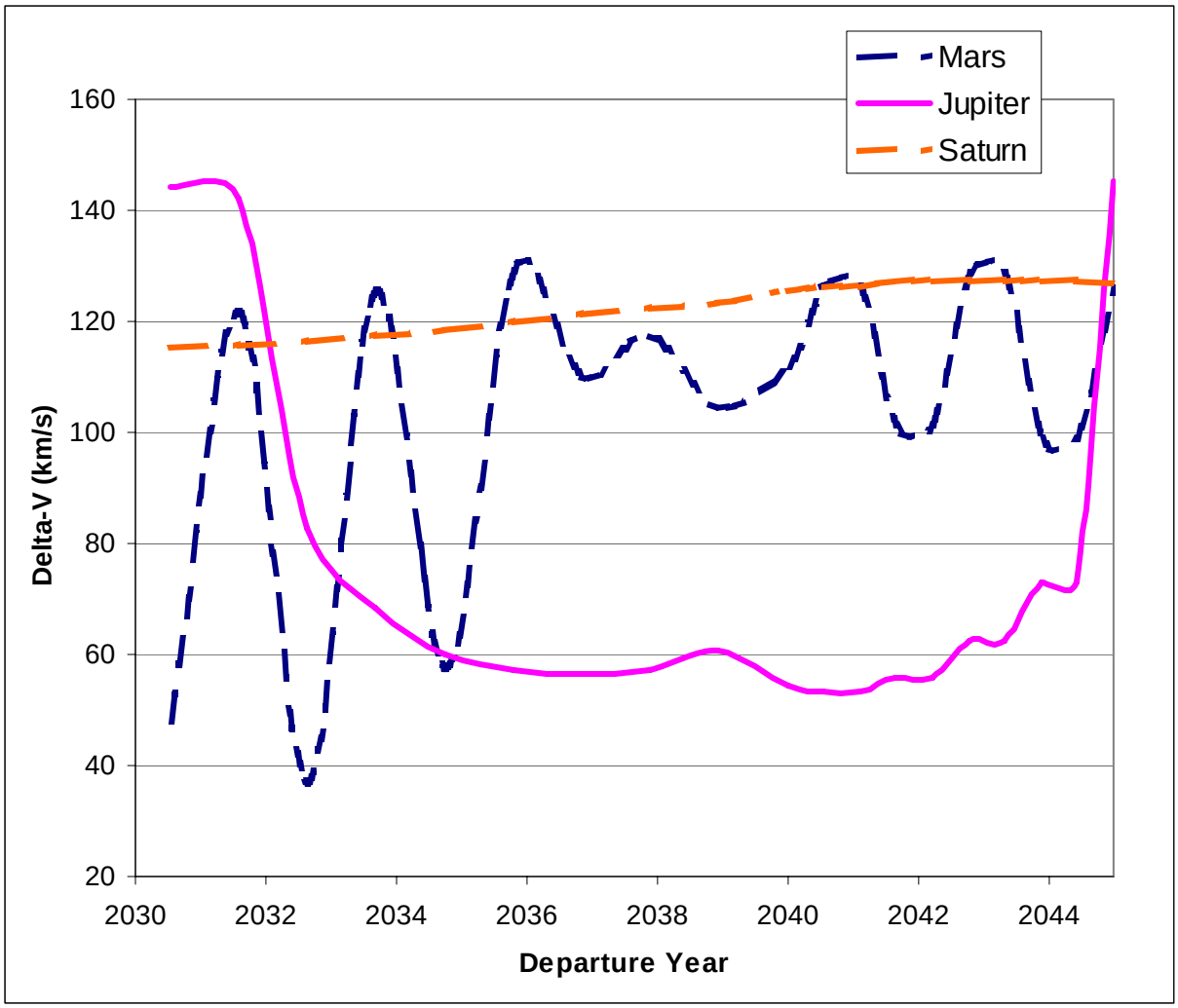

Figure 4-18. Hybrid Delta-V vs. Departure Year

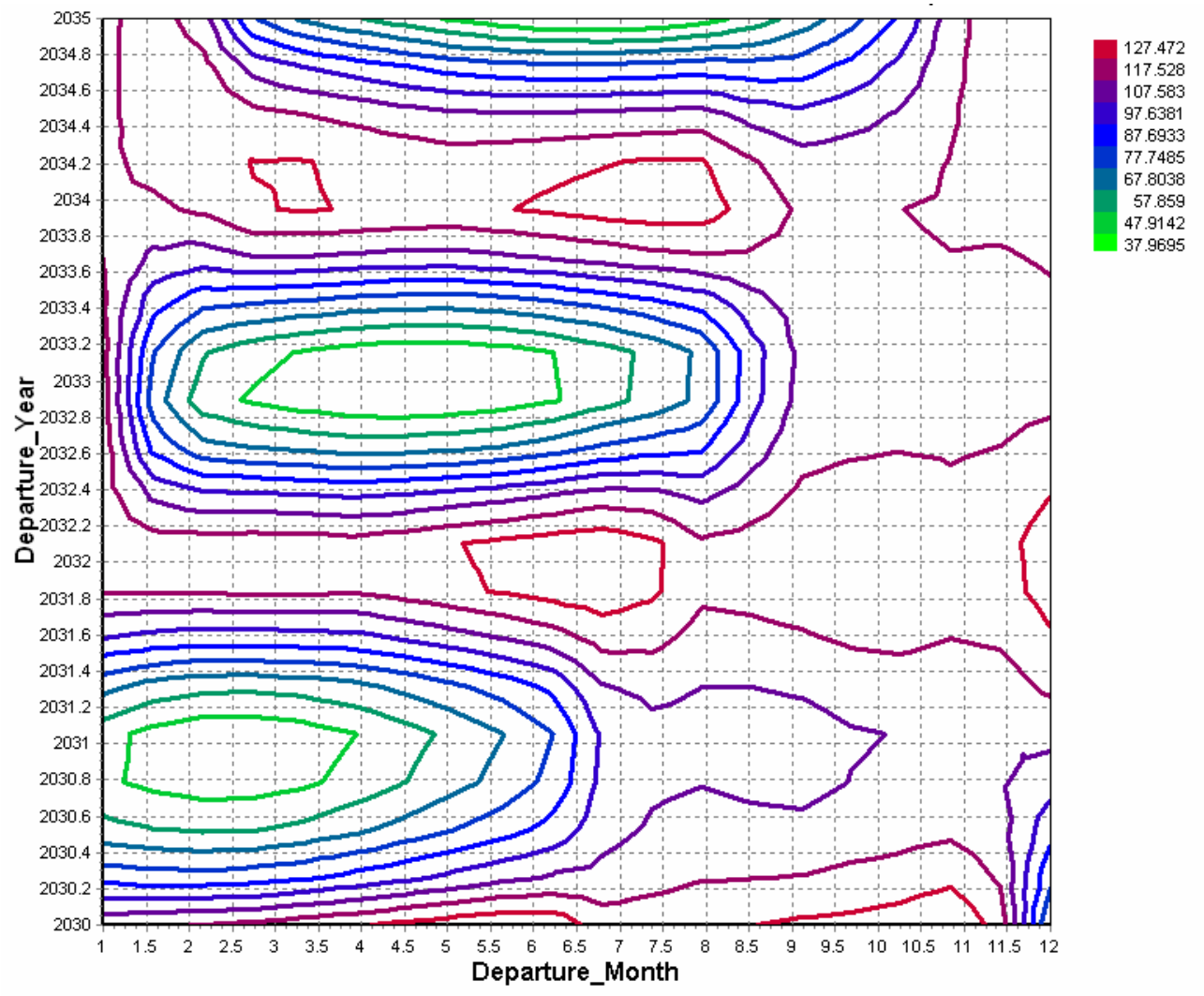

Figure 4-19. Hybrid Mars Delta-V vs. Departure Year and Month

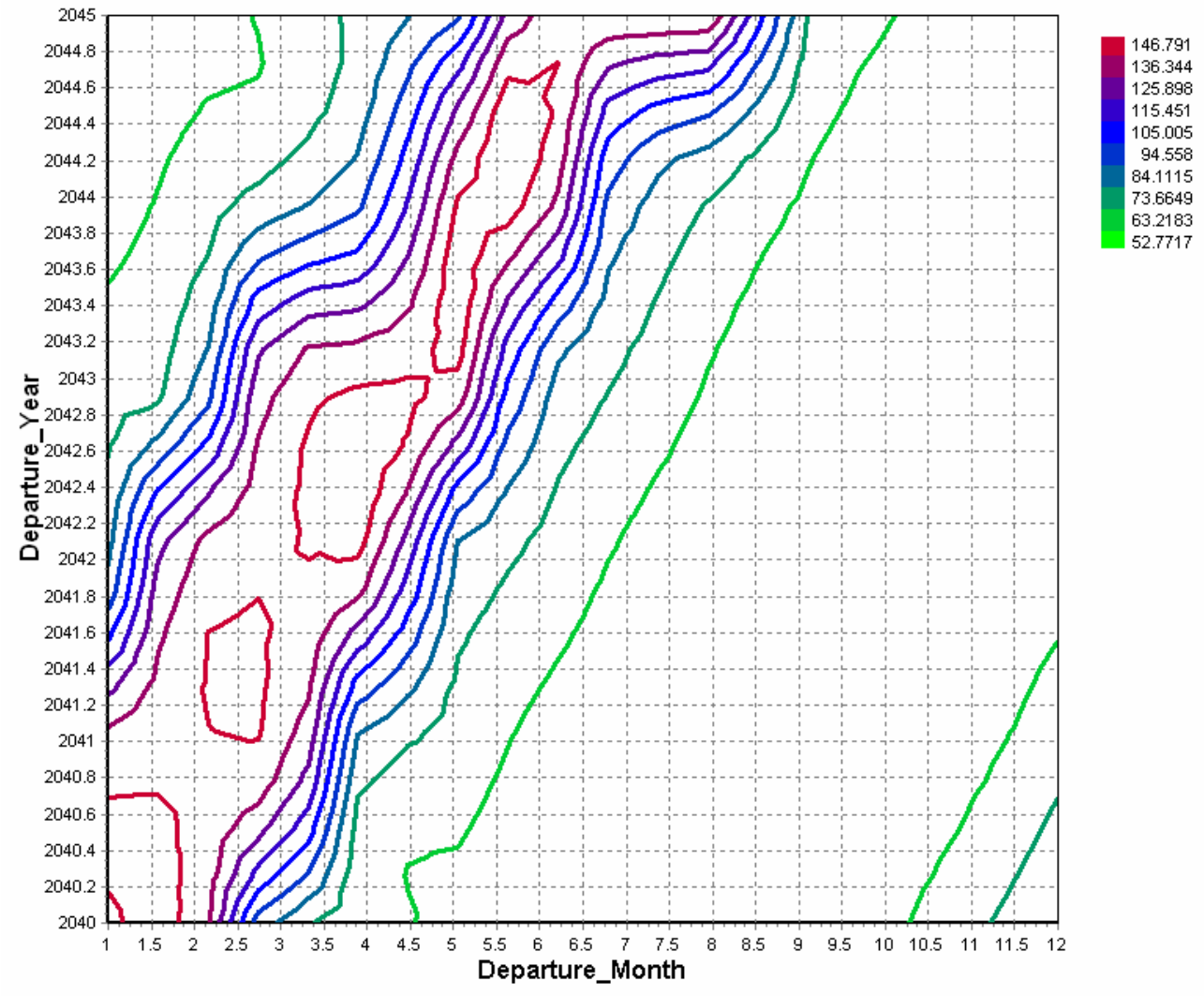

Figure 4-20. Hybrid Jupiter Delta-V vs. Departure Year and Month

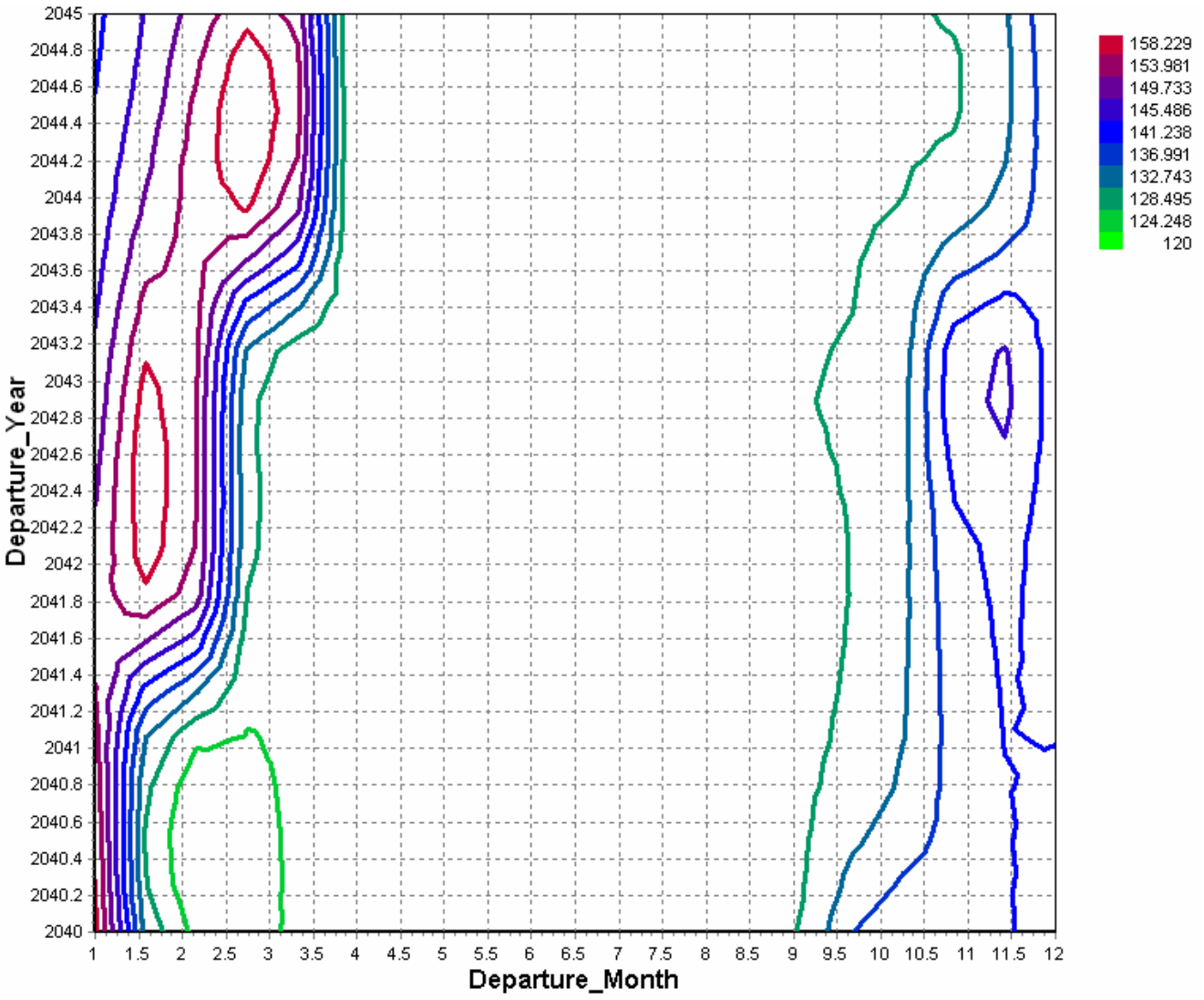

Figure 4-21. Hybrid Saturn Delta-V vs. Departure Year and Month

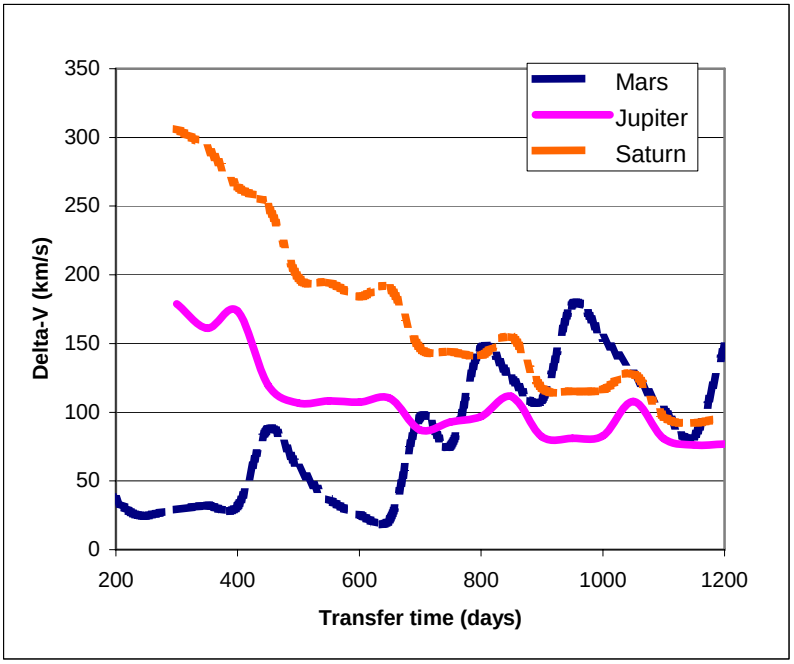

Figure 4-22. Hybrid Delta-V vs. Transfer Time

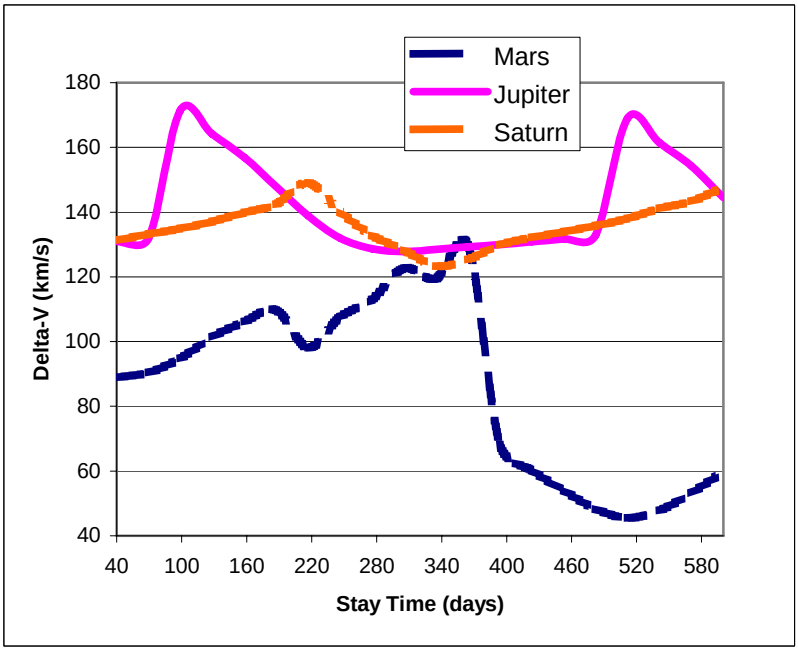

Figure 4-23. Hybrid Delta-V vs. Stay Time

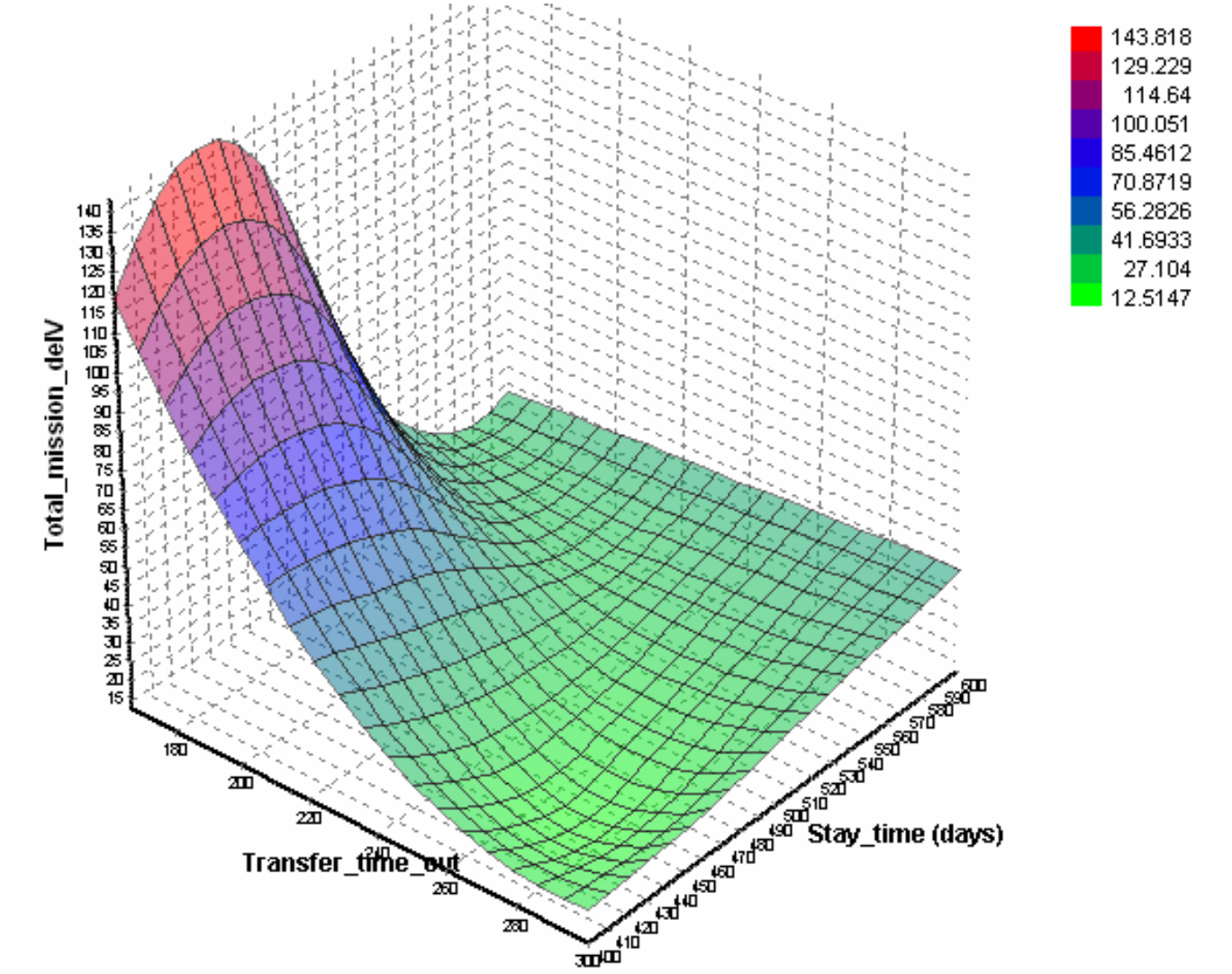

Figure 4-24. Hybrid Mars Delta-V vs. Transfer and Stay Time

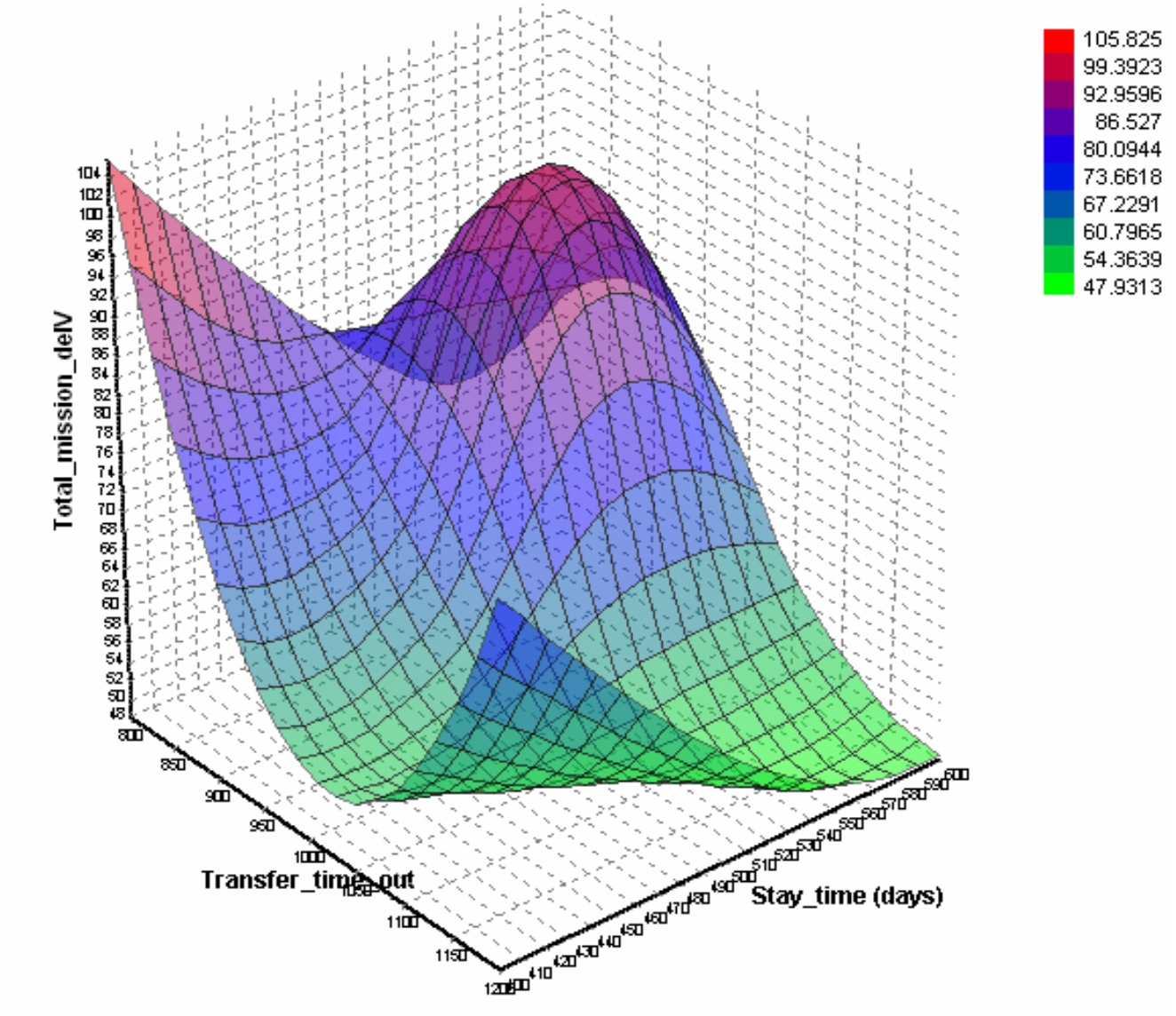

Figure 4-25. Hybrid Jupiter Delta-V vs. Transfer and Stay Time

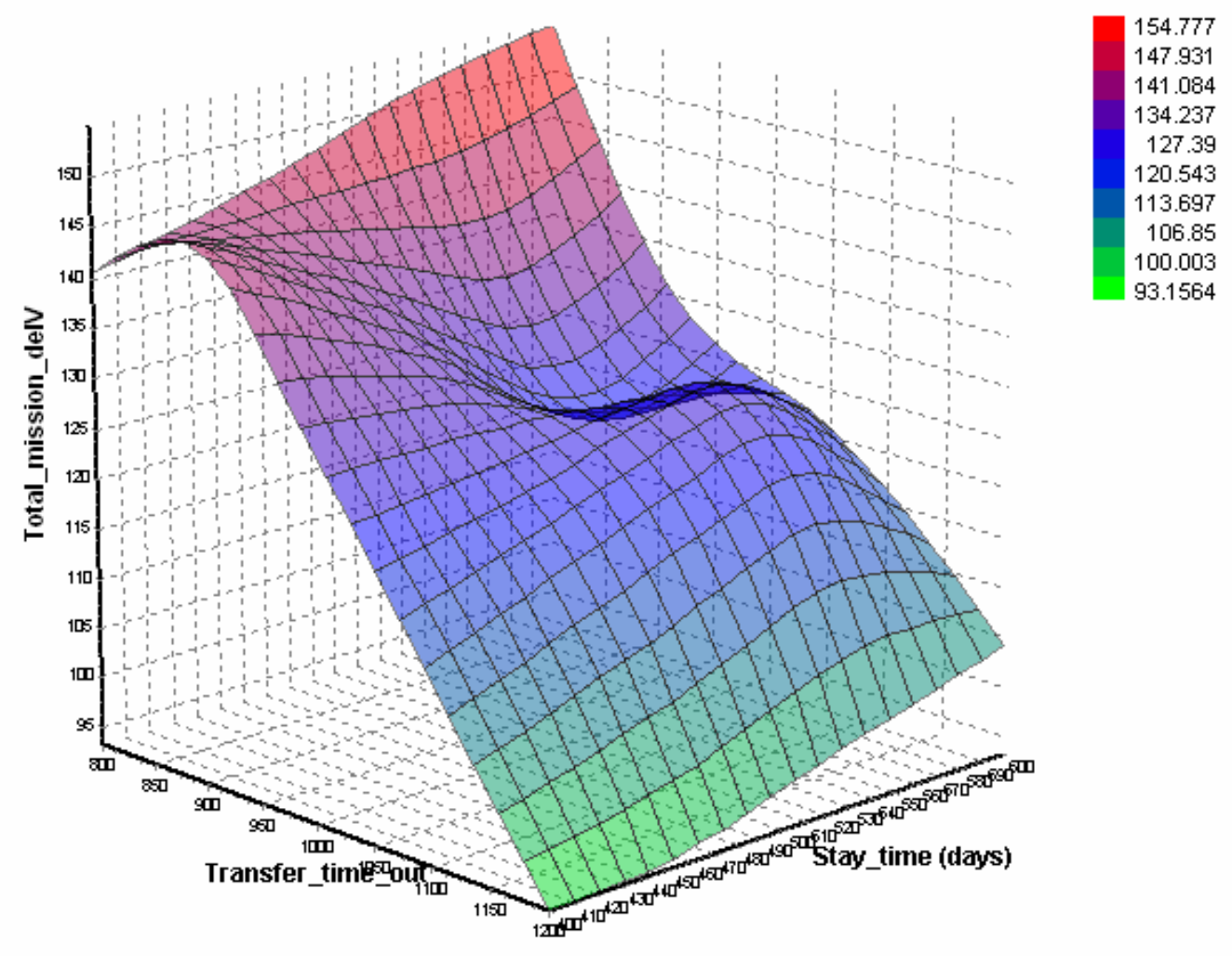

Figure 4-26. Hybrid Saturn Delta-V vs. Transfer and Stay Time

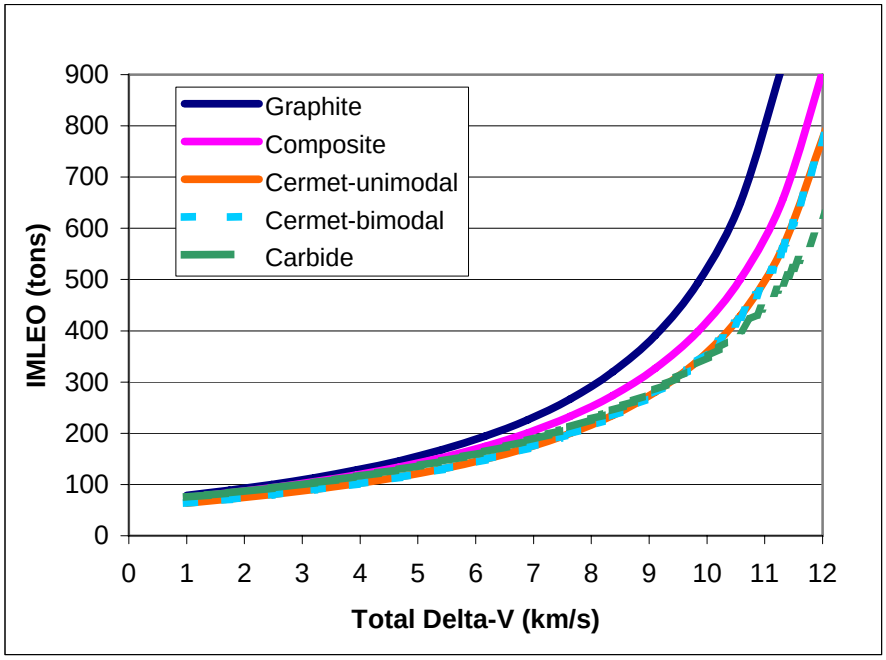

Figure 4-27. NTR IMLEO vs. Delta-V

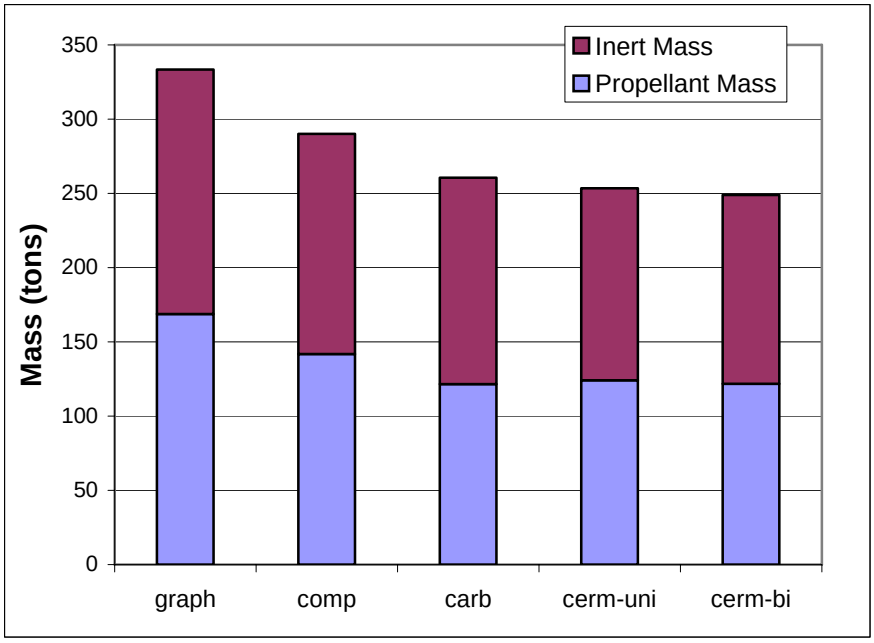

Figure 4-28. NTR Mass Breakdown vs. Fuel Type

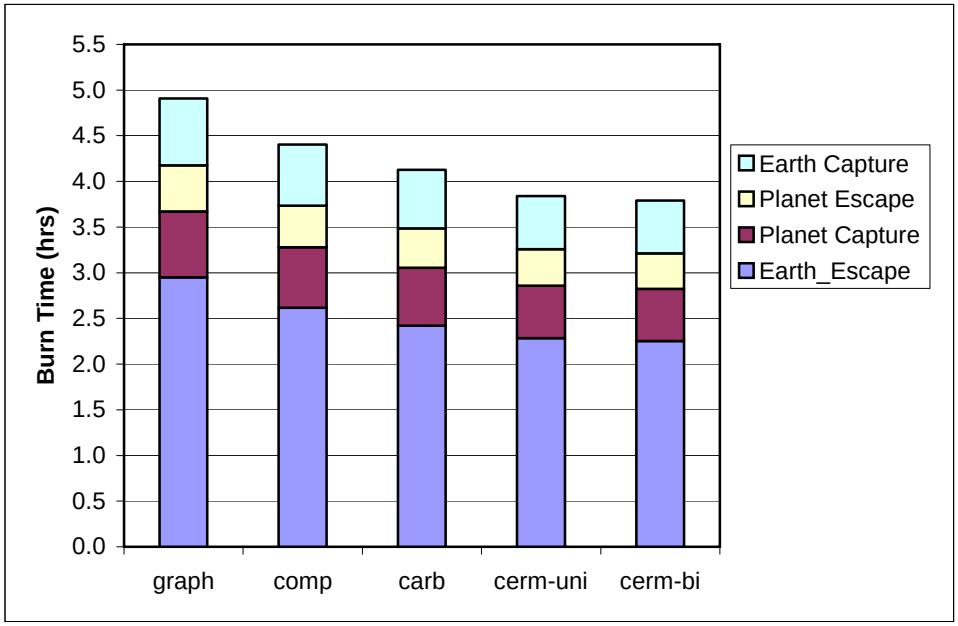

Figure 4-29. NTR Burn Time vs. Fuel Type

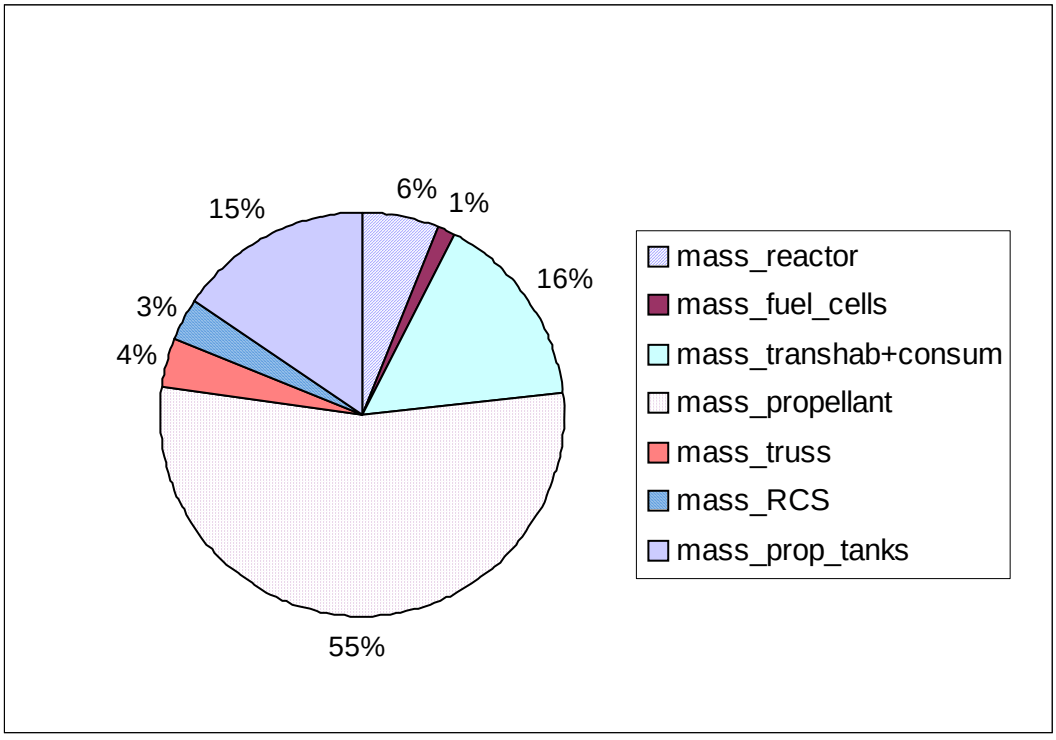

Figure 4-30. NTR Vehicle Mass Breakdown

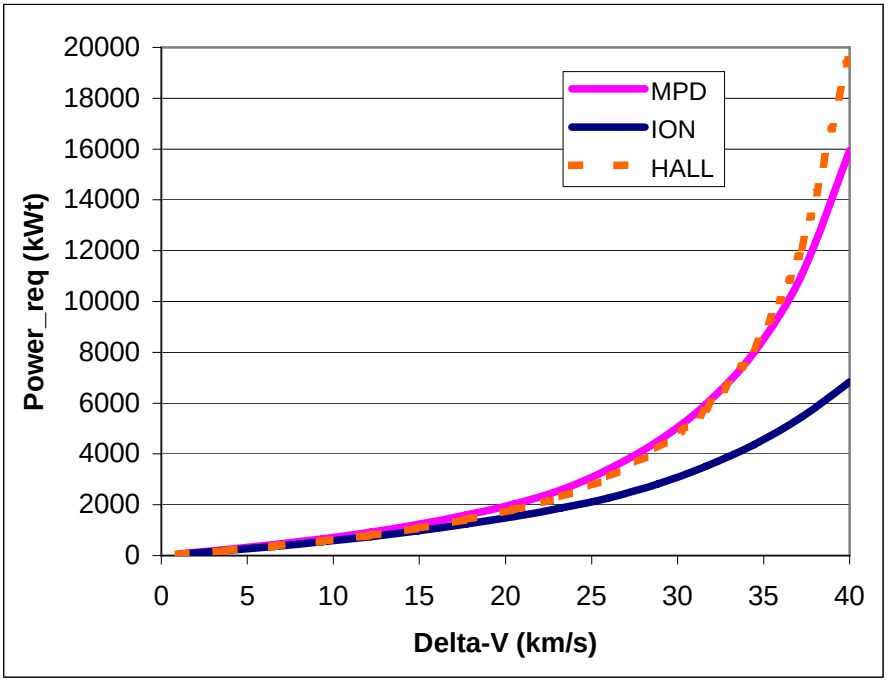

Figure 4-31. NEP Power vs. Delta-V

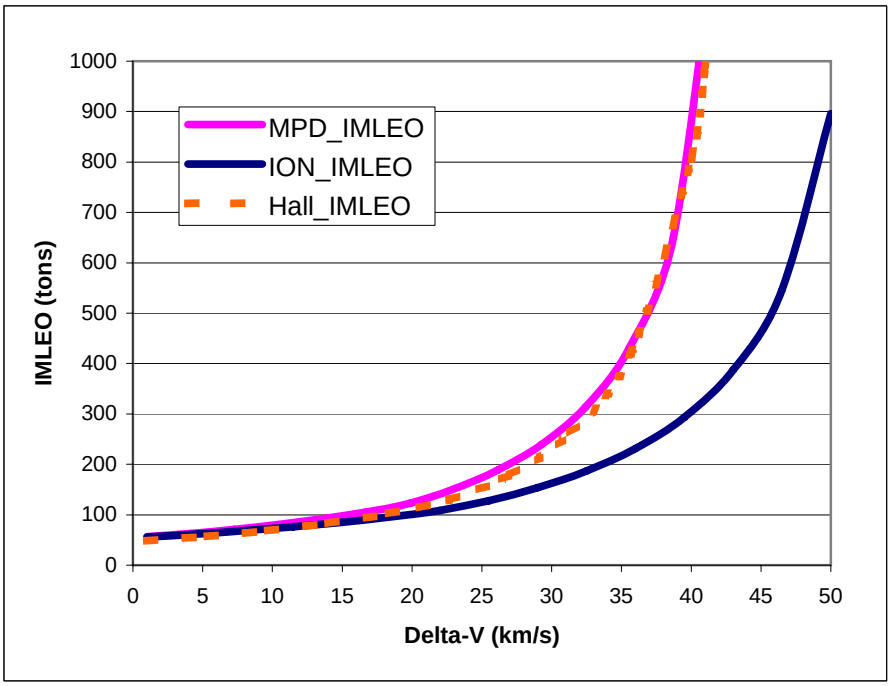

Figure 4-32. NEP IMLEO vs. Delta-V

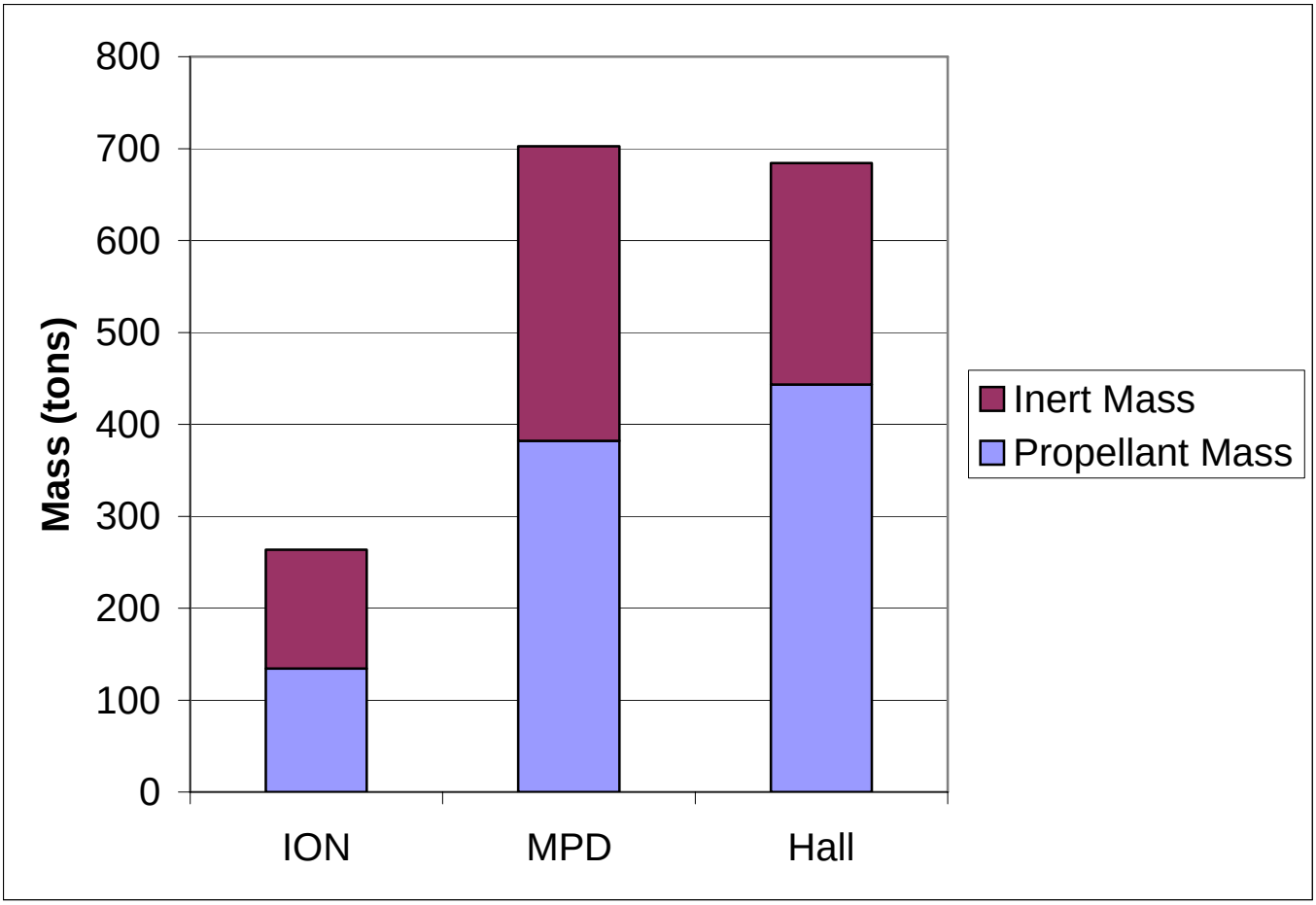

Figure 4-33. NEP Mass Breakdown vs. Thruster Type

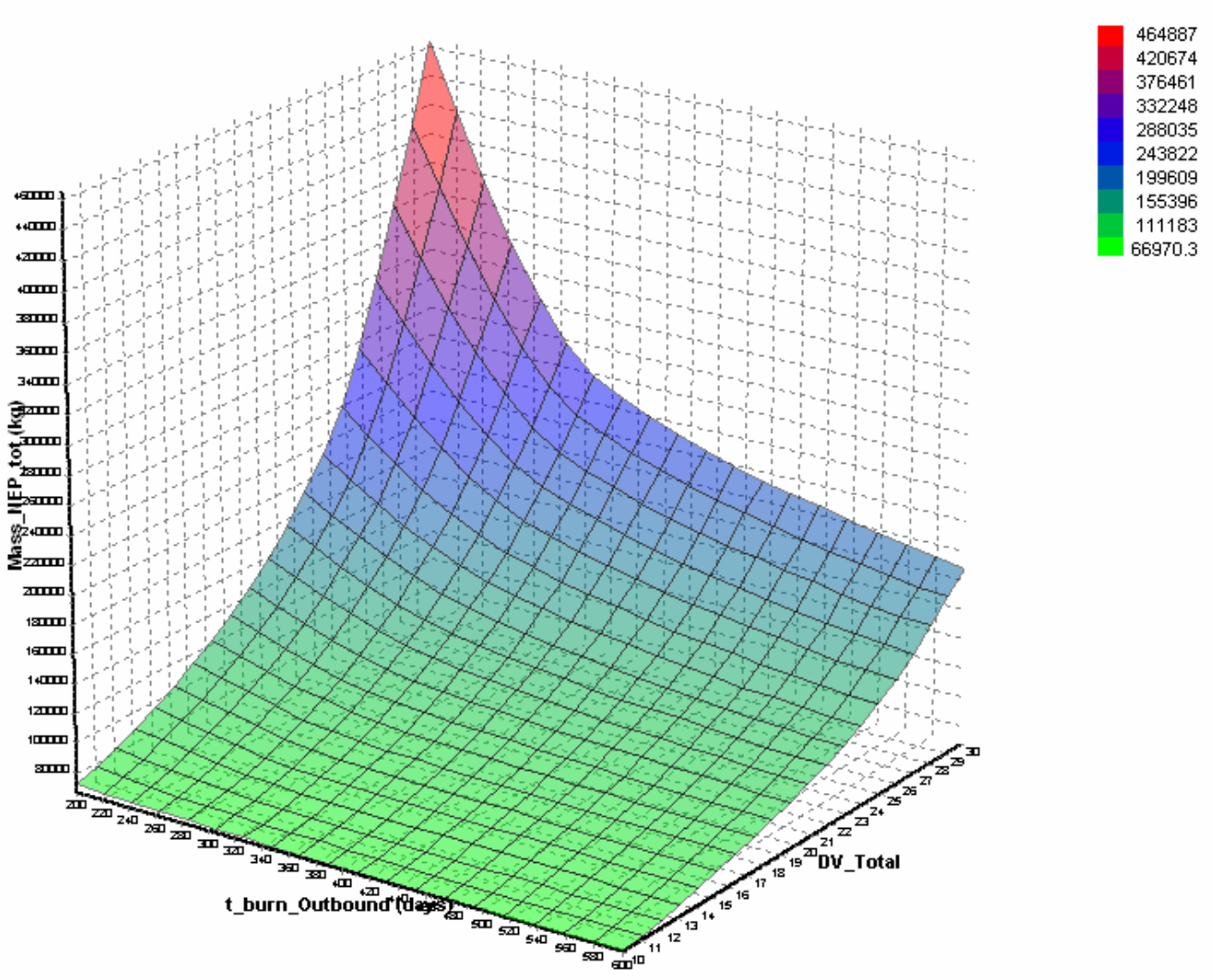

Figure 4-34. NEP IMLEO vs. Burn Time and Delta-V

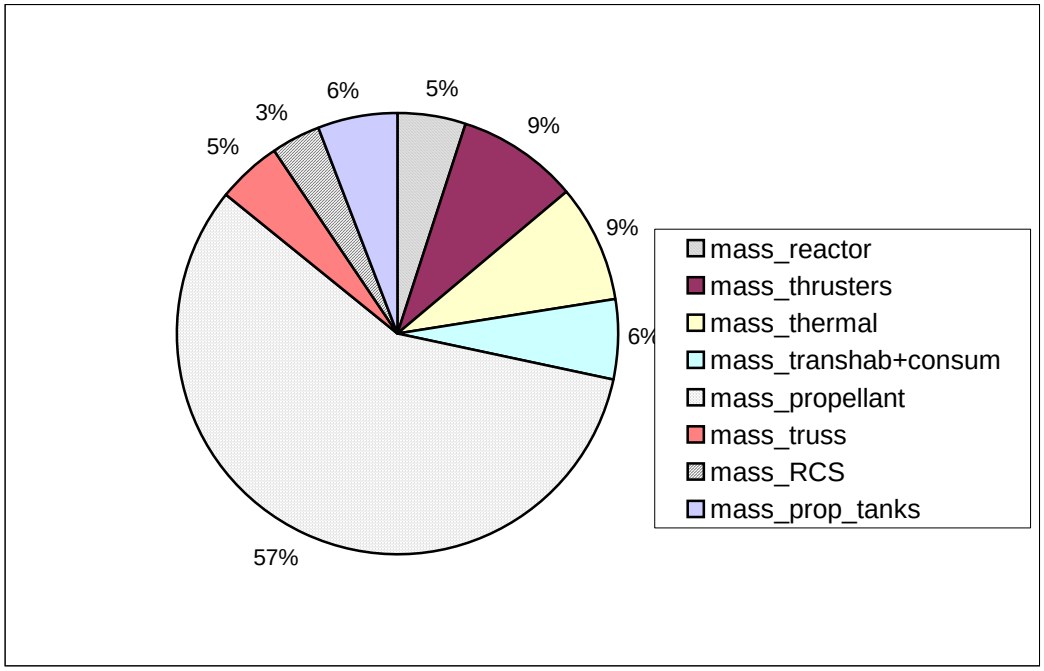

Figure 4-35. NEP Vehicle Mass Breakdown

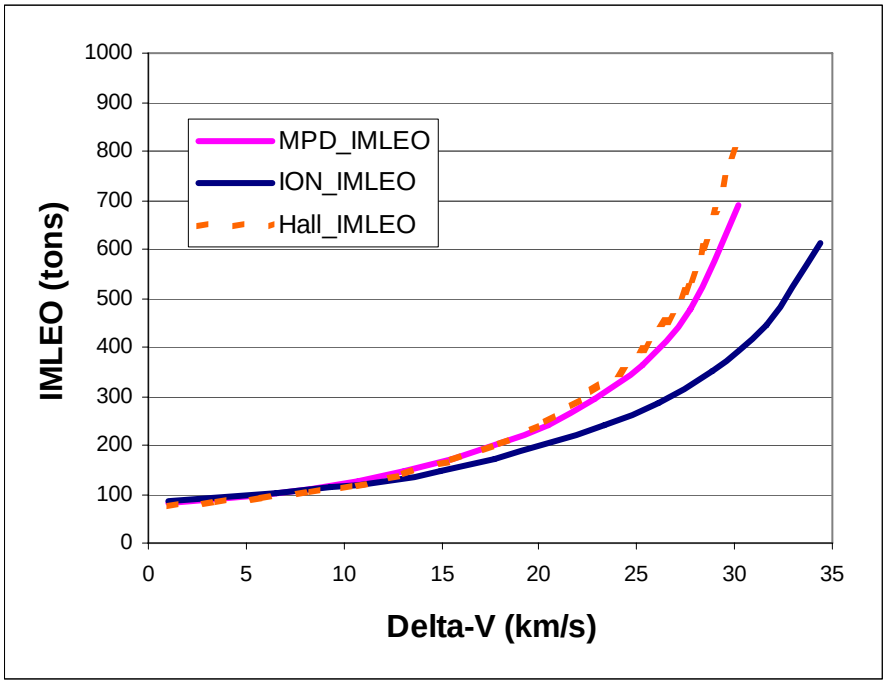

Figure 4-36. Hybrid IMLEO vs. Delta-V

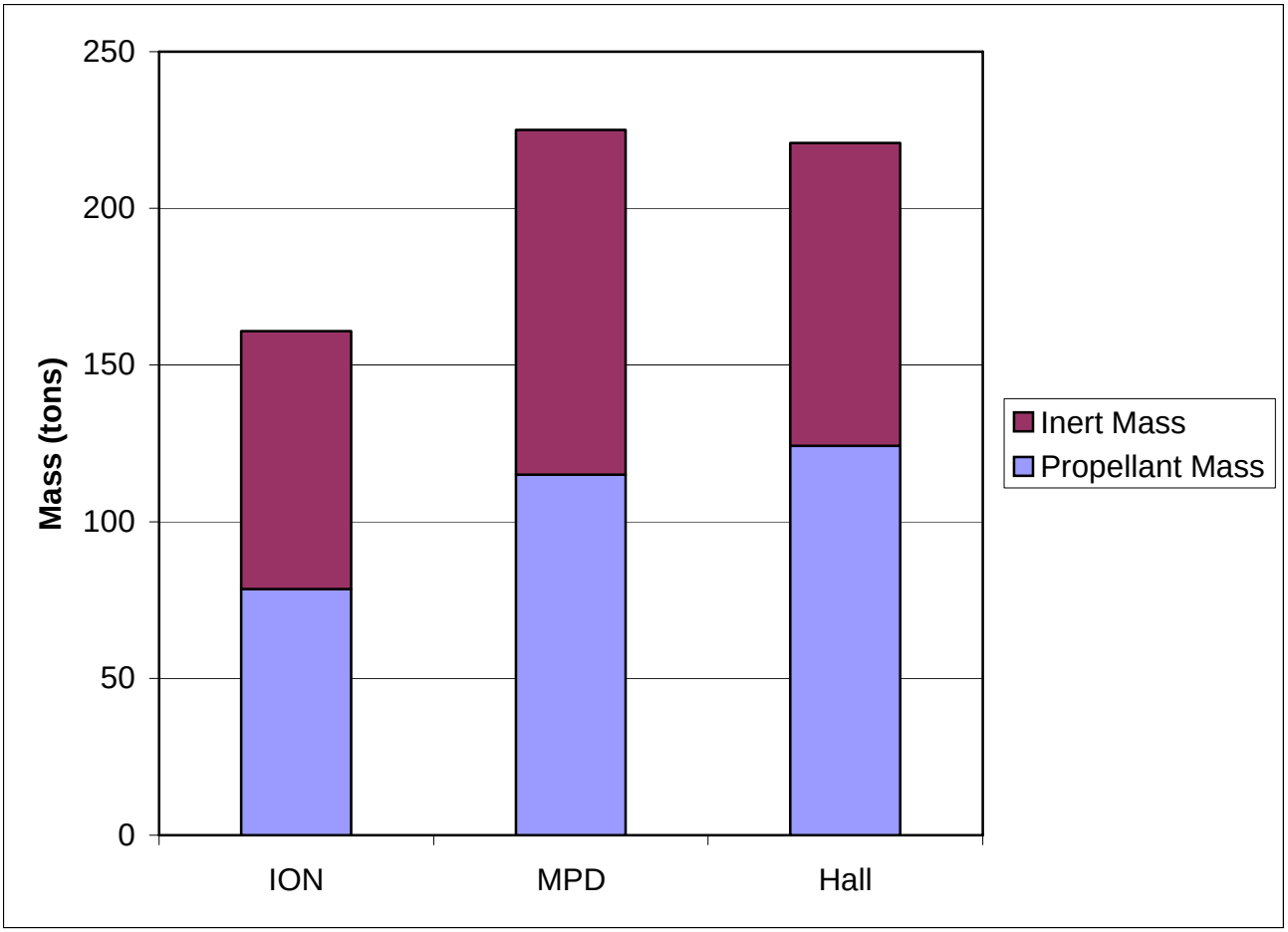

Figure 4-37. Hybrid Mass Breakdown vs. Thruster Type

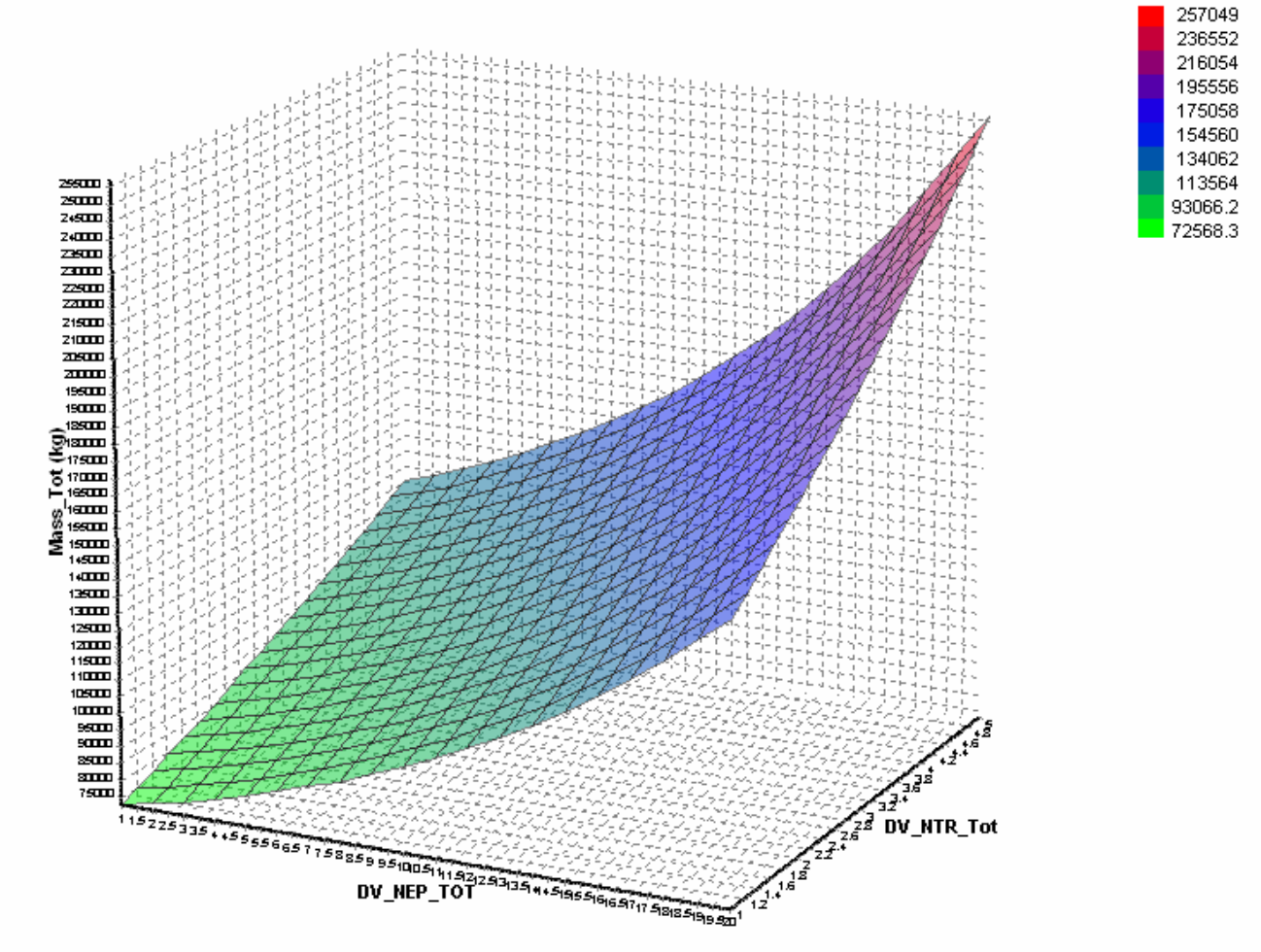

Figure 4-38. Hybrid IMLEO vs. NEP and NTR Delta-V

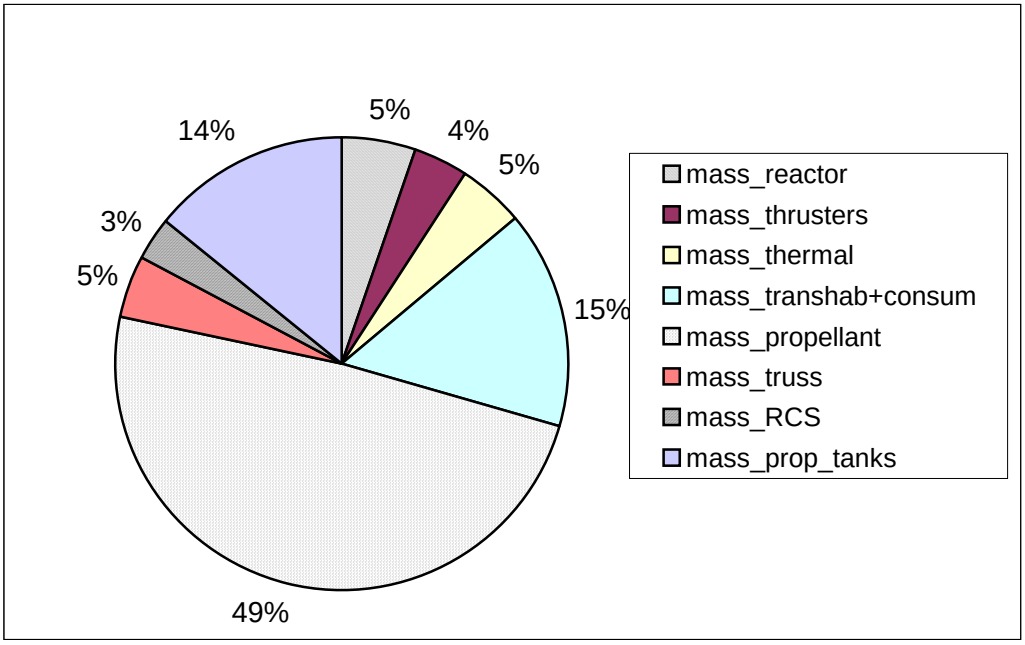

Figure 4-39. Hybrid Vehicle Mass Breakdown

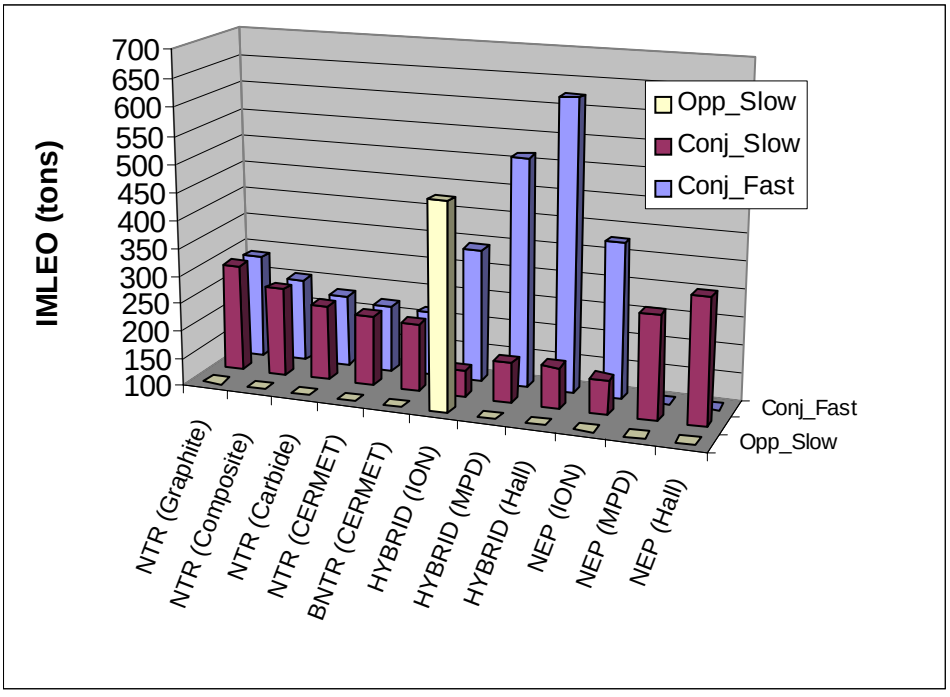

Figure 4-40. Mars Mission IMLEOs

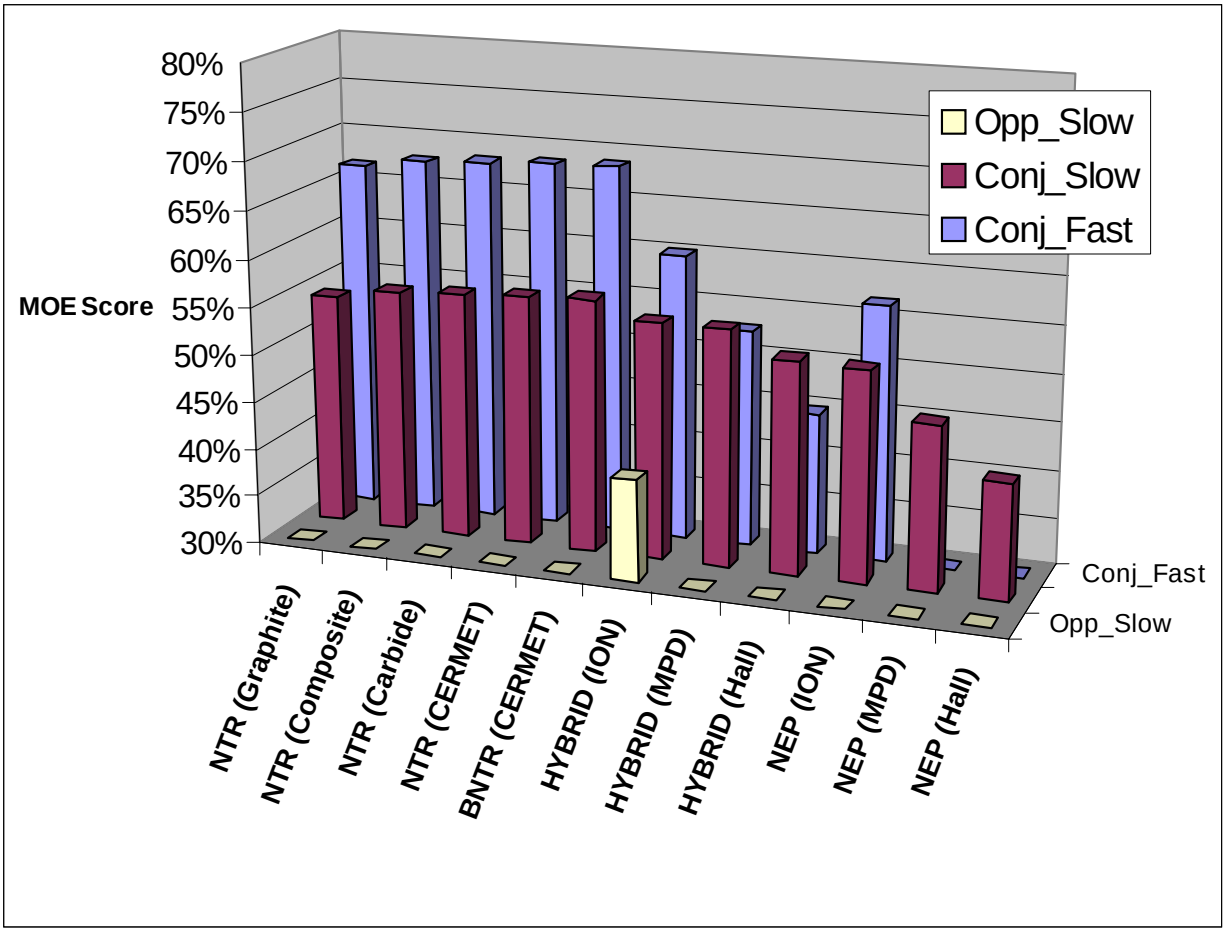

Figure 4-41. Tradespace MOE Scores for Mars Missions

CHAPTER 5
CONCLUSION

Study Contributions

One of the primary contributions of this thesis was to produce a mission analysis trade study with results that were on an order of magnitude not seen before in the short list of interplanetary mission analysis studies. This trade study compared three different vehicle architectures that were all based upon nuclear reactor power sources and broke these architectures down further into configurations based upon reactor fuel or electric thruster type. In addition to the eleven vehicle configurations that resulted from this framework, missions beyond Mars, to Jupiter and even Saturn were attempted. These destinations were aimed for while maintaining a sense of awareness for the duration that astronauts may safely travel in space.

A secondary contribution was to examine NEP, NTR, and Hybrid vehicles in a way that was unbiased, essentially analyzing each system side-by-side when tasked to perform the same type of mission. This contribution is significant as it is difficult to find any literature source that compares one architecture with another. This is a real challenge in industry because an expert in one area will no doubt be an advocate for the type of vehicle that falls into his/her area of expertise.

Creating a trade study from a mission analysis study and using a tradespace matrix was in itself another significant contribution to this area of research. The tradespace matrix served to represent high-level requirements that may be given in the future to interplanetary mission planners. More often than not, the decision on which technology to choose to satisfy these requirements will not lie in the hands of an engineer with the technical knowledge of how these systems work. Therefore, it is paramount that the engineer be able to analyze the systems'

capabilities in meeting specific requirements, and then present this analysis in a simple and often qualitative manner.

The addition of a systems engineering tradespace methodology was thus used in this thesis to help draw straightforward, unbiased, and meaningful results as to which type of power and propulsion system may be most suitable for manned interplanetary missions. Unfortunately, the results fail to give any vehicle configuration that could complete a Saturn or Jupiter mission. It is not believed that these results signify a failure in the models developed for this study. They are simply a reflection of the great demands in energy required to allow humanity to explore our vast solar system. It is thus believed at this time that new analysis cannot solve this problem without the development of new physical concepts for reaching these destinations.

It is important to note that the results of this study do not provide a veritable 'best answer' to the question of which propulsion and power system should be used for crewed interplanetary missions. This analysis instead serves to provide a comparison of specific system designs based on estimated operating parameters, applied to a range of reference missions. One must be aware of the fact that the IMLEO and MOE scores found for these systems were very sensitive to the selected operating parameters. Changing the value of an important system parameter such as ISP could entirely change the results, revealing a much different ranking matrix. This is an especially vital point, since the selected operating parameters were a mix of current and projected values. It is thus reiterated that the results of this trade study are meant only to reveal the performance of specific vehicle models, and do not assert that a specific power and propulsion system is better or worse than another.

Areas of Future Work

The results found in this study only open the door further for new work to be done in both the areas of mission analysis and in advanced nuclear and aerospace technologies. Although this

study allowed for increased breadth and depth of mission analysis as compared to any study found through an in-depth literature search, it is important that mission designs be even further optimized based on the unique capabilities of each power and propulsion system. Although optimization of mission parameters was a key utility in this study, it was done under the umbrella of maintaining homogeneity in mission design between the vehicle architectures. Thus, energy-saving maneuvers such as planetary swingbys and Earth flybys upon return were not used in this study. For instance, the NTR architecture had trouble completing the Mars opposition-class missions, yet it is common in mission analysis studies to lower delta-V through a Venus swingby gravity assist. It will be important, however, to incorporate such things into future analysis while stemming any bias towards one power and propulsion system.

The technology readiness level of many of the technologies needed for interplanetary travel must also see a sharp increase before these missions become a reality. In the EP field, special attention should be paid to power conversion units to allow for higher electric power draw to electric thrusters while minimizing weight of these units. The thruster power processing units must also be improved, as they are the heaviest part of the electric thruster hardware component. In the NTR field, reactor fuel testing must also continue in order to increase ISP while remaining below temperature limits of the materials being used. Nuclear thermal rocket testing must be reinstated before the results and know-how from the 1960s and 1970s are completely lost upon new engineers. Lastly, special attention should be paid to developing the complex, but achievable bimodal reactors, which performed strongly in this trade study, and must be advanced before Hybrid vehicles may come to fruition.

Final Comments

Despite the findings in this study that nearly half of the missions to Mars and no missions beyond Mars could be completed with the advanced technologies analyzed herein, there is no

doubt in the mind of this author that any of these missions could be achieved in the future. Reasonable results for some Mars opportunities were found given power and propulsion system hardware that was being tested nearly 40 years ago. Now, due to limited financial resources and political motivation, preparation for these Mars missions has been constrained to mostly paper studies. These studies do, however, keep alive the motivation to make these interplanetary missions a reality. This research was performed with that same spirit of hope that someday scientists and engineers will be given the opportunity to make the dream of interplanetary travel come true.

APPENDIX A
LIST OF ABBREVIATIONS

ADCS	Attitude Determination and Control System
BNTR	Bimodal Nuclear Thermal Rocket
C&DH	Command and Data Handling
CERMET	CERamic-METallic; Uranium-fueled/refractory metal matrix reactor core
CHEBYTOP	Chebyshev Trajectory Optimization Program
cSv	Centi-Sievert
CTV	Crew Transfer Vehicle
DOE	Department of Energy
DRM	Design Reference Mission
ECRV	Earth Crew Return Vehicle
EP	Electric Propulsion
FEEP	Field Emission Electric Propulsion
GCR	Galactic Cosmic Radiation
GUI	Graphical User Interface
HIVHAV	High Voltage Hall Accelerator
HLLV	Heavy Lift Launch Vehicles
IMLEO	Initial Mass in Low Earth Orbit
IPREP	Interplanetary PREProcessor
IPS	Integrated Propulsion Systems
ISP	Specific Impulse
ISS	International Space Station
JIMO	Jupiter Icy Moons Orbiter

K	Kelvin
kg	Kilogram
klbf	Kilo-Pound-Force
km	Kilometer
kWe	Kilo-Watt Electric
LEO	Low Earth Orbit
m	Meter
MOE	Measure of Effectiveness
MOP	Measure of Performance
Mpa	MegaPascal
MPD	Magneto-Plasma-Dynamic
MPDT	Magneto-Plasma-Dynamic Thruster
MSFC	Marshall Space Flight Center
MW	Mega-Watt (Thermal)
N	Newton
NASA	National Aeronautics and Space Administration
NDR	NERVA Derivative Reactor
NEP	Nuclear Electric Propulsion
NERVA	Nuclear Engine for Rocket Vehicle Applications
NTR	Nuclear Thermal Rocket
PMAD	Power Management and Distribution
PPU	Power Processing Unit
psia	Pounds per Square Inch, Absolute (referenced to a vacuum)

RCS	Reaction Control System
s	Second
SEP	Solar Electric Propulsion
SOI	Sphere of Influence
SPE	Solar Particle Events
t	Ton
TRL	Technology Readiness Level
TT&C	Tracking, Telemetry, and Command
T/W	Thrust to Weight

APPENDIX B
TRADESPACE MISSION ARCHITECTURE RESULTS

Table B-1. NTR Optimized Ephemeris Results

Dest.	Mars (2030-2035)			
Stay	Conjunc.(400-600)		Oppos.(40-60)	
Transfer	F(100-200)	S(200-300)	F(100-200)	S(200-300)
Departure Day	3	2	2	2
Departure Month	4	1	9	1
Departure_Year	2033	2031	2034	2033
Transfer (days)	200	294	199	243
Stay (Days)	600	443	46	46
Dest.	Jupiter (2040-2045)			
Stay	Conjunc.(400-600)		Oppos.(40-60)	
Transfer	F(800-1000)	S(1000-1200)	F(800-1000)	S(1000-1200)
Departure Day	1	24	14	4
Departure Month	1	12	1	1
Departure_Year	2041	2040	2041	2041
Transfer (days)	1000	1200	1000	1200
Stay (Days)	480	461	60	60
Dest.	Saturn (2040-2045)			
Stay	Conjunc.(400-600)		Oppos.(40-60)	
Transfer	F(800-1000)	S(1000-1200)	F(800-1000)	S1000-1200)
Departure Day	1	1	14	2
Departure Month	1	1	1	1
Departure_Year	2041	2041	2041	2041
Transfer (days)	1000	1200	1000	1200
Stay (Days)	475	461	60	60

Table B-2. NEP Optimized Ephemeris Results

Dest.	Mars (2030-2035)			
Stay	Conjunc.(400-600)		Oppos.(40-60)	
Transfer	F(100-200)	S(200-300)	F(100-200)	S(200-300)
Departure Day	24	6	25	15
Departure Month	3	5	3	3
Departure_Year	2033	2035	2033	2033
Transfer (days)	198	296	200	300
Stay (Days)	500	464	40	52
Dest.	Jupiter (2040-2045)			
Stay	Conjunc.(400-600)		Oppos.(40-60)	
Transfer	F(800-1000)	S(1000-1200)	F(800-1000)	S(1000-1200)
Departure Day	16	3	27	23
Departure Month	8	9	10	11
Departure_Year	2040	2042	2043	1044
Transfer (days)	1000	1200	984	1191
Stay (Days)	400	520	41	54
Dest.	Saturn (2040-2045)			
Stay	Conjunc.(400-600)		Oppos.(40-60)	
Transfer	F(800-1000)	S(1000-1200)	F(800-1000)	S1000-1200)
Departure Day	27	12	15	25
Departure Month	9	8	9	8
Departure_Year	2040	2041	2041	2040
Transfer (days)	992	1197	1000	1097
Stay (Days)	445	519	44	40

Table B-3. Hybrid Optimized Ephemeris Results

Dest.	Mars (2030-2035)			
Stay	Conjunc.(400-600)		Oppos.(40-60)	
Transfer	F(100-200)	S(200-300)	F(100-200)	S(200-300)
Departure Day	5	21	27	13
Departure Month	4	1	1	12
Departure_Year	2033	2033	2031	2030
Transfer (days)	182	297	200	298
Stay (Days)	587	488	400	40
Dest.	Jupiter (2040-2045)			
Stay	Conjunc.(400-600)		Oppos.(40-60)	
Transfer	F(800-1000)	S(1000-1200)	F(800-1000)	S(1000-1200)
Departure Day	15	15	10	21
Departure Month	9	8	11	10
Departure_Year	2041	2041	2042	2043
Transfer (days)	993	1197	987	1042
Stay (Days)	490	543	51	56
Dest.	Saturn (2040-2045)			
Stay	Conjunc.(400-600)		Oppos.(40-60)	
Transfer	F(800-1000)	S(1000-1200)	F(800-1000)	S1000-1200)
Departure Day	22	24	14	29
Departure Month	5	10	8	9
Departure_Year	2040	2040	2040	2040
Transfer (days)	1000	1000	948	1000
Stay (Days)	400	596	404	599

Table B-4. NTR Graphite Tradespace Results

Dest.	Mars (2030-2035)			
Stay	Conjunc.(400-600)	Oppos.(40-60)		
Transfer	F(100-200)	S(200-300)	F(100-200)	S(200-300)
IMLEO	287057.8	294324.4	NA	NA
Mass_Inert	114294.6	116823.1	NA	NA
Mass_Propellant	152117.5	156855.7	NA	NA
delta-V1	3.5	3.6	10.8	4.2
delta-V2	1.4	1.4	7.7	2
delta-V3	1.2	0.9	1.1	3.9
delta-V4	0.9	1.5	0.9	4.7
Crewed_days	1000	1031	NA	NA
MOE_Score	66.65%	54.38%	0.00%	0.00%
Dest.	Jupiter (2040-2045)			
Stay	Conjunc.(400-600)	Oppos.(40-60)		
Transfer	F(800-1000)	S(1000-1200)	F(800-1000)	S(1000-1200)
delta-V1	6.2	6.4	22.8	7.9
delta-V2	5.5	5.6	20.6	5.8
delta-V3	7.3	8.3	9.8	7.7
delta-V4	22.7	25.6	6.7	23
MOE_Score	0.00%	0.00%	0.00%	0.00%
Dest.	Saturn (2040-2045)			
Stay	Conjunc.(400-600)	Oppos.(40-60)		
Transfer	F(800-1000)	S(1000-1200)	F(800-1000)	S1000-1200)
delta-V1	9.2	8.9	11.1	9.1
delta-V2	9.3	7	9.1	7
delta-V3	10	7.5	9.6	7.3
delta-V4	6.2	5.4	8.9	6.9
MOE_Score	0.00%	0.00%	0.00%	0.00%

Table B-5. NTR Composite Tradespace Results

Dest.	Mars (2030-2035)			
Stay	Conjunc.(400-600)		Oppos.(40-60)	
Transfer	F(100-200)	S(200-300)	F(100-200)	S(200-300)
IMLEO	252334.7	258895.6	NA	NA
Mass_Inert	105397	107729.1	NA	NA
Mass_Propellant	129039.9	133268.8	NA	NA
delta-V1	3.5	3.6	10.8	4.2
delta-V2	1.4	1.4	7.7	2
delta-V3	1.2	0.9	1.1	3.9
delta-V4	0.9	1.5	0.9	4.7
Crewed_days	1000	1031	NA	NA
MOE_Score	67.63%	55.40%	0.00%	0.00%
Dest.	Jupiter (2040-2045)			
Stay	Conjunc.(400-600)		Oppos.(40-60)	
Transfer	F(800-1000)	S(1000-1200)	F(800-1000)	S(1000-1200)
delta-V1	6.2	6.4	22.8	7.9
delta-V2	5.5	5.6	20.6	5.8
delta-V3	7.3	8.3	9.8	7.7
delta-V4	22.7	25.6	6.7	23
MOE_Score	0.00%	0.00%	0.00%	0.00%
Dest.	Saturn (2040-2045)			
Stay	Conjunc.(400-600)		Oppos.(40-60)	
Transfer	F(800-1000)	S(1000-1200)	F(800-1000)	S1000-1200)
delta-V1	9.2	8.9	11.1	9.1
delta-V2	9.3	7	9.1	7
delta-V3	10	7.5	9.6	7.3
delta-V4	6.2	5.4	8.9	6.9
MOE_Score	0.00%	0.00%	0.00%	0.00%

Table B-6. NTR Carbide Tradespace Results

Dest.	Mars (2030-2035)			
Stay	Conjunc.(400-600)		Oppos.(40-60)	
Transfer	F(100-200)	S(200-300)	F(100-200)	S(200-300)
IMLEO	229760	235744.4	NA	NA
Mass_Inert	98681.7	100853.3	NA	NA
Mass_Propellant	111622.7	115435.4	NA	NA
delta-V1	3.5	3.6	10.8	4.2
delta-V2	1.4	1.4	7.7	2
delta-V3	1.2	0.9	1.1	3.9
delta-V4	0.9	1.5	0.9	4.7
Crewed_days	1000	1031	NA	NA
MOE_Score	68.01%	55.81%	0.00%	0.00%
Dest.	Jupiter (2040-2045)			
Stay	Conjunc.(400-600)		Oppos.(40-60)	
Transfer	F(800-1000)	S(1000-1200)	F(800-1000)	S(1000-1200)
delta-V1	6.2	6.4	22.8	7.9
delta-V2	5.5	5.6	20.6	5.8
delta-V3	7.3	8.3	9.8	7.7
delta-V4	22.7	25.6	6.7	23
MOE_Score	0.00%	0.00%	0.00%	0.00%
Dest.	Saturn (2040-2045)			
Stay	Conjunc.(400-600)		Oppos.(40-60)	
Transfer	F(800-1000)	S(1000-1200)	F(800-1000)	S1000-1200)
delta-V1	9.2	8.9	11.1	9.1
delta-V2	9.3	7	9.1	7
delta-V3	10	7.5	9.6	7.3
delta-V4	6.2	5.4	8.9	6.9
MOE_Score	0.00%	0.00%	0.00%	0.00%

Table B-7. NTR CERMET-Unimodal Tradespace Results

Dest.	Mars (2030-2035)			
Stay	Conjunc.(400-600)	Oppos.(40-60)		
Transfer	F(100-200)	S(200-300)	F(100-200)	S(200-300)
IMLEO	220997.8	227047.7	NA	NA
Mass_Inert	99218.5	101408.4	NA	NA
Mass_Propellant	113014.7	116874.8	NA	NA
delta-V1	3.5	3.6	10.8	4.2
delta-V2	1.4	1.4	7.7	2
delta-V3	1.2	0.9	1.1	3.9
delta-V4	0.9	1.5	0.9	4.7
Crewed_days	1000	1031	NA	NA
MOE_Score	68.45%	56.24%	0.00%	0.00%
Dest.	Jupiter (2040-2045)			
Stay	Conjunc.(400-600)	Oppos.(40-60)		
Transfer	F(800-1000)	S(1000-1200)	F(800-1000)	S(1000-1200)
delta-V1	6.2	6.4	22.8	7.9
delta-V2	5.5	5.6	20.6	5.8
delta-V3	7.3	8.3	9.8	7.7
delta-V4	22.7	25.6	6.7	23
MOE_Score	0.00%	0.00%	0.00%	0.00%
Dest.	Saturn (2040-2045)			
Stay	Conjunc.(400-600)	Oppos.(40-60)		
Transfer	F(800-1000)	S(1000-1200)	F(800-1000)	S1000-1200)
delta-V1	9.2	8.9	11.1	9.1
delta-V2	9.3	7	9.1	7
delta-V3	10	7.5	9.6	7.3
delta-V4	6.2	5.4	8.9	6.9
MOE_Score	0.00%	0.00%	0.00%	0.00%

Table B-8. NTR CERMET-Bimodal Tradespace Results

Dest.	Mars (2030-2035)			
Stay	Conjunc.(400-600)	Oppos.(40-60)		
Transfer	F(100-200)	S(200-300)	F(100-200)	S(200-300)
IMLEO	216602.9	222076.8	NA	NA
Mass_Inert	94236.6	96161.7	NA	NA
Mass_Propellant	110767.3	114316	NA	NA
delta-V1	3.5	3.6	10.8	4.2
delta-V2	1.4	1.4	7.7	2
delta-V3	1.2	0.9	1.1	3.9
delta-V4	0.9	1.5	0.9	4.7
Crewed_days	1000	1031	NA	NA
MOE_Score	68.67%	56.49%	0.00%	0.00%
Dest.	Jupiter (2040-2045)			
Stay	Conjunc.(400-600)	Oppos.(40-60)		
Transfer	F(800-1000)	S(1000-1200)	F(800-1000)	S(1000-1200)
delta-V1	6.2	6.4	22.8	7.9
delta-V2	5.5	5.6	20.6	5.8
delta-V3	7.3	8.3	9.8	7.7
delta-V4	22.7	25.6	6.7	23
MOE_Score	0	0	0	0
Dest.	Saturn (2040-2045)			
Stay	Conjunc.(400-600)		Oppos.(40-60)	
Transfer	F(800-1000)	S(1000-1200)	F(800-1000)	S1000-1200)
delta-V1	9.2	8.9	11.1	9.1
delta-V2	9.3	7	9.1	7
delta-V3	10	7.5	9.6	7.3
delta-V4	6.2	5.4	8.9	6.9
MOE_Score	0.00%	0.00%	0.00%	0.00%

Table B-9. Hybrid Ion Tradespace Results

Dest.	Mars (2030-2035)			
Stay	Conjunc.(400-600)		Oppos.(40-60)	
Transfer	F(100-200)	S(200-300)	F(100-200)	S(200-300)
IMLEO	342639.3	147146.7	NA	471985.9
Mass_Inert	161842	78653.5	NA	190950.1
Mass_Propellant	156310.6	55095.9	NA	251892.3
delta-V1 (NTR)	3.2	3.2	3.2	3.2
delta-V2 (NEP)	13.5	7.7	15.7	9.4
delta-V3 (NTR)	0.2	0.2	0.2	0.2
delta-V4 (NEP)	12.8	6.5	44.7	28.9
Crewed_days	951	1082	NA	636
Burn_Days	363.8	593.7	NA	595.8
Power_Elec	4664.4	719.8	NA	6018.1
No. Thrusters	128.5	19.8	NA	165.8
MOE_Score	60.06%	54.81%	0.00%	40.67%
Dest.	Jupiter (2040-2045)			
Stay	Conjunc.(400-600)		Oppos.(40-60)	
Transfer	F(800-1000)	S(1000-1200)	F(800-1000)	S(1000-1200)
delta-V1 (NTR)	3.2	3.2	3.2	3.2
delta-V2 (NEP)	23.3	20.9	23.4	22
delta-V3 (NTR)	4.5	4.5	4.5	4.5
delta-V4 (NEP)	22	20.3	22.5	22.1
MOE_Score	0.00%	0.00%	0.00%	0.00%
Dest.	Saturn (2040-2045)			
Stay	Conjunc.(400-600)		Oppos.(40-60)	
Transfer	F(800-1000)	S(1000-1200)	F(800-1000)	S1000-1200)
delta-V1 (NTR)	3.2	3.2	3.2	3.2
delta-V2 (NEP)	58.7	57	56.2	44.4
delta-V3 (NTR)	2.3	2.3	2.3	2.3
delta-V4 (NEP)	51.8	52.4	56.1	41.9
MOE_Score	0.00%	0.00%	0.00%	0.00%

Table B-10. Hybrid MPD Tradespace Results

Dest.	Mars (2030-2035)			
Stay	Conjunc.(400-600)		Oppos.(40-60)	
Transfer	F(100-200)	S(200-300)	F(100-200)	S(200-300)
IMLEO	514107.3	171516.1	NA	NA
Mass_Inert	229630.7	89795.6	NA	NA
Mass_Propellant	249265.5	67807.8	NA	NA
delta-V1 (NTR)	3.2	3.2	3.2	3.2
delta-V2 (NEP)	13.5	7.7	15.7	9.4
delta-V3 (NTR)	0.2	0.2	0.2	0.2
delta-V4 (NEP)	12.8	6.5	44.7	28.9
Crewed_days	951	1082	NA	NA
Burn_Days	363.9	593.7	NA	NA
Power_Elec	7618.8	937.4	NA	NA
No. Thrusters	1.8	0.2	NA	NA
MOE_Score	52.69%	54.79%	0.00%	0.00%
Dest.	Jupiter (2040-2045)			
Stay	Conjunc.(400-600)		Oppos.(40-60)	
Transfer	F(800-1000)	S(1000-1200)	F(800-1000)	S(1000-1200)
delta-V1 (NTR)	3.2	3.2	3.2	3.2
delta-V2 (NEP)	23.3	20.9	23.4	22
delta-V3 (NTR)	4.5	4.5	4.5	4.5
delta-V4 (NEP)	22	20.3	22.5	22.1
MOE_Score	0.00%	0.00%	0.00%	0.00%
Dest.	Saturn (2040-2045)			
Stay	Conjunc.(400-600)		Oppos.(40-60)	
Transfer	F(800-1000)	S(1000-1200)	F(800-1000)	S1000-1200)
delta-V1 (NTR)	3.2	3.2	3.2	3.2
delta-V2 (NEP)	58.7	57	56.2	44.4
delta-V3 (NTR)	2.3	2.3	2.3	2.3
delta-V4 (NEP)	51.8	52.4	56.1	41.9
MOE_Score	0.00%	0.00%	0.00%	0.00%

Table B-11. Hybrid Hall Tradespace Results

Dest.	Mars (2030-2035)			
Stay	Conjunc.(400-600)		Oppos.(40-60)	
Transfer	F(100-200)	S(200-300)	F(100-200)	S(200-300)
IMLEO	624351.9	173573.2	NA	NA
Mass_Inert	256258.6	85559.4	NA	NA
Mass_Propellant	333371.2	74474.5	NA	NA
delta-V1 (NTR)	3.2	3.2	3.2	3.2
delta-V2 (NEP)	13.4	7.7	15.7	9.4
delta-V3 (NTR)	0.2	0.2	0.2	0.2
delta-V4 (NEP)	12.7	6.5	44.7	28.9
Crewed_days	951	1082	NA	NA
Burn_Days	363.9	593.7	NA	NA
Power_Elec	7495.5	780.2	NA	NA
No. Thrusters	533.5	55.5	NA	NA
MOE_Score	44.78%	52.29%	0.00%	0.00%
Dest.	Jupiter (2040-2045)			
Stay	Conjunc.(400-600)		Oppos.(40-60)	
Transfer	F(800-1000)	S(1000-1200)	F(800-1000)	S(1000-1200)
delta-V1 (NTR)	3.2	3.2	3.2	3.2
delta-V2 (NEP)	23.3	20.9	23.4	22
delta-V3 (NTR)	4.5	4.5	4.5	4.5
delta-V4 (NEP)	22	20.3	22.5	22.1
MOE_Score	0.00%	0.00%	0.00%	0.00%
Dest.	Saturn (2040-2045)			
Stay	Conjunc.(400-600)		Oppos.(40-60)	
Transfer	F(800-1000)	S(1000-1200)	F(800-1000)	S1000-1200)
delta-V1 (NTR)	3.2	3.2	3.2	3.2
delta-V2 (NEP)	58.7	57	56.2	44.4
delta-V3 (NTR)	2.3	2.3	2.3	2.3
delta-V4 (NEP)	51.8	52.4	56.1	41.9
MOE_Score	0.00%	0.00%	0.00%	0.00%

Table B-12. NEP Ion Tradespace Results

Dest.	Mars (2030-2035)			
Stay	Conjunc.(400-600)		Oppos.(40-60)	
Transfer	F(100-200)	S(200-300)	F(100-200)	S(200-300)
IMLEO	379199.6	161640.8	NA	NA
Mass_Inert	165437.9	84860.5	NA	NA
Mass_Propellant	189758.9	67888.2	NA	NA
delta-V1	21.2	16.6	21	18.1
delta-V2	20.7	16	63.2	40.6
Crewed_days	896	1056	NA	NA
Burn_Days	701.2	1418.1	NA	NA
Power_Elec	6076.8	1075	NA	NA
No. Thrusters	167.4	29.6	NA	NA
MOE_Score	56.78%	52.01%	0.00%	0.00%
Dest.	Jupiter (2040-2045)			
Stay	Conjunc.(400-600)		Oppos.(40-60)	
Transfer	F(800-1000)	S(1000-1200)	F(800-1000)	S(1000-1200)
delta-V1	35.2	32.4	34.5	32.1
delta-V2	36	32.5	36.9	38.1
MOE_Score	0.00%	0.00%	0.00%	0.00%
Dest.	Saturn (2040-2045)			
Stay	Conjunc.(400-600)		Oppos.(40-60)	
Transfer	F(800-1000)	S(1000-1200)	F(800-1000)	S1000-1200)
delta-V1	51.1	48.7	59.1	52.3
delta-V2	45.3	45.3	61.7	62
MOE_Score	0.00%	0.00%	0.00%	0.00%

Table B-13. NEP MPD Tradespace Results

Dest.	Mars (2030-2035)			
Stay	Conjunc.(400-600)		Oppos.(40-60)	
Transfer	F(100-200)	S(200-300)	F(100-200)	S(200-300)
IMLEO	NA	286161.4	NA	NA
Mass_Inert	NA	143767.1	NA	NA
Mass_Propellant	NA	131168.7	NA	NA
delta-V1	21.2	16.6	21	18.1
delta-V2	20.7	16	63.2	40.6
Crewed_days	NA	1056	NA	NA
Burn_Days	NA	1419.7	NA	NA
Power_Elec	NA	1994.9	NA	NA
No. Thrusters	NA	0.5	NA	NA
MOE_Score	0.00%	47.27%	0.00%	0.00%
Dest.	Jupiter (2040-2045)			
Stay	Conjunc.(400-600)		Oppos.(40-60)	
Transfer	F(800-1000)	S(1000-1200)	F(800-1000)	S(1000-1200)
delta-V1	35.2	32.4	34.5	32.1
delta-V2	36	32.5	36.9	38.1
MOE_Score	0.00%	0.00%	0.00%	0.00%
Dest.	Saturn (2040-2045)			
Stay	Conjunc.(400-600)		Oppos.(40-60)	
Transfer	F(800-1000)	S(1000-1200)	F(800-1000)	S1000-1200)
delta-V1	51.1	48.7	59.1	52.3
delta-V2	45.3	45.3	61.7	62
MOE_Score	0.00%	0.00%	0.00%	0.00%

Table B-14. NEP Hall Tradespace Results

Dest.	Mars (2030-2035)			
Stay	Conjunc.(400-600)		Oppos.(40-60)	
Transfer	F(100-200)	S(200-300)	F(100-200)	S(200-300)
IMLEO	NA	327884	NA	NA
Mass_Inert	NA	135316.6	NA	NA
Mass_Propellant	NA	181721.9	NA	NA
delta-V1	21.2	16.6	21	18.1
delta-V2	20.7	16	63.2	40.6
Crewed_days	NA	1056	NA	NA
Burn_Days	NA	1422.9	NA	NA
Power_Elec	NA	1850.3	NA	NA
No. Thrusters	NA	131.7	NA	NA
MOE_Score	0.00%	42.17%	0.00%	0.00%
Dest.	Jupiter (2040-2045)			
Stay	Conjunc.(400-600)		Oppos.(40-60)	
Transfer	F(800-1000)	S(1000-1200)	F(800-1000)	S(1000-1200)
delta-V1	35.2	32.4	34.5	32.1
delta-V2	36	32.5	36.9	38.1
MOE_Score	0.00%	0.00%	0.00%	0.00%
Dest.	Saturn (2040-2045)			
Stay	Conjunc.(400-600)		Oppos.(40-60)	
Transfer	F(800-1000)	S(1000-1200)	F(800-1000)	S1000-1200)
delta-V1	51.1	48.7	59.1	52.3
delta-V2	45.3	45.3	61.7	62
MOE_Score	0.00%	0.00%	0.00%	0.00%

APPENDIX C
MODELCENTER TEMPLATE AND FILEWRAPPER

CHEBYTOP Hybrid Ephemeris Model Template:

```
$input
 HEAD='Mars Bimodal Hybrid propulsion system 1'
 SHOTA='Earth', ; departure planet
 BULSI='Mars', ; arrival planet
 jdl=2033,4,1,  ; Julian date (year, month, day)
 iprnt=2, ;forces printing of intermediate ChebyTOP results
 jdate=0, ;Julian departure date bias from epoch of jdl
 nv1=2, ;Departure velocity bias flag (2=hyp)
 nv2=2, ; Arrival velocity bias flag (2=hyp)
 npow=0, ; constant power source (0=nucl)
 p0=5000,500,8000, ; initial power- not used if nmuop > 0, units kW
 is=6000, ;elect_prop_specific_impulse
 bb=.315, ; elect_prop_thruster efficiency
 dd=0., ; elect_prop_thruster_eff_isp
 kt=.05, ; electric_prop_tankage fraction
 ALFA=15,0.0, ; prop_system_specific_mass
 nb1=2, ;departure date flag (use jdl given)
 nb2=2, ; arrival date flag (use jdl given)
 radep=6785.,  ; elliptical departure apo
 tend=300.,-0,300.0, ; mission duration relative to jdl
 vhl=0, 0.0, 0., ;departure excess velocity
 vhp=0,0.0,0., ;arrival excess velocity
 nlv=0, ;launch vehicle number
 m0d=180000., ; initial mass_tot_system
 depart=t, ; if true depart from Earth orbit
 jetisd=t, ; high thrust departure model, jettison mass
 ispd=915, ;ISP of nuclear prop system
 glossd=1.015, ;high thrust departure model gravity loss
 kd=.25,0,
 rpdep=6787., ; departure parking orbit perigee (km)
 rarr=37190, ; arrival apo
 retro=t, ; simulate high thrust retro stage at arrival
 jetis=t, ; simulate jettison of high thrust retro stage
 cisp=915,
 kr=.25,15.606, ; retro stage tankage fraction
 rparr=3640., ;arrival peri
 flyby=f,
 rn=0, ;heliocentric revolution count
 keep=f, ;if 't' save intermediate values for next run
 ncop=0, ;optimal Isp flag,1 keeps it constant (keep=0)
 nmuop=1, ;optimal power flag (keep=1)
$nctopt=2 ; constant thrust
$end
```

CHEBYTOP Hybrid Ephemeris Model FileWrapper:

```
# ChebyTOP Earth Mars File Wrappe98765
#RunCommands
{
generate inputFile
       run "chebytop cheby_Hybrid.inp"
parse outputFile

templateFile: cheby_Hybrid.template
initializationFile: cheby_Hybrid.template
fileToGenerate: cheby_Hybrid.inp

      setDelimiters "=,'"
```

```
      removeMissingVariables: true

#          name   type  row   field
#-------------------------------------------
markAsBeginning "$input"
#variable: Title  string      2     2     description="Trajectory
Title/Description"
#variable: rp                 integer     9     2     description="must be 0
when using alta" enumValues="0"
#variable: nctopt       integer 23  2     description="1=compute constant
thrust solution" enumValues="0,1" default="1"
#variable: copla        string      28    2     description="Coplanar Solution
Flag" enumValues="True,False"
#variable: DepartureYear            integer     5     2     units="year
(jdl(1))"
#variable: DepartureMonth     integer     5     3     units="month (jdl(2))"
#variable: DepartureDay       integer     5     4     units="day (jdl(3))"
#variable: DepDtFlag          integer 17  2     description="Departure Date
Flag:0=optimal travel angle solution,1=optimal date min J,2=use date and TOF
supplied (nb1)" enumValues="1,2" default="2"
#variable: ArrDtFlag          integer 18  2     description="Arrival Date
Flag:0=optimal travel angle solution,1=optimal date min J,2=use date and TOF
supplied (nb2)" enumValues="1,2" default="2"
#variable: OptPwrFlag         integer     40    2     description="1=Optimal
Power Flag (nmuop)" enumValues="0,1" default="1"
#variable: SaveIntValues            string      39    2     description="If
true, save intermediate values for next run (keep)" enumValues="True,False"
default="False"

#10/25/2001 modification: add ' to delimiters group and remove ' ' from planet
names
setGroup "MissionInfo"
variable: DepartureYear       integer     5     2     units="year (jdl(1))"
variable: DepartureMonth      integer     5     3     units="month (jdl(2))"
variable: DepartureDay        integer     5     4     units="day (jdl(3))"
variable: DeparturePlanet     string      3     2     description="Departure
Body (shota)"
variable: ArrivalPlanet       string      4     2     description="Arrival
Body (bulsi)"
variable: HelioTripTime_max   double      20    2
      description="Heliocentric transfer time-max (tend)" units="days"
variable: HelioTripTime_min   double      20    4
      description="Heliocentric transfer time-min (tend)" units="days"
variable: Power_Source        integer     10    2     enumValues="0,1"
description="Nuclear=0,Solar=1 (npow)"
variable: Flyby               string      37    2     enumValues="True,False"
variable: DepartureApo        double      19    2     description="Departure
planet apo (radep)" units="kilometers"
variable: DeparturePeri         double  30      2       description="Departure
planet perigee(rpdep)"
variable: ArrivalApo          double      31    2     description="Arrival
Apogee (rarr)" units="kilometers"
variable: ArrivalPeri           double  36      2       description="Arrival
Perigee"
#variable: DepVelBias         integer     8     2     description="Departure
velocity bias flag:0=none,1=asym,2=hyp,3=spiral (nv1)" enumValues="0,1,2,3"
default="3"
#variable: ArrVelBias         integer 9   2     description="Arrival velocity
bias flag:0=none,1=asym,2=hyp,3=spiral (nv2)" enumValues="0,1,2,3" default="3"
variable: DepHypVel           double      21    2     description="Departure
excess velocity for use when nv1=1 or 2 (vhl)" units="kilometers/second"
default="0"
```

```
variable: ArrHypVel           double      22    2     description="Arrival
excess velocity for use when nv2=1 or 2 (vhp)" units="kilometers/second"
default="0"
#variable: Helio_Rev_Count    double      38    2
      description="Heliocentric revolution count, default=0"
variable: Outbound_v_bias       double  8       2       description="Velocity
bias, 1=asymp,2=hyper,3=tangen"
variable: Inbound_v_bias        double  9       2       description="Velocity
bias, 1=asymp,2=hyper,3=tangen"

setGroup "Prop_systems"
variable: InitialMass_tot     double      24    2     description="Initial
Mass (m0d)" units="kilograms"
variable: InitialPower        double      11    2     description="Initial
Power at 1 AU (p0)" units="kilowatts"
variable: Alpha                 double  16      2       description="power
system alpha kw/kg"
variable: Isp_elec            double      12    2     description="Specific
Impulse (is)" units="seconds"
#variable: AlphaSlope         double      16    2     description="Propulsion
System Specific Mass (alpha(1))" units="kilograms/kilowatts"
#variable: AlphaIntercept     double      16    3     description="Propulsion
System Fixed Mass (alpha(2))" units="kilograms" default="0"
variable: Efficiency_elec     double      13    2     description="Thruster
Efficiency (bb)" default="0.6"
#variable: EfficiencyIsp      double      14    2     description="Thruster
Efficiency (Isp) (dd)" units="seconds" default="0"
variable: TankageFrac_elec    double      15    2     description="Tankage
Fraction (kt)" default="0"
#variable: StructuralFrac     double      31    2     description="Structural
Fraction (ks)"
#variable: StationKeepingPower      double      15    2
      description="Station Keeping Power, subtracts from p0 (sap)"
units="kilowatts" default="0"
variable: Isp_nucl            double      27    2     description="Specific
Impulse_nuclear_prop (ispd)" units="seconds"
#variable: Isp_flag           double      41    2     description="Optimal Isp
flag (when non-zero, does not work)
variable: Depart_nucl           string  25      2       description=="If 't',
depart from Earth orbit"  enumValues="True,False"
variable: Retro_tank_frac     double      35    2     description="Retro Stage
Tankage Fraction"
variable: Retro_nucl          string      32    2     description="If 't',
simulate high thrust retro stage at arrival"  enumValues="True,False"
variable: Jettison            string      33    2     description="If 't',
simulate jettison of high thrust retro stage"  enumValues="True,False"

}

RowFieldOutputFile outputFile
{
fileToParse: cheby_Hybrid.out
setDelimiters whitespace

removeMissingVariables: true
#resize=true
#          name   type  row   field
#-----------------------------------------------
clearMarks

markAsBeginning "Chebytop 3"
setGroup "Dates"
variable: DepDtJulian   double       4    7     ignoreConversionErrors=true
description="Julian departure date"
```

```
variable: DepMonth      string       4    4     description="departure month"
variable: DepDay  string       4    5     description="departure day"
variable: DepYear integer      4    6     ignoreConversionErrors=true
description="departure year"
variable: ArrDtJulian   double       5    7     ignoreConversionErrors=true
description="Julian arrival date"
variable: ArrMonth      string       5    4     description="arrival month"
variable: ArrDay  string       5    5     description="arrival day"
variable: ArrYear integer      5    6     ignoreConversionErrors=true
description="arrival year"

markAsBeginning "Solution time="
setGroup "NTR_DeltaV"
variable: TMI_Burn      double   3      8      description="init.delta V from
main engine (nuclear)system"

markAsBeginning "Spacecraft parameters"
setGroup "NEP_1st_Iter"
variable: Elec_Delta_V      double   6       7      description="total del-V
for elec_prop sys"
variable: Burn_time1         string   3       16
#variable: Burn_time_highpe string   3         15     description="total
thruster on time (solar is approximated at 1AU) (tp)"
units="days"ignoreConversionErrors=false
markAsEnd "Solution time="
setGroup "NEP_2nd_Iter"
variable: Elec_Delta_V          double  -4       7
#variable: Burn_time_highpe      string  -7       15
variable: Burn_time2             string  -7       16

#markAsBeginning "Spacecraft parameters"
#setGroup "Trajectory_values"
#array:      x            double         24:-26    2     description="plotting
data" ignoreConversionErrors=true
#array:      y            double         24:-26    3     description="plotting
data" ignoreConversionErrors=true
#array: rdata             double            24:-26      5
      description="plotting data" ignoreConversionErrors=true
#array: thetadata         double         24:-26    6     description="plotting
data" ignoreConversionErrors=true


# Unused Variables
#markAsBeginning "Constant specific impulse solutions"
#variable: jv     double      3     12    ignoreConversionErrors=false
#variable: jc     double      7     14    ignoreConversionErrors=false
#variable: jc     double      7     -3    ignoreConversionErrors=false
#variable: initialaccel double 7 -11      description="a0" units="mm/day^2"
ignoreConversionErrors=true
#variable: initialaccel2 string 7 4 description="used when accel# runs into a0
variable name"
#array: timedata         double 10  1     description="plotting data"
ignoreConversionErrors=true
#array: phidata double 10:-25 7     description="plotting data"
ignoreConversionErrors=true
#array: magadata double 10:-25  8   description="plotting data"
ignoreConversionErrors=true
#array: pwrratiodata double 10:-25 8      description="plotting data"
ignoreConversionErrors=true
#array: conedata double 10:-25      10    description="plotting data"
ignoreConversionErrors=true
#array: clockdata double 10:-25 11  description="plotting data"
ignoreConversionErrors=true
#markAsEnd "Solution time="
```

```
#setGroup "Summary_Parameters"
#variable: tot_TOF            double      4     6     description="total
flight time (tf)" units="days"
#array: ThrusterSwitching        string -3       1:-1
      description="Thruster switching information"
#variable: EqiDv        double      9     -11   ignoreConversionErrors=false
#variable: PowerTxt     string  7         1     description="used when power
so large it runs into preceding text"
#variable: Power        double      7     2     description="Optimal Power"
units="kiloWatts" ignoreConversionErrors=false
#variable: JetPower     double      9     2     description="Jet Power =
pwr*efficiency" units="kiloWatts" ignoreConversionErrors=false
#variable: MOC_burn   double  5       11       description="retro delta V from
main engine (nuclear)system"
#variable: Power_elec    double  6       2       description="total power"
#variable: PayloadMass  double      4     10    description="Payload Mass =
FinalMass-PropSys-Tankage-Structure (mn)" units="kilograms"
ignoreConversionErrors=false
#variable: FinalMass    double      4     4     description="Final Mass = Mo-
prop (mf)" units="kilograms" ignoreConversionErrors=false
#variable: PropMass     double      4     6     description="Propellant Mass
(mp)" units="kilograms" ignoreConversionErrors=false
#variable: PropSysMass  double      4     8     description="Propulsion System
Mass = Pwr*alpha (mps)" units="kilograms" ignoreConversionErrors=false
#variable: m0_pe  double      6     11    description="Initial Mass/Power"
ignoreConversionErrors=true
}
```

LIST OF REFERENCES

[1]Wade, M., 2007, “Von Braun Mars Expedition-1952,” Encyclopedia Astronautica, http://www.astronautix.com/craft/vonn1952.htm, Jan 2007.

[2]Griffin, B., Thomas, B., Vaughan, D., “A Comparison of Transportation Systems for Human Missions to Mars,” 40th AIAA/ASME/SAE/ASEE Joint Propulsion Conference and Exhibit, 11-14 July 2004, Fort Lauderdale, FL.

[3]Stafford, T.P., 1991, “America at the Threshold,” Report of the Synthesis Group on America’s Space Exploration Initiative,” http://history.nasa.gov/staffordrep/main_toc.PDF, Jan 2007.

[4]“Space Transfer Concepts and Analysis for Exploration Missions,” Boeing Aerospace and Electronics, Fourth Quarterly Review, NASA Contract NAS8-37857, Oct. 17, 1990.

[5]Borowski, S.K., Corban, R.R., McGuire, M.L., Beke, E.G., “Nuclear Thermal Rocket/Vehicle Design Options for Future NASA Missions to the Moon and Mars,” NASA Lewis Research Center.

[6]Roy, S., 2006, “For Fuel Conservation in Space, NASA Engineers Prescribe Aerocapture,” Marshall Space Flight Center study, http://www.nasa.gov/vision/universe/features/aerocapture.html, Jan 2007.

[7]Borowski, S.K., McGuire, M.L., Mason, L.M., Gilland, J., “High Power MPD Nuclear Electric Propulsion (NEP) for Artificial Gravity HOPE Missions to Callisto,” NASA/TM--2003-212349.

[8]Accettura, A.G., Bruno, C., Casotto, S., Marzari, F., “Mission to Mars Using Integrated Propulsion Concepts: Considerations, Opportunities, and Strategies,” Acta Astronautica 54 (2004) 471-486.

[9]Borowski, S.K., Dudzinski, L.A., “Bimodal Nuclear Electric Propulsion: Enabling Advanced Performance with Near-Term Technologies,” AIAA 2002-3653, 38th AIAA/ASME/SAE/ASEE Joint Propulsion Conference & Exhibit, Indianapolis, Indiana, July 7-10, 2002.

[10]Beaty, James S., *Glossary of Optical Communication Terms*, DOT/FAA/CT-TN91-9, U.S. Department of Transportation, Federal Aviation Administration, Technical Center, Atlantic City International Airport, NJ 08405, April 1991.

[11]Belfiore, M., “The Five-Billion-Star Hotel,” Popular Science Magazine, General Technology Section, 2005.

[12]Bates, R.R., Mueller, D.D., White, J.E., "Fundamentals of Astrodynamics," Dover Publications, INC., New York.

[13]Conway, B.A., Prussing, J.E., "Orbital Mechanics," Oxford University Press, 1993.

[14]Sutton, G.P, Biblarz, O., "Rocket Propulsion Elements," John Wiley & Sons, Inc., 2001.

[15]Eagle, C.D., 2007, "Orbital Mechanics with Numerit: The Hohmann Orbit Transfer," Science Software, http://www.cdeagle.com/omnum/hohmann.pdf, Jan 2007.

[16]Wertz, J.R., Larson, W.J, "Space Mission Analysis and Design," Microcosm Press & Kluwer Academic Publishers, 3rd edition, 2003.

[17]Striepe, S.A., Braun, R.D., "Effects of A Venus Swingby Periapsis Burn During an Earth-Mars Trajectory," The Journal of Astronautical Sciences, Vol. 39, No. 3, July-September 1991.

[18]Borowski, S.K., Dudzineki, L.A., McGuire, M.L, "Bimodal Nuclear Thermal Rocket (NTR) Propulsion for Power-Rich Artificial Gravity Human Exploration Missions to Mars," IAA-01-IAA.13.3.05, NASA Glenn Research Center, 2001.

[19]Benton, M.G., "Conceptual Design for Interplanetary Spaceship Discovery," American Institute of Physics 0-7354-0305-8, 2006.

[20]"Space Transfer Concepts and Analysis for Exploration Missions," Fourth Quarterly Review, Boeing Aerospace and Electronics, October 17, 1990.

[21]"Exploration Studies Technical Report; Volume 1: Mission and Integrated Systems," The Office of Exploration, FY 1989 Annual Report.

[22]Sakai, T., 2004, "A Study of Variable Thrust, Variable Specific Impulse Trajectories for Solar System Exploration," Georgia Institute of Technology, Aerospace Engineering Dissertation, http://etd.gatech.edu/theses/available/etd-11212004-151326/, Jan 2007.

[23]Navagh, J., 1993, "Optimizing Interplanetary Trajectories with Deep Space Maneuvers," NASA Contractor Report 4546, http://ntrs.nasa.gov/archive/nasa/casi.ntrs.nasa.gov, Dec. 2006.

[24]Riehl, J.P., 2007 "Tools used by the Analysis & Integration Group: Chebytop," NASA Glenn Research Center: Space Propulsion & Mission Analysis Office, http://trajectory.grc.nasa.gov/tools/chebytop.shtml, Feb 2007.

[25]Polsgrove, "CHEBYTOP User's Manual," NASA internal document, April 2006.

[26]Humble, R.W., Henry, G.N., Larson, W.J., "Space Propulsion Analysis and Design," McGraw-Hill Companies, 1995.

[27]Pike, J., 2007, "Nuclear Resources: Reactor Concepts," Federation of American Scientists, http://www.fas.org/nuke/space/c02early.htm, Jan 2007.

[28]Cinnamon, J.D., 2005, "Nuclear Thermal Rocket Propulsion: Design Issues and Concepts," Texas Space Grant Consortium, University of Texas at Austin, Department of Aerospace Engineering, http://www.tsgc.utexas.edu/archive/fulltext/nuke.pdf, Jan 2007.

[29]Howe, S., "Assessment of the Advantages and Feasibility of a Nuclear Rocket for a Manned Mars Mission," Los Alamos National Laboratory LA-UR-85-2442, Los Alamos, New Mexico, 1985.

[30]Bixler, C.H., Gunther, N.A., Rochow, R.F., Polansky, G.F., "A Bimodal Power and Propulsion System Based on Cermet Fuel and Heat Pipe Energy Transport," Sandia National Laboratories, US. DOE contract DE-AC04-96AL85000.

[31]"Nuclear Thermal Rocket (NTR) Engine System Assessment: Status Review," NASA Contract No. NA53-25809, Science Applications International Corporation, Nov.7, 1990.

[32]McGuire, M.L., Martini, M.C., Packard, T.W., Weglian, J.E., Gilland, J.H., "Use of High-Power Brayton Nuclear Electric Propulsion (NEP) for a 2033 Mars Round-Trip Mission," NASA/TM-2006-214106.

[33]Choueiri, E.Y., "A Critical History of Electric Propulsion: The First 50 Years (1906-1956)," Journal of Propulsion and Power, Vol. 20, No. 2, 2004.

[34]Dunning, J.W., Hamley, J.A., Jankovsky, R.S., Oleson, S.R., "An Overview of Electric Propulsion Activities at NASA," Glenn Research Center, Cleveland, Ohio, 2004.

[35]Jahn, R.G., Choueiri, E.Y., "Electric Propulsion." Encyclopedia of Physical Science and Technology, Third Edition, Volume 5, 2002.

[36]Peradzynski, Z., 2006, "Electric Propulsion Research," Institute of Fundamental Technological Research, Polish Academy of Science, http://fluid.ippt.gov.pl/sbarral/index.html, Jan 2007.

[37]Charania, A., St. Germain, B., Wallace, J.G., Olds, J.R., "REACIONN: A Nuclear Electric Propulsion Mission Concept to the Outer Solar System," 40th AIAA/ASME/SAE/ASEE Joint Propulsion Conference and Exhibit, Fort Lauderdale, FL, July 11-14, 2004.

[38]Jacobson, D.T., Manzella, D.H., Hofer, R.R., Peterson, P.Y., "NASA's 2004 Hall Thruster Program," AIAA conference paper.

[39]"MMWe NEP Charts," NASA Glenn Research Center Internal Document.

[40]Pinero, L.R., 2005, "Multikilowatt Power Module Designed and Fabricated for High-Power Hall Thrusters," NASA Glenn Research Center study, http://www.grc.nasa.gov/WWW/RT/2003/5000/5430pinero.html, Feb. 2007.

[41]Borowski, S.K., "Bimodal Nuclear Thermal Rocket (BNTR) Propulsion for Future Human Mars Exploration Missions," presentation at the 2003 NASA Seal/Secondary Air System Workshop, November 5-6, 2003.

[42]Lindroos, M., 2007, "TransHab Module," Encyclopedia Astronautica, http://www.astronautix.com/craft/traodule.htm, Jan 2007.

[43]"Guidelines and Capabilities for Designing Human Missions, Chapter 5: Radiation," NASA Technical Report, PB2003-101438.

[44]Wilson, J.W., et.al., "Galactic and Solar Cosmic Ray Shielding in Deep Space," NASA Technical Paper 3682, Dec., 1997.

[45]G.L. Kulcinski, "NEEP 423 Course Notes, Lecture 2," University of Wisconsin, 1996.

[46]Hodus, S., 2006, "ModelCenter 7.0: Design Your Success," Phoenix Integration, Inc., http://www.phoenix-int.com, Jan 2007.

[47]Joyner, R., Lentati, A., Cichon, J., "Mission Analysis Trades Using Nuclear Propulsion Design Options Apllied to a Human Mars Mission," American Institute of Aeronautics and Astronautics, working paper, 2006.

[48]Sproles, N. "Establishing Measures of Effectiveness for Command and Control: A Systems Engineering Perspectivethe Journal of The International Council on Systems Engineering, Vol. 4, No.2, 2001.

BIOGRAPHICAL SKETCH

Jaclyn Cichon grew up in Tampa, FL and graduated from the Academy of the Holy Names in May 2001. In fall 2001, her passion for aerospace engineering led her to the Massachusetts Institute of Technology. Upon graduating with her Aeronautical/Astronautical Engineering degree in June 2005, she moved back to Florida to begin graduate studies at the University of Florida. Here she entered the Nuclear Engineering Department, which enabled her to pursue her interests in propulsion through study in the area of nuclear space propulsion. She worked under Dr. Samim Anghaie with the Innovative Nuclear Space Power and Propulsion Institute and focused her thesis work on mission analysis studies for interplanetary crewed missions. Upon graduating with her Master of Science degree in nuclear engineering in May 2007, she will begin work as a Missile Defense Agency contractor with the Boeing Company in Washington DC.